SCE Notes and Follow-up Items from
09-07-2023 Engineer-to-Engineer Meeting and Tour of SONGS
Prepared by Southern California Edison
10-25-2023

Context:

Southern California Edison hosted a tour of the San Onofre Nuclear Generating Station's Independent Spent Fuel Storage Installation on Sept. 7, 2023, and an engineer-to-engineer meeting largely focused on a beyond-design-basis flooding analysis of the Holtec UMAX ISFSI. Primary external participants were engineers Paul Blanch and David Lochbaum. SCE was represented by engineers Jerry Stephenson and Randall Granaas as well as seismic/tsunami specialist Bob Yales. Observers from the local communities were Gary Headrick, Charles Langley, and Dan Stetson. Observing from SCE was Manuel Camargo. Lochbaum and Stetson participated in the technical discussion virtually, via Microsoft Teams.

This document captures several key discussion points from the engineer-to-engineer discussion. This document also includes new detail regarding the elevation of remnant tsunami deposits in north coastal area of San Diego County as provided by the third party consulting firm, Coastal Environments.

ISFSI Specific Safety Issues:

1. Cavity Enclosure Container (CEC) and Divider Shell material and thickness, and UMAX air passage.

During the walkdown of the ISFSI, SCE stated the CEC is ¾" thick 304 stainless steel. The divider shell is ½" thick carbon steel. There is a 6" air passage at the base of the CEC (i.e., between the base of the CEC and bottom of the divider shell), which extends around the entire 360° circumference.

2. Inlet and outlet vent radiation readings.

SCE engineer Granaas carried an RO-2 radiation survey meter during the tour of the ISFSI. An RO-2 reads in millirem/hour, which are the units generally recorded on radiation surveys of the NUHOMS and UMAX inlet and outlet vents[1].

For the NUHOMS system, the outlet vent radiation reading is lower than the inlet, due to the design of the module's concrete shielding. For the UMAX system, the outlet vent reading is also typically the same, or lower, than the inlet vent radiation reading, due to design of the module's shielding.

SCE does not routinely survey the NUHOMS system outlet vents, due to their location approximately 20' above grade. Working at this elevation on a routine basis is an avoidable industrial safety risk. Routine surveys of the ISFSI include radioactive contamination surveys, which would identify a release of radioactive particulate from the outlet vent of a NUHOMS module.

[1] Micro-rem/hour may also be used, if applicable to the survey instrument used.

SCE Notes and Follow-up Items from
09-07-2023 Engineer-to-Engineer Meeting and Tour of SONGS
Prepared by Southern California Edison
10-25-2023

However, in response to an assertion made by a member of the public that SCE and the NRC were hiding radiation levels from the outlet vents, SCE arranged to have an independent contractor survey the outlet vents in October of 2020. Reference:

https://www.songscommunity.com/_gallery/get_file/?file_id=5fbdad4f2cfac2529449d162&ir=1&file_ext=.pdf

The independent contractor found no radioactive contamination at the outlet vents. Measured outlet vent radiation levels were lower than inlet vent radiation levels.

The canisters used at SONGS are designed, fabricated, and processed in accordance with NRC regulations and guidance. The canisters are leak-tested in accordance with ANSI standards and have redundant closure lids. Radiological surveys of the ISFSI area performed by SCE are consistent with the canister design and NRC requirements.

3. SONGS ISFSI Radiation Monitoring System (IRMS).

During the tour of the ISFSI, Jerry Stephenson (SCE ISFSI engineering manager) pointed out three radiation monitors installed adjacent to the storage modules (a fourth control monitor is installed near the owner-controlled area boundary). The group observed a 15 micro-rem/hour reading on the monitor on the northeast corner of the UMAX ISFSI.

The group discussed whether the monitors may detect a breach of the canister's confinement boundary. The monitors are not gaseous monitors, and therefore would not detect a gaseous release, if a breach occurred in a canister containing fuel with breached cladding[2]. The monitors would detect a significant release of radioactive material from a canister, or significant damage to the shielding surrounding the dry storage canister. A microscopic breach in the confinement boundary of a dry storage canister will not result in a significant release of radioactive particulate.

4. Chloride Induced Stress Corrosion Cracking (CISCC).

CISCC cannot occur unless all three of the below elements are present:

1. Tensile stress (present in weld areas);
2. Susceptible environment (e.g., marine);
3. Susceptible material (e.g., 304 stainless steel).

[2] Gaseous activity (primarily Krypton-85 for spent fuel) is normally confined within an intact fuel rod but may be released through a cladding breach. The dose resulting from a release of gaseous activity from a dry storage cask is well below applicable regulatory limits, as reported in Table 10 of NRC NUREG-1140*, A Regulatory Analysis on Emergency Preparedness for Fuel Cycle and Other Radioactive Material Licensees*.

SCE Notes and Follow-up Items from
09-07-2023 Engineer-to-Engineer Meeting and Tour of SONGS
Prepared by Southern California Edison
10-25-2023

CISCC is a slow process, if it occurs at all[3]. For the SONGS site, a through-wall crack would not occur sooner than approximately 80 years[4] (if it occurs at all).

The weld areas of SONGS Holtec canisters have been laser peened, which relieves tensile stress and creates compressive stress. This negates the potential for CISCC to occur on the Holtec canisters: without tensile stress, cracking cannot occur.

The effect of CISCC on canister structural integrity was discussed during the meeting. Randall Granaas stated the canisters are very flaw tolerant[5]. Therefore, CISCC is unlikely to affect a dry storage canister's structural integrity.

Red staining has been observed on the shell during inspection of Holtec canisters. The red stains were caused by free iron transferred from the coated carbon steel transfer cask liner (breaches in the coating exposed carbon steel). Red stains—i.e., corrosion—can be a precursor to CISCC, but is not actual cracking. The free iron will likely be expended through oxidation, after which corrosion will cease. SCE will be monitoring red stains in weld areas to ensure CISCC is not occurring, in accordance with the Inspection and Maintenance Program approved by the California Coastal Commission. In addition, as noted earlier, the affected canisters have been laser peened, removing the tensile stress required for CISCC to occur.

5. Detection of a through-wall crack.

SCE follows industry guidance to select canisters for inspection that are most susceptible to chloride induced stress corrosion cracking[6].

If a canister that has not been inspected were to develop an undetected through-wall crack, it is unlikely routine radiological surveys of the ISFSI area would identify the crack. This is due to the microscopic nature of chloride induced stress corrosion cracking, which will restrict the release of radioactive particulate through the crack.

6. Retrievability.

10 CFR Part 72.122 (l) specifies the requirement for the retrieval of spent nuclear fuel as follows:

Retrievability. Storage systems must be designed to allow ready retrieval of spent fuel, high-level radioactive waste, and reactor-related GTCC waste for further processing or disposal.

The retrievability requirement applies to all general license ISFSIs, such as for SONGS, and specific licensed ISFSIs. The NRC is responsible to verify by its review of license applications for ISFSIs and by pre-

[3] For example, there are many welded stainless-steel pipes and tanks in marine environments that have not experienced cracking.
[4] EPRI report *Flaw Growth and Flaw Tolerance Assessment for Dry Cask Storage Canisters*, 3002002785, Table 3-3. Note the table assumes a 0.5" thick shell; SONGS canisters use a 0.625" thick shell.
[5] EPRI report *Flaw Growth and Flaw Tolerance Assessment for Dry Cask Storage Canisters*, 3002002785, Chapter 4.
[6] EPRI Report *Aging Management Guidance to Address Potential Chloride-Induced Stress Corrosion Cracking of Welded Stainless Steel Canisters*, 3002008193.

operational inspection of dry storage systems under a general license that the retrievability requirement of 10 CFR Part 72.122 (I) is met. The NRC carries out its reviews and inspections using NRC approved procedures and, where needed, NRC approved Interim Staff Guidance (ISG) documents, such as ISG No. 2, Fuel Retrievability (note that ISG No. 2 has been incorporated into NUREG-2215).

The SONGS dry storage systems have demonstrated their compliance with NRC regulations, including retrievability, by the NRC's extensive licensing reviews performed for both the UMAX and NUHOMS systems, which confirmed compliance with their respective Safety Analysis Report, Certificate of Compliance (CoC), and other applicable NRC regulations. During its licensing reviews the NRC determined, as documented in separate Safety Evaluation Reports (SERs), that both systems meet the requirements of 10 CFR Part 72, including retrievability.

Prior to canisters containing spent fuel being loaded into the SONGS ISFSIs, the NRC also performed pre-operational inspections of each system in accordance with NRC Inspection Procedure 60854 (IP 60854). Among other objectives, IP 60854 requires verification of retrievability. As documented in the inspection reports, the demonstration tests required by each CoC and witnessed by the NRC in 2003 for the NUHOMS dry storage system and 2017 for the UMAX system confirmed compliance with all CoC requirements, including retrievability, and returning a canister to a pool to be opened, if required.

NUREG-2215, NRC's Standard Review Plan for Spent Fuel Dry Storage Systems and Facilities, section 16.4.5 defines ready retrieval as the ability to safely remove the spent fuel from storage for further processing or disposal. To demonstrate the ability for ready retrieval, a licensee should demonstrate it has the ability to perform any of the three options below. These options may be utilized individually or in any combination or sequence, as appropriate:

A. Remove individual or canned spent fuel assemblies from wet or dry storage.
B. Remove a canister loaded with spent fuel assemblies from a storage cask or overpack, as applicable.
C. Remove a cask or DSF storage container, as applicable, loaded with spent fuel assemblies from the storage location.

The dry storage canisters stored within the SONGS ISFSIs are retrievable in accordance with option B above.

Note the definition of retrievability does not explicitly include retrieving a canister for repair or maintenance. Furthermore, the NUHOMS and UMAX FSARs do not require the ability to retrieve a canister from its storage module for repair. However, the definition of retrievability implies appropriate measures will be taken to ensure canisters remain retrievable, which could potentially include planned retrieval of a canister for maintenance or repair. The design of the dry storage canisters (e.g., material selection) and inspection programs implemented by SONGS ensure canisters will remain retrievable. SONGS has developed a method to repair UMAX canisters in-situ, in the unlikely event of the need arising. SONGS has also developed a method to repair NUHOMS canisters, which requires withdrawing (retrieving) the canister into the transfer cask.

Regular inspections of the SONGS ISFSIs continue to be performed by the NRC to assure compliance with applicable NRC regulations. These ongoing inspections will ensure retrievability is maintained over time.

SCE Notes and Follow-up Items from
09-07-2023 Engineer-to-Engineer Meeting and Tour of SONGS
Prepared by Southern California Edison
10-25-2023

The NRC verified the NUHOMS canisters will remain retrievable during the period of extended operation (renewal). Reference the NRC's SER for renewed CoC 72-1029:

https://www.nrc.gov/docs/ML2125/ML21258A020.pdf.

For example:

• *The staff reviewed the applicant's supplemental evaluation to assess whether there was reasonable assurance that CISCC will not result in a loss of confinement or prevent retrieval of a CoC 1029 DSC during the period of extended operation, for a total of 60 years of storage. As noted in the CoC 1029 renewal application, the analysis was based on the CoC 1004 renewal application (ADAMS Accession No. ML16279A372), which the staff previously evaluated and documented in the CoC 1004 renewal application SER (ADAMS Accession No. ML17338A121). Specifically, Section 3.3.2 of the CoC 1004 renewal application SER addresses the staff's evaluation of the applicant's analysis of (1) DSC shell temperatures, (2) critical temperatures, relative humidity, and chloride concentration, (3) time for CISCC initiation, and (4) CISCC crack growth rate. Likewise, Section 3.4.13 of the CoC 1004 renewal application SER addresses the staff's evaluation of the applicant's analysis for DSC shell thickness to maintain the ASME Code limits during retrieval.*

• *The staff also reviewed the applicant's assessment that it relied on to support its conclusion that the evaluations conducted for the CoC 1004 renewal application are valid for the Standardized Advanced NUHOMS® System and sufficient for the CoC 1029 renewal application.*

The discussion of retrievability eventually turned toward options for long-term disposition of the spent fuel. Jerry Stephenson suggested that with the ongoing changes in the way nuclear power is viewed politically, it would not surprise him if the fuel wound up being reprocessed, instead of storing or disposing.

7. Onsite transfer equipment.

SCE owns and stores onsite a transfer cask for the NUHOMS system, and a transfer cask for the UMAX system.

SCE also owns and stores onsite the auxiliary equipment necessary to remove a NUHOMS canister from its storage module.

SCE does not own the specialized crane (vertical cask transporter [VCT]) required to remove a UMAX canister from its storage module.

SCE does not keep a trained and qualified crew on standby to operate the transfer equipment. In the unlikely event of a need to remove a canister from a storage module, two to three months would be required to bring personnel onsite, train the cask handling crew, bring a VCT onsite, and preoperationally test the transfer equipment prior to use.

8. Are canisters required to be inspected prior to transportation?

SCE Notes and Follow-up Items from
09-07-2023 Engineer-to-Engineer Meeting and Tour of SONGS
Prepared by Southern California Edison
10-25-2023

David Lochbaum raised this question. Randall Granaas responded that he would check the individual certification of compliance (CoC) for each canister model. He further offered that SCE would likely inspect canisters prior to offsite transportation, even if not required by the CoC.

There are three (3) transportation CoCs associated with SONGS dry storage canisters. Whether a canister contains high burnup fuel (HBF) may influence whether a pre-shipment inspection is required. Storage of HBF within the 24PT1 canister is not authorized.

Canister Model (Stores)	Certificate of Compliance (CoC)	Canister inspection/integrity verification requirement for non-HBF?	Canister inspection/integrity verification requirement for HBF?
NUHOMS 24PT1 (Unit 1 Fuel)	71-9255	No	N/A
NUHOMS 24PT4 (Units 2/3 Fuel)	71-9302	Yes	Yes
Holtec MPC-37 (Units 2/3 Fuel)	71-9373	No	Yes

9. UMAX module flooding.

For the SONGS site, the maximum credible tsunami height is 27’ above the Mean Lower Low Water (MLLW) sea level datum, and the maximum flooding elevation for the ISFSI is approximately 21.5’ MLLW. Since the inlet vents of the UMAX system are at approximately 31.5’ above sea level, flooding of the SONGS UMAX storage modules is not credible.
In the event of a beyond design basis tsunami or flood that fills the UMAX modules with water, SCE staff would keep the modules filled with water until the air passage at the bottom of the CEC is verified clear of debris, sediment, etc. This direction is included in a site procedure for responding to beyond design basis flooding.

It is important to distinguish between a credible event, and a credible event that is beyond design basis. Flooding of the SONGS ISFSI is credible. Furthermore, flooding is considered a credible event in the UMAX FSAR, and is thus evaluated within the FSAR. However, flooding of the SONGS ISFSI to the height of the Vertical Ventilated Module (VVM) inlet vents is not credible. In other words, the boundaries for credible events are site-specific.

A flooded VVM would hold approximately 2,500 gallons of water. This is similar to the volume of water contained within the fuel cavity of a Holtec dry storage canister after the canister is first removed from the spent fuel pool. SCE trended the heat-up rate of cavity water during inner lid welding activities: the heat-up rate was approximately 2° F/hour. The cavity water reached a maximum temperature of about 130° F when inner lid welding activities were completed, at which time bulk water was removed from the cavity to commence drying operations.

The highest heat-load of SONGS Holtec multi-purpose canisters (MPC) is approximately 28 kW, or approximately 95.5 BTU/hour. Conservatively assuming adiabatic heat transfer, it would take about 30

SCE Notes and Follow-up Items from
09-07-2023 Engineer-to-Engineer Meeting and Tour of SONGS
Prepared by Southern California Edison
10-25-2023

hours to raise the temperature of 2,500 gallons of water (approximately 20,000 lb.) from 70° F to boiling temperature. Subsequently boiling 2,000 gallons of water, leaving 500 gallons of cooling water within the module, would take approximately 165 hours.

Using the more realistic estimate of 2° F/hour rise, consistent with heating of fuel cavity water during welding activities, it would take about three days for flood water in a storage module to start boiling.

Using the most conservative (adiabatic) case, SONGS staff has approximately 30 hours to begin adding water to a VVM before the water would start to boil. Staff would have approximately 195 hours to begin adding water before 2,000 gallons of the original 2,500 gallons boiled to steam.

Jerry Stephenson noted that the effects of tsunamis are limited to coastal areas. Thus, equipment necessary to keep the storage modules flooded, and to support full recovery (e.g., sediment removal), could be obtained from inland areas, if necessary, by helicopter.

Holtec's proprietary analysis of VVM flooding, Section 4.6.2.5 of the UMAX FSAR, was discussed. Randall Granaas offered that he has read the analysis, and that it is essentially intuitive: water has orders of magnitude better heat transport properties, as compared to air. In response, David Lochbaum stated (paraphrasing): "If Holtec used tried and true methods, they would not make it proprietary."

10. Consequences of floodwater entering a SONGS dry storage canister.

For both the NUHOMS and UMAX canisters, the fuel was loaded in accordance with the criticality analysis for their respective transportation CoC. The transportation CoC criticality analysis assumes the canister is flooded with unborated water; the fuel remains subcritical.

Therefore, water entering a SONGS NUHOMS or UMAX dry storage canister will not result in a criticality event.

11. Technical Specification compliance.

Two different technical specifications were discussed during the meeting, which may have been conflated at times:

1. LCO 3.1.1, "The MPC shall be dry and helium filled."
2. LCO 3.1.2, "The SFSC Heat Removal System shall be operable."

Reference https://www.nrc.gov/docs/ML2034/ML20349A209.pdf .

The applicability of LCO 3.1.1 ends after the MPC has been dried, leak-tested, and backfilled; "APPLICABILITY: Prior to TRANSPORT OPERATIONS."

The applicability of LCO 3.1.2 begins after an MPC has been stored within a VVM.

During the meeting, it was asserted that SONGS must maintain a spent fuel pool to comply with Required Action D.1 of LCO of 3.1.1. As discussed above, LCO 3.1.1 is no longer applicable after the MPC

SCE Notes and Follow-up Items from
09-07-2023 Engineer-to-Engineer Meeting and Tour of SONGS
Prepared by Southern California Edison
10-25-2023

has been dried, leak-tested, backfilled, and transferred to the ISFSI. Required Action D.1 may be implemented if, for example, there were a defect in the canister, which prevented achieving leak-tightness prior to transfer to the ISFSI.

During the meeting, it was asserted that SCE must maintain the capability to transfer an MPC to a transfer cask, to comply with Required Action C.2.2 of LCO 3.1.2.

Per the UMAX FSAR Bases, Chapter 13:

The intent of this LCO is to address those occurrences of air duct screen blockage that can be reasonably anticipated to occur from time to time at the ISFSI (i.e., Design Event I and II class events per ANSI/ANS-57.9). These events are of the type where corrective actions can usually be accomplished within one operating shift to restore the heat removal system to operable status (e.g., removal of loose debris).

This LCO is not intended to address low frequency, unexpected Design Event III and IV class events (ANSI/ANS-57.9) such as design basis accidents and extreme environmental phenomena that could potentially block one or more of the air ducts for an extended period of time (i.e., longer than the total Completion Time of the LCO). This class of events is addressed by site procedures as required by the CoC.

In addition to Required Action C.1, efforts must continue to restore cooling to the SFSC. Efforts must continue to restore the heat removal system to operable status by removing the air flow obstruction(s) unless optional (emphasis added) Required Action C.2.2 is being implemented.

Section 3.4.12 of Appendix B of the CoC, Amendment 4, states:

For those users whose site-specific design basis includes an event or events (e.g., flood) that result in the blockage of any VVM inlet or outlet air ducts for an extended period of time (i.e., longer than the total Completion Time of LCO 3.1.2), an analysis or evaluation may be performed to demonstrate adequate heat removal is available for the duration of the event. Adequate heat removal is defined as fuel cladding temperatures remaining below the short term temperature limit. If the analysis or evaluation is not performed, or if fuel cladding temperature limits are unable to be demonstrated by analysis or evaluation to remain below the short term temperature limit for the duration of the event, provisions shall be established to provide alternate means of cooling to accomplish this objective.

Required Action C.2.2 is optional, and there are no credible events at SONGS, such as flooding or burial in debris, which results in blockage of any VVM inlet or outlet air ducts for longer than the total completion time of LCO 3.1.2.

Therefore, it is not necessary to maintain equipment available to remove an MPC from a storage module per Action C.2.2 of LCO 3.1.2. Furthermore, SCE is not required to perform an analysis or evaluation to demonstrate adequate heat removal. However, as discussed above, maintaining a VVM full of water (in the case of beyond design basis flooding) until the air passages can be verified free of obstruction will provide adequate cooling (superior to air cooling).

12. 10 CFR 72.48 reviews.

SCE Notes and Follow-up Items from
09-07-2023 Engineer-to-Engineer Meeting and Tour of SONGS
Prepared by Southern California Edison
10-25-2023

During the meeting, Randall Granaas and Jerry Stephenson emphasized SCE, as the licensee, is ultimately responsible for the quality and content of 10 CFR 72.48 reviews performed by Holtec, if accepted by SCE for use at the SONGS site.

Granaas and Stephenson stated that Holtec provides copies of all 10 CFR 72.48 evaluations affecting the Holtec Certificate of Compliance used at SONGS (72-1040). This is required by 10 CFR 72.48(d)(6)(iii). SCE documents review of the 10 CFR 72.48 evaluation for applicability to the SONGS site in the SONGS corrective action program.

Tsunami and Flooding General Issues:

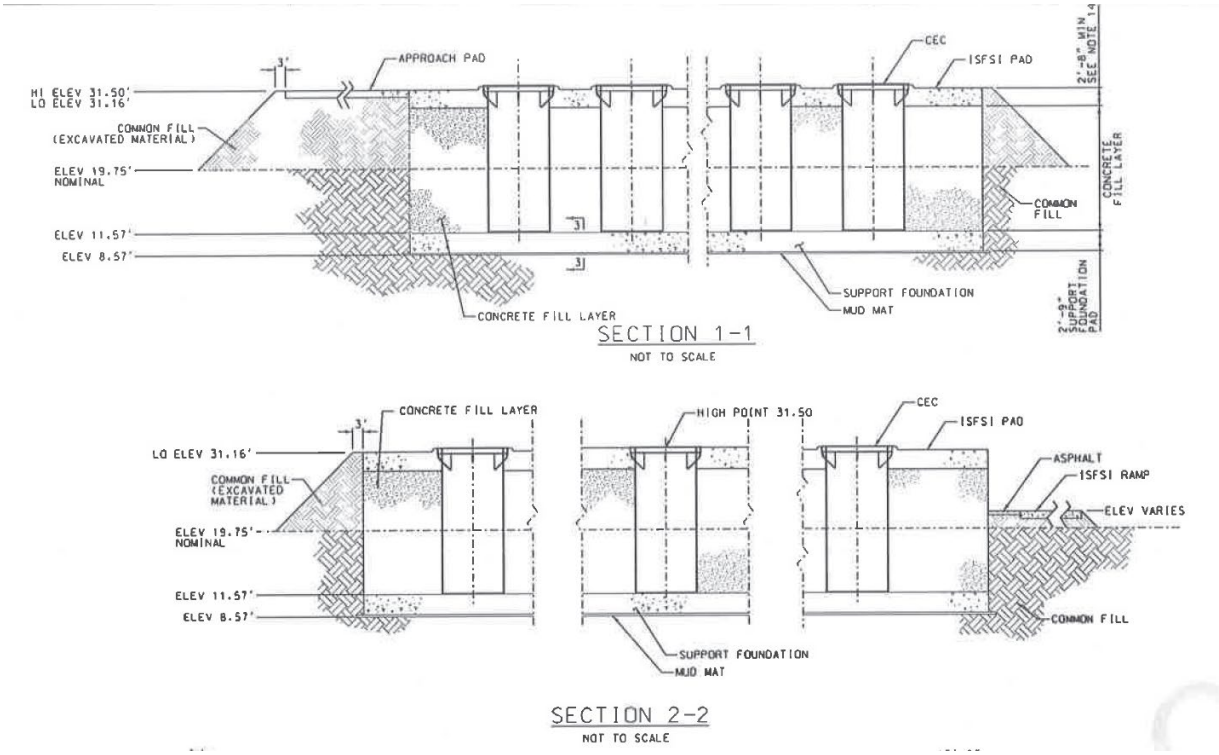
1. UMAX ISFSI Pad Elevation, Height of VVM Inlet Vent, and Flooding

Per the Holtec engineering drawings, the UMAX ISFSI pad elevation varies between el. 31.50‘ (slab high point) and 31.16’ (slab low point) and is sloped to drain rainwater from the pad surface. The bottom of the inlet opening is about 6” above the surface of the ISFSI pad. Therefore, flood water would have to reach a level above el. 31.5’ MLLW to enter the VVM inlet openings.

For the SONGS site, the design basis water level during a tsunami is el. 27’ Mean Lower Low Water (MLLW), and the maximum flooding elevation for the ISFSI during the Probable Maximum Precipitation (PMP) event is approximately 21.5’ MLLW.

Since the inlet vents of the SONGS UMAX system at approximate el. 31.5’ MLLW are well above the analyzed water elevations during either a tsunami or PMP event, water entering the VVM inlet vents during a flooding event is not considered credible.

SCE Notes and Follow-up Items from
09-07-2023 Engineer-to-Engineer Meeting and Tour of SONGS
Prepared by Southern California Edison
10-25-2023



2. Design Basis Tsunami Water Level

The SONGS Updated Final Safety Analysis Report, Section 2.4 available on the NRC's online database (San Onofre, Units 2 & 3 Final Safety Analysis Report, 2.4 Hydrologic Engineering Through 2.4.15 References 1-49. (nrc.gov)), addresses how elevation 27 feet was established as the SONGS design basis.

Section 2.4.6.1 titled *Probable Maximum Tsunami* states *detailed specific analyses were completed by Dr. Basil W. Wilson*.

The study concluded that the wave induced by 7-foot sea floor displacement and occurring during simultaneous high tide and storm surge would have a maximum runup to elevation +15.6 feet MLLW at the Unit 2 and 3 seawall.

Section 2.4.5.3 describes wave action as producing *the lowest and highest instantaneous water elevations* while storm surge is described in section 2.4.5.2.3 and is the abnormal rise in seawater level during a storm, measured as the height of the water above the normal predicted astronomical tide.

Section 2.4.6.6 titled *Effects on Safety-Related Facilities* states *When storm waves are superimposed, the predicted maximum runup is to elevation +27 MLLW, as discussed in paragraph 2.4.5.3*. Superimposing storm waves is conservative. This elevation for maximum water elevation during a tsunami remains the SONGS design basis and was accepted by the Nuclear Regulatory Commission during review of the SONGS 2&3 Final Safety Analysis Report.

SCE Notes and Follow-up Items from
09-07-2023 Engineer-to-Engineer Meeting and Tour of SONGS
Prepared by Southern California Edison
10-25-2023

3. Recent Tsunami Hazard Studies for SONGS

As part of the NUHOMS ISFSI permit extension process required by the California Coastal Commission, SCE engaged oceanographic engineering & environmental consulting company Coastal Environments to prepare an updated tsunami hazard report. The purpose of the report was to understand the current tsunami hazards at the waste storage facility based on information available in 2022. The analysis was performed using deterministic worst-case scenarios, both for far-field and near-field tsunamis. The assessments used a conservative maximum still water level called an "extreme water level." This extreme water level includes astronomical tides, storm surge, limited wave setup caused by breaking waves, and sea level rise using the extreme H++ scenario (2.8 ft in year 2050).

The studies were submitted to the California Coastal Commission, reviewed by their staff geologist, and summarized in the CCC Staff report for permit extension for the NUHOMS ISFSI. Findings from the 2022 CE Tsunami Hazards report, as summarized in the CCC Staff Report, are as follows:

Near-field tsunamis

Near-field tsunamis may be generated by earthquakes on the Newport-Inglewood/Rose Canyon (NIRC) fault system, which is the closest fault system offshore SONGS. The hypothetical near-field modeling conducted by SCE included earthquakes ranging from M7.62 to M7.44 and with seafloor uplift ranging from 13.1 ft to 8.2 ft. The analysis found a maximum potential water elevation at the waste storage facility of 23.6 ft MLLW, with a water depth above ground surface of 3.9 ft. Although inundation would be present in this scenario, the predicted water levels are lower than those predicted to be generated from a worst-case far-field tsunami source.

Far-field tsunamis

The updated analysis found that tsunamis originating from earthquakes on the AlaskaAleutians subduction zone, particularly the eastern portion of the subduction zone, would produce the highest tsunami wave heights offshore of SONGS. Tsunami sources from this region were used to model a worst-case scenario for tsunamis on top of the extreme water level discussed above.

The worst-case hypothetical far-field tsunami would come from a M9.5 earthquake in the eastern Aleutians. In the worst-case scenario, which would include 2.8 ft of sea level rise (H++ projection for 2050), the maximum potential water elevation at the waste storage facility would be 29.8 ft MLLW, with a water depth above ground surface of 9.1 ft around the NUHOMS waste storage facility. [Note: Reducing for future sea level rise, the current estimate is el. 27.0 ft MLLW]. The worst-case scenario was modeled without the seawall present to demonstrate that the waste storage facility was not reliant on existing shoreline protection devices. The presence of the seawall is expected to reduce the waste storage facility exposure to tsunamis.

Submarine landslide tsunamis

Finally, offshore submarine landslides occurring along the steep escarpments present on the southern California seafloor have also been considered as potential tsunami sources. Prior simulations performed for SCE have found that tsunami runup from submarine landslides along

SCE Notes and Follow-up Items from
09-07-2023 Engineer-to-Engineer Meeting and Tour of SONGS
Prepared by Southern California Edison
10-25-2023

the Thirtymile Bank formation towards the San Diego Trough and from the Fortymile Bank formation into the North San Clemente Basin are the most significant potential local landslide sources of tsunamis. One of these simulations found high water levels on the cliffs adjacent to SONGS of 21.7 ft MLLW from Thirtymile Bank and 18.7 ft MLLW from Fortymile Bank. Although significant, both of these predictions are lower than the water levels predicted to be generated from a worst-case far-field tsunami source. The worst-case far-field tsunami therefore remains the most extreme worst-case tsunami scenario.

Conclusion

The worst-case scenario tsunamis from far-field, near-field, and local landslide sources may all inundate the waste storage facility site (conservatively assuming for analytical purposes that the sea wall is not present). Most predicted inundation is expected to be below 4 ft. The maximum depth of inundation is expected to be 9.1 ft from a far-field source in the eastern Aleutians after a M9.53 earthquake.

In summary, flooding of the SONGS site due to a tsunami resulting from even the most extreme environmental hazards does not result in a water depth above el. 27.0 ft MLLW. Since the inlet vents of the UMAX storage modules are at el. 31.5 ft MLLW, flooding of the SONGS UMAX storage modules is not credible.

Links to the CCC staff reports are as follows:

2015 CCC staff report (Tu14a-10-2015.pdf (ca.gov))

2022 CCC Staff Report (Th12a-10-2022-report.pdf (ca.gov))

4. The SONGS Seawall

The SONGS North Industrial Area (formerly Unit 1) seawall was built to protect SONGS Unit 1 from a potential tsunami hazard. Following the decommissioning of SONGS Unit 1 and transfer of spent fuel into the existing ISFSI, the seawall was no longer required for tsunami protection. Although the seawall continues to provide some level of site protection from a tsunami hazard, it is not required by either the TN NUHOMS ISFSI or the Holtec HI-STORM UMAX system as they are designed to safely withstand flooding effects, including complete submergence up to 50 feet and 125 feet, respectively. The NIA seawall continues to function as a physical security barrier between publicly accessible areas (i.e., the beach walkway and San Onofre State Beach) and the SONGS site.

The seawall extends along the seaward side of the North Industrial Area (NIA) which includes the ISFSI site. The seawall is constructed of 3/8" thick steel sheet piling approximately 36' long with a soil embedment depth of 22'. The top of the seawall is at elevation (El.) 28.2' referenced to the site mean lower low water (MLLW) tidal datum. The sheet pile seawall is protected from the marine environment with a 2.5" thick layer of gunite on both faces. It was originally designed to maintain structural integrity during a SONGS design basis earthquake followed by the design basis tsunami to water elevation 27.0’ MLLW.

SCE Notes and Follow-up Items from
09-07-2023 Engineer-to-Engineer Meeting and Tour of SONGS
Prepared by Southern California Edison
10-25-2023

Although the ISFSI does not rely upon the NIA seawall for protection against tsunami does not mean the structure provides no environmental hazard protection for the SONGS site. The seawall remains a robust structure that is periodically inspected, and repairs are performed when conditions warrant. The steel sheet pile members are protected against corrosion by an active cathodic protection system as well as the existing gunite cover.

5. **Gerald G. Kuhn [2005],** ***Paleoseismic features as indicators of earthquake hazards in North Coastal, San Diego County, California, USA***

The purpose of this 2005 scientific paper was to evaluate the seismic hazard of the north coastal area of San Diego County due to tsunami deposits and paleoseimically deformed sediments exposed by new road cut and mass-grading excavations. He found that remnant tsunami deposits occur up to 100+ m in elevation around the modern coastal lagoons and estuaries.

The 2005 Kuhn paper has been used and referenced numerous times for studies related to the seismic and tsunami hazard at SONGS. Most recently, the paper was referenced in the geological hazards study completed by Coastal Environments in 2022 for the NUHOMS ISFSI permit extension and used to establish the worst-case earthquake that could occur on the Newport-Inglewood/Rose Canyon fault system. The earthquake information was then used as input for computer-generated tsunami prediction model summarized in the 2022 CE Tsunami Hazards Report.

Because the elevation of remnant tsunami deposits described in the Kuhn (2005) paper were located at elevations greater than results of the 2022 Coastal Environments (CE) Tsunami Hazards Report, SCE requested a review of the issue by CE for potential impact to the conclusions of the 2022 Tsunami Hazards Report. Their findings are summarized as follows:

> Most of the tsunami deposits identified by Kuhn (2005) are located on marine terrace surfaces remnant from past sea level high water levels which exist throughout the Southern California area. Prominent marine terraces include the Nestor (120,000 years) and Bird Rock (80,000 years) in the San Diego area. Stuart Mesa in the Oceanside/Camp Pendleton area exists at elevation 32 m and represents an ~225,000 year surface (Kern and Rockwell, 1992). Remnant tsunami deposits found on these marine terraces are due to geological uplift. Although uplift rates of these terraces have been estimated, these are long term (100,000 years) values and may be in inaccurate for the most recent tectonics conditions as the convergence proceeds. The average estimate for uplift in southern California varies from 0.13 mm/year (millimeter) to 0.25 mm/year.
>
> The Tsunami deposits elevation found by Kuhn (2005) at elevations between 6.7-9.14 m, MSL (Mean Sea Level) and other deposits at lower elevations (3.04-3.35 m, MSL) are consistent with tsunami modeling for San Onofre site performed by CE in 2022.
>
> CE is not aware of any “Known” historic tsunamis with run up in the Southern California Region greater than that presented in the 2022 Tsunami Hazards Report. The prehistoric tsunami deposits identified by Kuhn in his study at the Batiquitos lagoon with run up to 6.70 m - 9.14 m el. MSL do not have established age controls. Even if present sea level is used, the maximum run

SCE Notes and Follow-up Items from
09-07-2023 Engineer-to-Engineer Meeting and Tour of SONGS
Prepared by Southern California Edison
10-25-2023

up elevation in the Batiquitos lagoon may have been achieved due to local channeling in the lagoon that otherwise would not have been observed elsewhere along the coastline.

Coastal Environments concluded that the results described in the 2022 CE Tsunami Hazards Report remains a credible upper bound for tsunami run up at SONGS and are consistent with the observations found in the Kuhn (2005) study.

C8601216 - 19

RECEIVED
FEB 15 1973
Civil/Structural
Nuclear Facilities Group

ESTIMATE OF TSUNAMI EFFECT AT SAN ONOFRE NUCLEAR GENERATING STATION UNITS 2 AND 3, CALIF.

12-31-72

orig

by
Basil W. Wilson

Prepared for
SOUTHERN CALIFORNIA EDISON COMPANY
Rosemead, California

PP

Contract P. O. No. T. 2202015

RECEIVED
JAN 20 1986
CDM/GO

December, 1972

Basil W. Wilson. D.Sc.
Consulting Oceanographic Engineer.
529 South Winston Ave., Pasadena, California, 91107.

TABLE OF CONTENTS

	Page No.
TABLE OF CONTENTS	i
LIST OF FIGURES	iii
LIST OF TABLES	vi
SUMMARY AND CONCLUSIONS	
1. Design Earthquake Magnitude, Fault Location and Ground Displacement	S-1
2. Time Dependency of Earthquake Dislocation	S-1
3. Elastic Displacements and Practical Evaluation of Earth Movements	S-2
4. The Formal Hydrodynamic Problem of Tsunami Wave Generation	S-3
5. Assumed Initial Form of Water Surface Elevation	S-3
6. Amplification of Wave Effects at the San Onofre Coastline	S-3
7. Modes of Free Oscillation of the Shelf off San Onofre	S-4
8. Tsunami Run-up and Draw-down at the Coast	S-5
9. Maximum Velocities of Uprush and Drawdown near San Onofre	S-6
10. Effects of the Offshore Islands and Ocean Basins	S-7
11. Possible Effects of Strike Slip Displacement, X	S-7
12. Broad Conclusions and Recommendations	S-8
1. INTRODUCTION	1
2. THE DESIGN EARTHQUAKE MAGNITUDE AND FAULT LOCATION	1
3. GROUND DISPLACEMENT OF DESIGN EARTHQUAKE	2
4. DURATION TIME OF EARTHQUAKE DISLOCATION	11
5. ELASTIC DISPLACEMENTS	17
6. PRACTICAL EVALUATION OF VERTICAL EARTH MOVEMENTS	20
7. THE HYDRODYNAMIC PROBLEM OF TSUNAMI WAVE GENERATION	21
8. ASSUMED INITIAL FORM OF WATER SURFACE ELEVATION	29
9. AMPLIFICATION OF WAVE EFFECTS AT THE SAN ONOFRE COASTLINE	34

TABLE OF CONTENTS (CONT'D)

		Page No.
10.	TSUNAMI WAVE REFRACTION OVER THE CONTINENTAL SHELF	40
11.	MODES OF FREE OSCILLATION OF THE SHELF OFF SAN ONOFRE	43
12.	TSUNAMI RUN-UP AND DRAW-DOWN AT THE COAST	48
13.	MAXIMUM VELOCITIES OF UPRUSH AND DRAWDOWN NEAR SAN ONOFRE	62
14.	OSCILLATING PROPERTIES OF THE OCEANIC BASINS	69
	a. Dana Point-Rose Canyon Shelf	70
	b. Gulf of Santa Catalina from Newport Beach to La Jolla	71
	c. Oceanic Quasi-Basin between San Clemente Island and the Mainland	74
	d. Oceanic Quasi-Basin from the Santa Barbara Channel Islands to San Diego	76
15.	POSSIBLE TSUNAMI EFFECTS FROM THE STRIKE-SLIP COMPONENT OF EARTHQUAKE DISPLACEMENT ON THE FAULT	77
REFERENCES		79
APPENDIX A		82
APPENDIX B		83

LIST OF FIGURES

Fig. No.		Page No.
1.	Detailed Bathymetry of the Ocean Basins off California	3
2.	General Bathymetry of the Ocean Basins off California	4
3.	Apparent Trends of Dependence of Maximum Resultant Ground Displacement on Earthquake Magnitude (adapted from Wilson 1964, 1969)	5
4.	Horizontal Earth Movements in the Tango Earthquake of March 7, 1927, Island of Honshu, Japan (adapted from Davison, 1936)	8
5.	Horizontal Displacements East and West of the Gomura Fault near Shimooka, Tango Earthquake of March 7, 1927, Japan	9
6.	Integrated Horizontal Components of Velocity and Displacement of Ground Motion (about 30 miles from epicenter) in El Centro, Calif., Earthquake of May 18, 1940 (adapted from Berg and Housner, 1961)	10
7.	Relationship between Duration of Strong Shaking and Earthquake Magnitude	12
8.	Integrated Horizontal Components of Velocity and Displacement of Ground Motion (about 45 miles from epicenter) in Olympia, Washington, Earthquake of April 13, 1949 (from Berg and Housner, 1961)	14
9.	Integrated Vertical Components of Earthquake Ground Velocity and Displacement; (a) El Centro, Calif., Earthquake of May 18, 1940; (b) Olympia, Washington, Earthquake of April 13, 1949 (from Berg and Housner, 1961	15
10.	Vertical Component of Sea Bed Movement (Empirical Model, Eq. 24 i) at three Locations off Southern California Coast	22
11.	Schematic Diagram of Vertical (Dip-Slip) Movement on Earthquake Fault and Accompanying Effect on Sea Surface	23
12.	Schematic Diagram of Sea Disturbance (exaggerated saw-tooth model) Resulting from Vertical Dip-Slip Faulting of Sea-Bed	30
13.	Maximum Profile of Sea Surface at Instant of Tsunami Generation for Three Assumed Dip-Slip Displacements of the Sea Bed of the Type Shown in Fig. 11	33

Fig. No.		Page No.
14.	Profile of Continental Shelf off San Onofre, California	36
15.	Network used for Numerical Computation of Tsunami Wave Refraction over Continental Shelf off San Onofre, California (Numbers indicate depths in meters at grid-points; spacings of grid points are 1794 ft. in both x and y directions	41
16.	Wave Refraction Diagram Showing Approach of Tsunami Waves to San Onofre, Calif., from Assumed Earthquake Fault at Edge of Continental Shelf	42
17.	Initial Maximum Profile of Sea Disturbance at Instant of Tsunami Generation, as at Low Tide and High Tide, for Dip-Slip Displacement on the Fault Z = 3.77 ft.	49
18.	Time Histories of Run-up (above low tide) of Tsunami Waves Generated by Various Magnitudes of Vertical Dip-Slip Offset, Z, (San Onofre)	51
19.	Time Histories of Run-up (above high tide) of Tsunami Waves Generated by Various Magnitudes of Vertical Dip-Slip Offset, Z, for Hypothetical Earthquake on Shelf-Edge Fault - (San Onofre)	52
20.	Approximate Profile of Sea-Bed in Neighborhood of San Onofre Nuclear Power Generating Plant	54
21.	Time Histories of Tsunami Elevation above Low Tide (MLLW) at 2640 ft from Coast near San Onofre for Two Magnitudes of Dip-Slip Offset, Z	55
22.	Time Histories of Tsunami Elevation above High Tide (MLLW + 8 ft) at 2640 ft from Coast near San Onofre for Two Magnitudes of Dip-Slip Offset, Z	56
23.	Values of Numerical Coefficients in Relationship for Run-up of Solitary Waves on Slopes of Various Grades	58
24.	Relationship between Maximum Tsunami Run-up at San Onofre and Vertical Dip Slip Offset	60
25.	Time History of Tsunami Current Velocity at Low Tide (MLLW) at 1800 ft. from Coast for Two Magnitudes of Dip-Slip Offset, Z	64
26.	Maximum Velocities of Draw-down Currents in the Tsunami near San Onofre for Various Magnitudes of Vertical Dip-Slip Offset, Z	68

Fig. No.		Page No.
27.	Bathymetry of Oceanic Basins off Southern California Showing Geometric Analogies for Basins Adjacent to San Onofre	72
28.	Vertical Profile of Ocean Bed between San Onofre and San Clemente Island, California	75

LIST OF TABLES

Table No.		Page No.
I	Most Probable Maximum Earthquake Surface Displacements (M = 7.5)	6
IA	Possible Extreme Maximum Earthquake Surface Displacements (M = 7.5)	6 a
II	Test of Adequacy of $f(t) \approx \tanh(\alpha t)$	16
III	Heights and Periods of Component Standing Waves Caused by the Hypothetical Earthquake	32
IV	Normalized Parameters of Tsunami Oscillation on Continental Shelf off San Onofre: Water Depths at Mean Low Low Water (MLLW)	44
V	Normalized Parameters of Tsunami Oscillation on Continental Shelf off San Onofre: Water Depths at (MLLW + 8 ft.)	45
VI	Comparison of Estimated and True Modal Periods for Tsunami Shelf Oscillation	47
VII	Coastal Heights and Periods of Modal Components of Tsunami Oscillation Caused by Hypothetical Earthquake (Water Depths to MLLW)	47
VIII	Estimated Maximum Runup, R, and Draw-Down, D, of Tsunami at the San Onofre Site	59
IX	Maximum Velocity Values and Times of Occurrence of Uprush and Drawdown Currents from Tsunami at Different Stations Offshore	65

SUMMARY AND CONCLUSIONS

1. Design Earthquake Magnitude, Fault Location and Ground Displacement

On the premise that a magnitude M = 7.5 earthquake occurs along 65 miles of a postulated fault along the edge of the shelf at a depth of 100 m between Newport Beach and La Jolla, statistical information is used to verify that the assumed rupture length is in keeping with such earthquake magnitude.

The fault plane is taken vertical and the sense of offset to be predominantly right lateral strike-slip with an associated small component of vertical dip-slip in relative amounts of 1/10, 2/10 and 3/10.

Statistical information comprising world data in a relationship of maximum ground displacement Δ to earthquake magnitude M (Fig. 3) is used to arrive at an engineering estimate of the expected value of Δ for M = 7.5. This is found to be $\Delta \approx 4$ m. A nominal maximum earth displacement of $\Delta \approx 7.5$ m is also selected as an approximate upperbound 75% confidence limit. Values of strike-slip and dip-slip components, X and Z respectively, for the two values of Δ are given in Tables I (p. 6) and IA (p. 6a).

Data from the Tango earthquake of 1927 in Japan (M = 7.5) is used next as a model for the type of dependence of X and Z upon horizontal distance, y, normal to the fault. It is shown that ground movements in the El Centro earthquake (M = 7.1) of 1940 in California are consistent with this model. An empirical equation [Eq. (5)] is then developed which satisfactorily fits the Tango-El Centro data and relates horizontal and vertical ground movements at any distance y from the fault to the values of X and Z on the fault.

2. Time Dependency of Earthquake Dislocation

An examination of duration times of strong shaking in relation to earthquake magnitude reveals that, except for very large earthquakes, the calculated time for the shear wave of rupture to travel the fault length, is an unreliable measure of shaking time.

Ground velocity and displacement data from the El Centro earthquake (M = 7.1) of 1940 in California and the Olympia earthquake (M = 7.1) of 1949 in Washington are then used to show that, besides the permanent displacements occurring in these earthquakes, relatively sizeable transient elastic displacements occurred in the horizontal and vertical directions (Figs 6, 8 and 9). In both these earthquakes the permanent displacement was attained in about 8 secs, as adduced from these data, and this length of time is supported by a calculation of Housner (1965) for the El Centro earthquake. A similar length of time for establishment of the permanent ground displacement in the Alaskan earthquake (M = 8.5) of 1964 has been inferred from hydrodynamic arguments related to tsunami effects.

To simulate this time dependency an empirical expression is developed (Eq. 10) to relate the horizontal and vertical components of permanent ground displacement, ξ and ζ respectively, at any distance y from the fault and any time t, with the values X and Z on the fault.

3. Elastic Displacements and Practical Evaluation of Earth Movements

The transient displacements in the El Centro and Olympia earthquakes were so significant that inclusion of their effect in the empirical equations for $\xi(y,t)$ and $\zeta(y,t)$ seemed essential. Dr. P.C. Jennings, noted earthquake engineer, was consulted on this aspect and pointed out that positive evidence for this transient displacement had been recorded in the Gobi Altai earthquake of 1957. Empirical Eqs (16) for $\xi(y,t)/X$ and $\zeta(y,t)/Z$ were thus made to include transient terms of 15 secs period with damping allowance in keeping with the El Centro and Olympia earthquake data.

The empirical equations in their final form [Eqs (23) and (24)] were used next to evaluate the vertical earth movement ζ as a function of time t for three specific values of y on the continental shelf off San Onofre (Fig. 10). Results are consistent with equivalent type data for the El Centro and Olympia earthquakes.

4. The Formal Hydrodynamic Problem of Tsunami Wave Generation

The (y,t) dependent vertical earth movement ζ on the shelf is next used in a formal attack on the hydrodynamic problem of determining the nature of the sea disturbance caused by uplift of sea bed on the shelf and equivalent down-drop on the continental slope and ocean floor. The hydrodynamic equations are developed in terms of a velocity potential and the evolving expression for the water surface elevation $\eta(y,t)$ for a vertical plane solution is given in Eqs (50) and (51). The general intangibility of these mathematical expressions and their need for extensive development led to an alternative engineering approach to the problem.

5. Assumed Initial Form of Water Surface Elevation

This approach consisted of making an assumption as to the shape of vertical water surface elevation $\eta(y)$ at time $t = 0$, taking the shelf to be of uniform depth. A saw-tooth shape (Fig. 12) was adopted on the basis that zero value of η must prevail over the fault ($y = 0$) because of the cancelling effects of ground uplift on the shelf side of the fault and down-drop on the continental slope side of the fault.

The Fourier series representation of the saw-tooth function, taken to the third harmonic, gives a satisfactory and desirable rounding of the saw-tooth (Fig. 13) and permits the approximate identification of amplitudes and periods of the harmonic components in the tsunami (Table III, p. 32) on the continental shelf.

6. Amplification of Wave Effects at the San Onofre Coastline

Formal hydrodynamic equations of motion and continuity of water particles on the shelf (Eqs 64) are next invoked for analyzing the tsunami-induced oscillations of the shelf waters. The equations are basicly similar to the equations of motion governing the vibration of a linear mass-spring system. It is pointed out that because the ground vibration is extremely rapid relative to the period of oscillation of the shelf waters, the effect of the former on the behavior of the water is quite minor, (except, of course, in respect of the initial uplift). Because of this the

problem can be treated as a free oscillation and the effect of the forcing function discarded as negligible.

The hydrodynamical equations are then solved numerically for the exact vertical profile shape of the continental shelf off San Onofre. The calculation is a finite-difference recursive procedure which "homes in" on the true values of the modal periods of free oscillation by using approximate values for a start. The approximate values needed for this were obtained by using Lamb's mathematical solutions for the free oscillations for a canal of uniformly sloping bed.

The numerical solution achieved via Eqs (71), makes allowance for the influence of the shelf in refracting tsunami waves. The refraction effect, computed separately, is illustrated in Fig. 16. Boundary requirements on the results of the calculation are that no horizontal velocity is possible against the vertical sea wall of San Onofre and that $\eta = 0$ at $y = 0$ and $t = 0$, in keeping with the initial sea disturbance over the fault. Numerical calculations, in the first instance, are evolved as displacement amplitudes of water particles, $\zeta(y)$ and $\nu(y)$, (ζ being in respect of vertical surface elevation of the water and ν in respect of horizontal movement, which is uniform with depth for long tsunami waves), all normalized to unit value of ζ at the coast. These normalized values of ζ_m and ν_m for each mode m(=1, 2, 3, 4) are given in Tables IV and V (pp. 44-45) for two conditions of water depth, (a) low tide at MLLW and (b) high tide (7 ft) with storm tide (1 ft), at MLLW + 8 ft, and for six values of vertical dip-slip Z.

7. Modes of Free Oscillation of the Shelf off San Onofre

The periods of oscillation, T_m, of the several modes m(=1, 2, 3, 4) found from the numerical calculations agree quite closely with the periods T_n (n=1, 2, 3) inferred from the Fourier analysis of the assumed initial sea disturbance (Table VI, p. 47). To improve the latter's representation of the initial sea disturbance, a sub-harmonic term ($n = \frac{1}{2}$) was introduced to allow for the permanent uplift of the sea bed [Eqs (79) and (80)].

The remaining problem was to determine the wave height scale factors (H_n) to be applied to the normalized values of the water displacements ζ_n and v_n. This was accomplished by linking H_n for each mode m(=1, 2, 3, 4) with the wave heights, H_n, for each harmonic n(=$\frac{1}{2}$, 1, 2, 3) of the assumed initial disturbance (as found from Fourier analysis). The basis for the link was the establishment of congruency in horizontal displacements of the water over the fault, as given by the normalized values of v_n (last rows of Tables IV and V), and the values of v_n based on linear wave theory and the use of H_n, as defining the flow of water at a node of the shelf oscillation in each mode. The scale factors thus calculated are given in Table VII (p. 47). This application concludes the use of the assumed initial water surface profile (Fig. 13) which is then replaced by a more accurate representation of initial profile (Fig. 16), which is in conformity with the hydrodynamic requirements of the irregularly shaped shelf.

8. Tsunami Run-up and Draw-down at the Coast

The final description of water surface elevation $\eta(y,t)$ and horizontal particle movement is given by Eqs (83), which combine the modal components (m = 1, 2, 3, 4). Figs 18 and 19 give the time histories of η at the coast for low and high tide conditions and five values of Z, and show that after a small initial draw-down, the worst effect comes from a wave crest at about 7 mins after the earthquake and a wave trough some 10 to 11 mins after the quake. Although Figs 18 and 19 show higher waves forming after this time, it is demonstrated [Eq. (86)] that, when appropriate damping effects are allowed for, they will actually be lesser waves.

By way of checking tsunami elevations at the coast, the height of the largest tsunami wave is calculated for a location offshore near the toe of the slope BCDE in Fig. 20. An empirical formula of Kishi and Saeki (1966) based on theoretical and experimental results for run-up of solitary waves on slopes of various steepnesses is then applied to estimate the final run-up at the coast. The comparison of results in Table VIII (p. 59) is quite good, the more accurate results of this study being conservative.

To permit evaluation of draw-down effect at low tide on cooling water intake and diffuser structures, draw-down levels are also given in Table VIII.

The calculation of run-up results for six values of Z enables a relationship between Z and run-up, R, to be defined in Fig. 24. The relationship is linear and can be extrapolated to indicate that the vertical dip-slip Z would have to exceed 5.5 m (18.2 ft) to generate a tsunami that could overtop the 28 ft height of the sea wall. Even this "out-of-this-world" result is conservative, because any appreciable value of Z would also require some vertical elevation of the entire coastline in approximate accord with Eq. (14).

It turns out, however, that a lesser value of Z, producing a tsunami on low tide (MLLW), could result in exposure of the cooling water intake head. Eq. (92) shows that this limiting value of Z is 4.5 m (14.8 ft). The value of the total earth movement, Δ, for such a value of Z at the 10 : 3 ratio for (X/Z) is 51.5 ft or 15.7 m. As Fig. 3 shows, such an earth movement has no precedent except for earthquakes of magnitude $M \approx 8.5$ and is considered wholly unlikely on a fault such as Rose Canyon or on postulated fault.

9. Maximum Velocities of Uprush and Drawdown near San Onofre

The drawdown conditions at low tide (MLLW) besides imposing the severer restriction on water level than runup also provide more severe conditions as regards velocities of scour. Velocities have been calculated via Eq. (94) and maxima for five values of Z, as a function of distance from the coast, are plotted in Fig. 26 and tabulated in Table IX (pp. 65-67). It would be advisable to increase the drawdown velocities shown in Fig. 26 (and Table IX) by a suitable factor to allow for the lessened depths of water resulting from permanent uplift of the sea bed. Such increased velocities in lessened depths would be needed to provide the same flux of water. At Station 1, (Fig. 16) or at about 1800 ft from the coast, Eq. (14) tells us that sea bed uplift, ζ_1, is

$$\zeta_1 = 0.20\ Z$$

For Z = 7.07 ft., then, water depth at that point is lessened by 1.39 ft from an original 18 ft to about 16.6 ft. Scour velocities then should be increased in the proportion (18/16.6) or by a factor 1.08. A nominal 10% increase on values given in Table IX or Fig. 26 should then be allowed.

It is pointed out that apart from the scour effects of velocities of withdrawal up to 13 ft/sec (for Z = 7.07 ft), consideration should be given in design to the effects of such velocities on the cooling water intake and diffuser structures, along with other concomitant wave forces from tides and waves.

10. Effects of the Offshore Islands and Ocean Basins

In the final phase of this report consideration is given to the possible effects of the tsunami in the adjacent oceanic basins. The oscillating properties of various such basins or quasi-basins are examined. In particular it appears that the deep ocean basin between San Clemente Island and the mainland can oscillate in modes with periods very similar to the periods of oscillation of the shelf.

In the case of a tsunami disturbance resulting from dip-slip on the edge of the shelf, both the shelf and the adjacent oceanic basin are set in oscillation, describing free oscillations for the coupled system. Because the initial sea upheaval over the shelf was assumed to occur with a corresponding subsidence of water level on the ocean side of the shelf-edge, the analysis of this study has in effect allowed for the coupling effect in a conservative way. Considerations of potential energy release suggest that amplitudes of oscillations in the ocean basins would be less than on the shelf and that velocities over the shelf-edge should therefore be somewhat less than prescribed.

11. Possible Effects of Strike Slip Displacement, X.

Because of the absence of any steeply inclined boundaries that are in any sense normal to the directions of fault movement there appears to be no likelihood that any significant effect on the sea would result from the horizontal component strike-slip movement of the fault. Precedents for saying this are cited in the cases of the San Francisco earthquake of 1906 and the Tango earthquake of 1927 in Japan.

12. Broad Conclusions and Recommendations

For convenience the following broad conclusions and recommendations are further summarized.

(a) A postulated earthquake of magnitude M ≈ 7.5 in the zone of deformation on the shelf edge, 5 miles from San Onofre, may be expected to cause an earth movement having a most probable value $\Delta \approx 4$ m (13.1 ft). A suggested design value for the San Onofre site is $\Delta \approx 7.5$ m (24.6 ft). This design value of Δ is as large as the most probable value of Δ for an earthquake of M = 7.95 magnitude, whose chance of occurrence on a minor fault is considered negligible. It is larger even than the movement recorded in the San Francisco earthquake of 1906 (M = 8.2, see Fig. 3). In any case, the statistical (Los Angeles Basin) frequency of occurrence of an earthquake of M = 7.5 on the postulated fault is 1 in 2000 years (Allen et al, 1965; Wilson, 1969). All these factors suggest that the recommended design value for Δ is conservative.

(b) For design purposes, it is recommended that the dip-slip component Z of earth movement be taken as 3/10 of the strike-slip component X, for which ratio, (for $\Delta = 7.5$ m) the design value of Z would be $Z \approx 2.2$ m (7.1 ft). This design value of Z is larger than any known value of vertical uplift in a California earthquake in recent history, at least since 1900. Considering the large recurrence interval (2000 years statistically) for an M = 7.5 earthquake in the Los Angeles Basin area, this recommended design value of Z is also conservative.

(c) Based upon evidence of earth movements in strike-slip earthquakes in Japan, California and Washington, it appears that magnitudes of vertical bed movement ζ_b can be predicted reasonably well by Eqs (16) or their empirically developed forms, Eqs (23) or (24). Results from Eqs (24 i) give results consistent with observations (Fig. 10).

(d) An odd-function shape for sea bed upheaval is assumed deriving from upthrust on the continental shelf and down-drop on the continental slope and ocean floor.

(e) Eqs (16), (23) or (24) show that some permanent upheaval of the entire coastline in the vicinity of San Onofre will occur. This effect would decrease water depths slightly and raise levels of cooling water intake structures and outfalls, etc. No problems should arise from distortion of the foundations which should be negligible.

(f) Maximum run-up and draw-down elevations likely to occur at San Onofre for the recommended value Z = 7.1 ft are respectively 4.8 m (15.6 ft) at high tide (MLLW + 7 ft. astronomical tide + 1 ft storm tide) and 2.8 m (9.3 ft) at low tide (MLLW).

(g) Low tide condition tends to be more critical in terms of scour or withdrawal velocities than high tide and draw-down velocities exceed those of uprush. For the suggested design value of Z = 7.1 ft., maximum velocities at 1800 ft offshore are + 5.3 ft/sec (uprush) and - 11.9 ft/sec (drawdown) on the low tide (MLLW). On the high tide (MLLW + 8 ft) they are + 3.6 ft/sec (uprush) and - 7.5 ft/sec (drawdown).

(h) Maximum withdrawal velocities are related to distance from the coast as shown in Fig. 26. The uppermost curve for Z = 7.1 ft is recommended for design and values should be increased an additional 10% over those plotted to allow for uplift of the sea bed.

(i) At the recommended design value of Z = 7.1 ft., cooling water intake structures at the design level of - 15.0 ft (below MLLW) should be safe from exposure. In the extreme they should be safe from an earthquake likely to occur on the postulated fault.

(j) It is recommended that outfall diffuser ports and cooling water intake structures, etc., be designed to withstand the maximum velocities of current mentioned along with concomitant accelerative flow conditions from wave and swells, storm tide and astronomical tide.

(k) Maximum accelerations in the design tsunami (at Z = 7.1 ft.) can be calculated for any location but are not given in this report.

(l) Results given generally in this study are considered to be conservative with respect to possible more exact treatment of the coupling effect

between shelf and oceanic oscillations.

(m) There is no likelihood that a local earthquake on the postulated fault could generate a tsunami capable of overtopping the sea wall at its height of + 28 ft. above MLLW. General uplift of land in such an event would tend to reduce the runup.

ESTIMATE OF TSUNAMI EFFECT AT SAN ONOFRE NUCLEAR GENERATING STATION UNITS 2 AND 3, CALIF.

Basil W. Wilson*

1. Introduction

This study is undertaken in general accord with the discussions between the writer and engineers of Southern California Edison Company on July 5, 1972, and their subsequent outline in writing of the requirements of the investigation and assumptions to be used. A summary of the statement of requirements forms Appendix A of this report. Appendix B contains the writer's original proposals for seeking answers to these requirements; some of these proposals have been subject to modification in the conduct of the present analysis.

2. The Design Earthquake Magnitude and Fault Location

The premise is adopted that an earthquake of Richter magnitude M = 7.5 will occur along 65 miles of postulated fault between Newport Beach and LaJolla, approximately along the edge of the continental shelf off Southern California. A statistical relationship between fault length L and earthquake magnitude M given by Tocher (1958) as

$$\text{Log}_{10} L = M - 5.6 \qquad (1)$$

for L in kms suggests that this premise is in reasonable accord with expectation (see also Wilson, 1969, Fig. 64). Thus for M = 7.5, Eq. (1) gives L ≈ 80 kms ≈ 50 miles. However, a result of Ambraseys and Zatopek (1968), namely

$$\text{Log}_{10} L = 1.13M - 6.4 \qquad (2)$$

gives L ≈ 125 kms ≈ 78 miles. The postulated fault rift of 65 miles is an approximate mean between the results from Eqs (1) and (2) for M = 7.5.

The fault location (as given) is approximately along the 60 m (200 ft) depth contour between Dana Point and Oceanside and along the 100 m (330 ft) depth contour between Newport Beach and Dana Point, as also between Oceanside and

* Consulting Oceanographic Engineer, Pasadena, California

LaJolla and is shown in Fig. 1. This figure shows the system of oceanic basins and islands which are a prominent feature of the topography of the ocean bed off Southern California. The topography is shown in more approximate form in Fig. 2. We shall refer to these features in the course of this study.

3. Ground Displacement of Design Earthquake

The fault plane (as given) is taken vertical and trending subparallel with the coastline, being nominally 5 miles distant from the San Onofre site. The sense of offset is assumed to be predominantly right lateral strike slip with an associated small component of vertical dipslip motion.

To arrive at an estimate of total (maximum) ground displacement Δ, where Δ is the resultant of the horizontal strike slip, X, and the vertical dip-slip, Z, at the fault, namely:

$$\Delta = (X^2 + Z^2)^{\frac{1}{2}} \qquad (3)$$

we refer to Fig. 3, which plots some of the available statistical information on the relationship between maximum ground displacement Δ and earthquake magnitude M. This diagram is adapted from Wilson (1964, 1969) and has been updated with the "Additional Data" recorded on the left hand side of the figure (Oakeshott, 1966; Ambraseys and Zatopek, 1968; King and Knopoff, 1968; Housner, 1971). The new data points, though scattered, do not unbalance the previously derived median curves given by the full and dash-lines. Although one might argue that the great scatter of data precludes any attempt to define a meaningful relationship, one might argue that part of this scatter undoubtedly shows the influence of additional parameters in the relationship, such as focal depth of earthquake, type and quality of basement rock, depth and quality of overlying alluvium, etc. From an engineering point of view the median curves do have a usefulness and meaning as an expression of the most probable trend of relationship when the variable parameters are averaged out. The curves could reasonably be considered to apply to shallow focus earthquakes whose focal depth might be of the order of 15 to 50 kms. The shaded zone represents the range within which 75% of all data points fall.

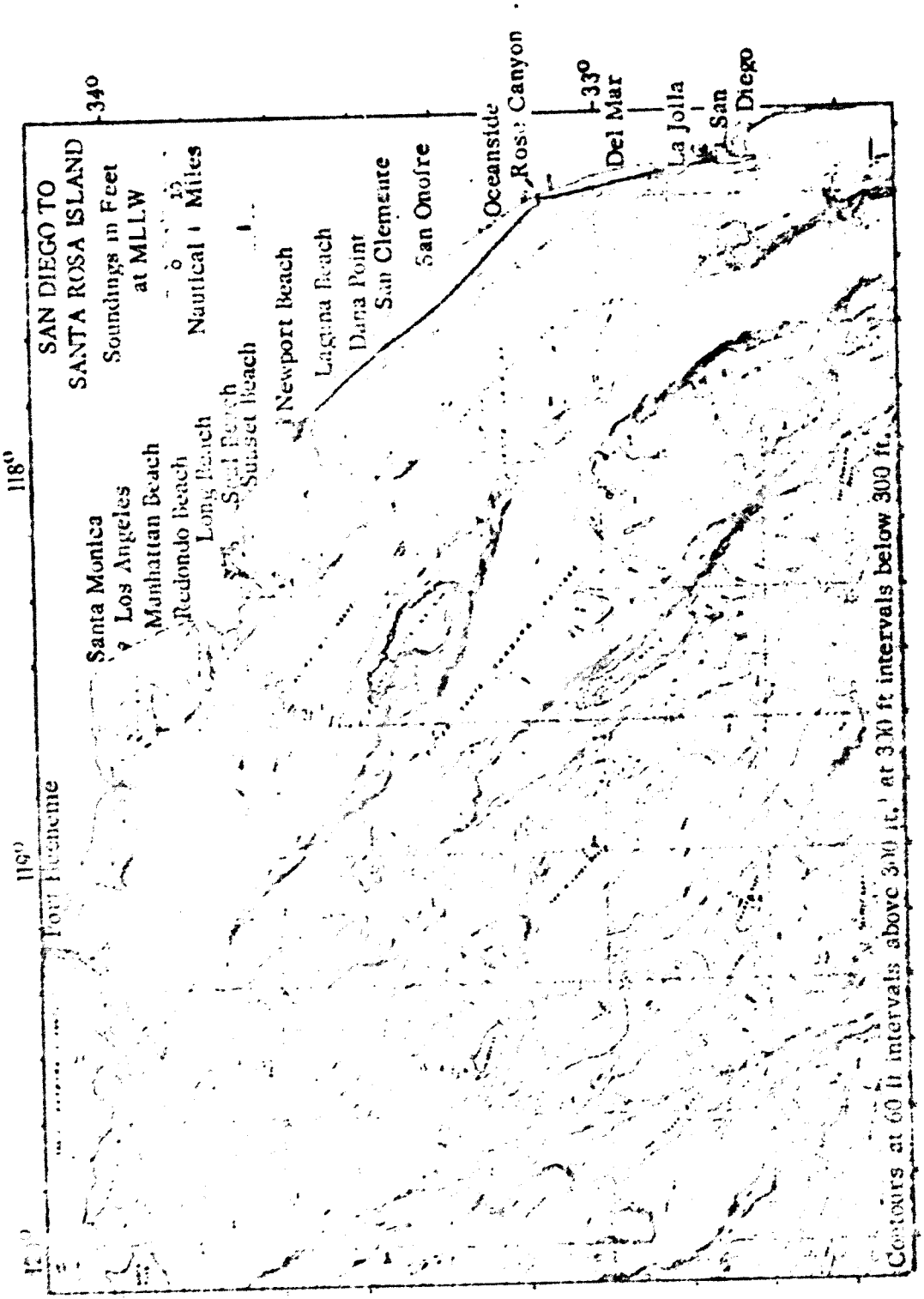


FIG. 1 DETAILED BATHYMETRY OF THE OCEAN BASINS OFF CALIFORNIA

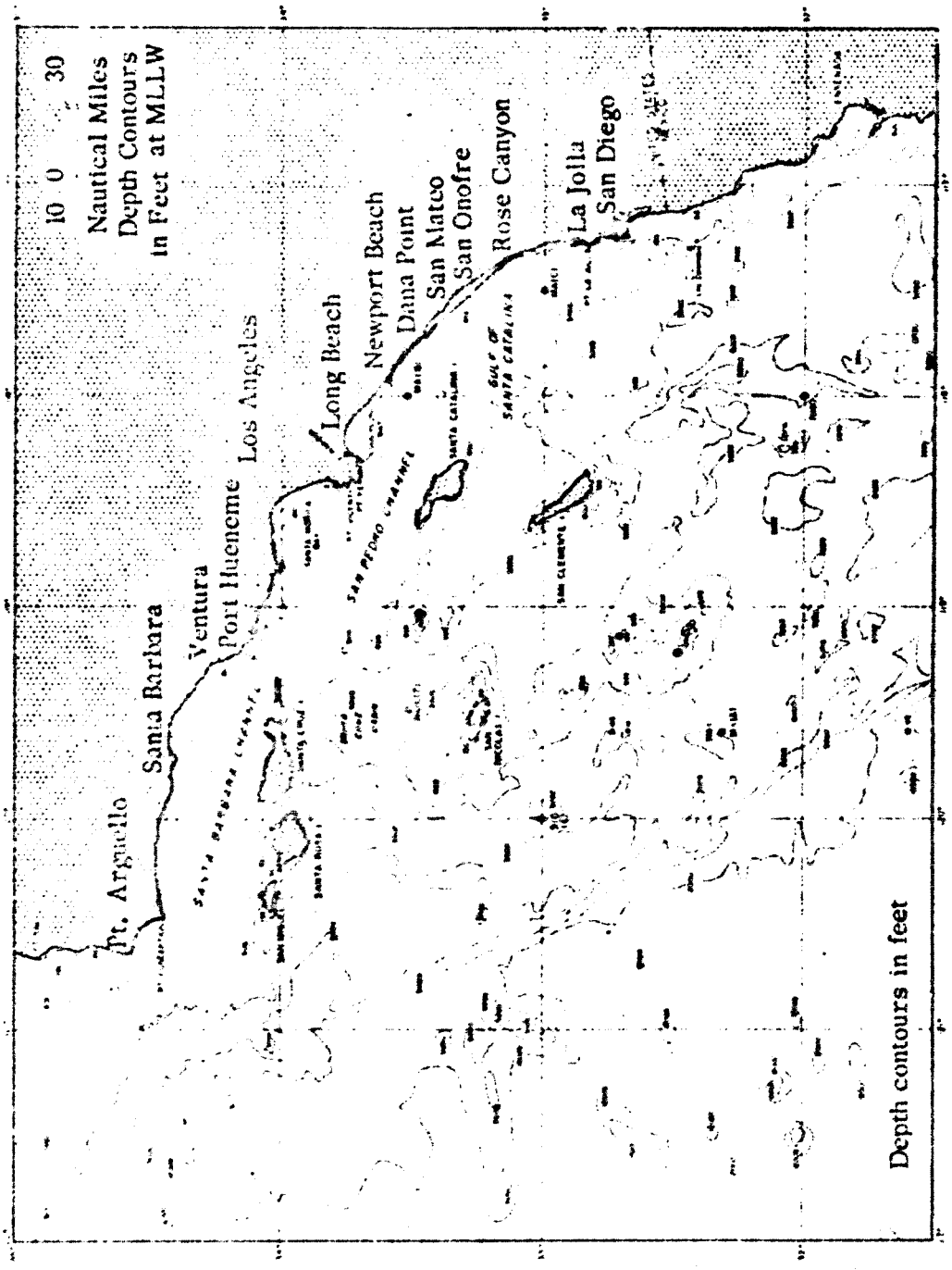


FIG. 2 - GENERAL BATHYMETRY OF THE OCEAN BASINS OFF CALIFORNIA

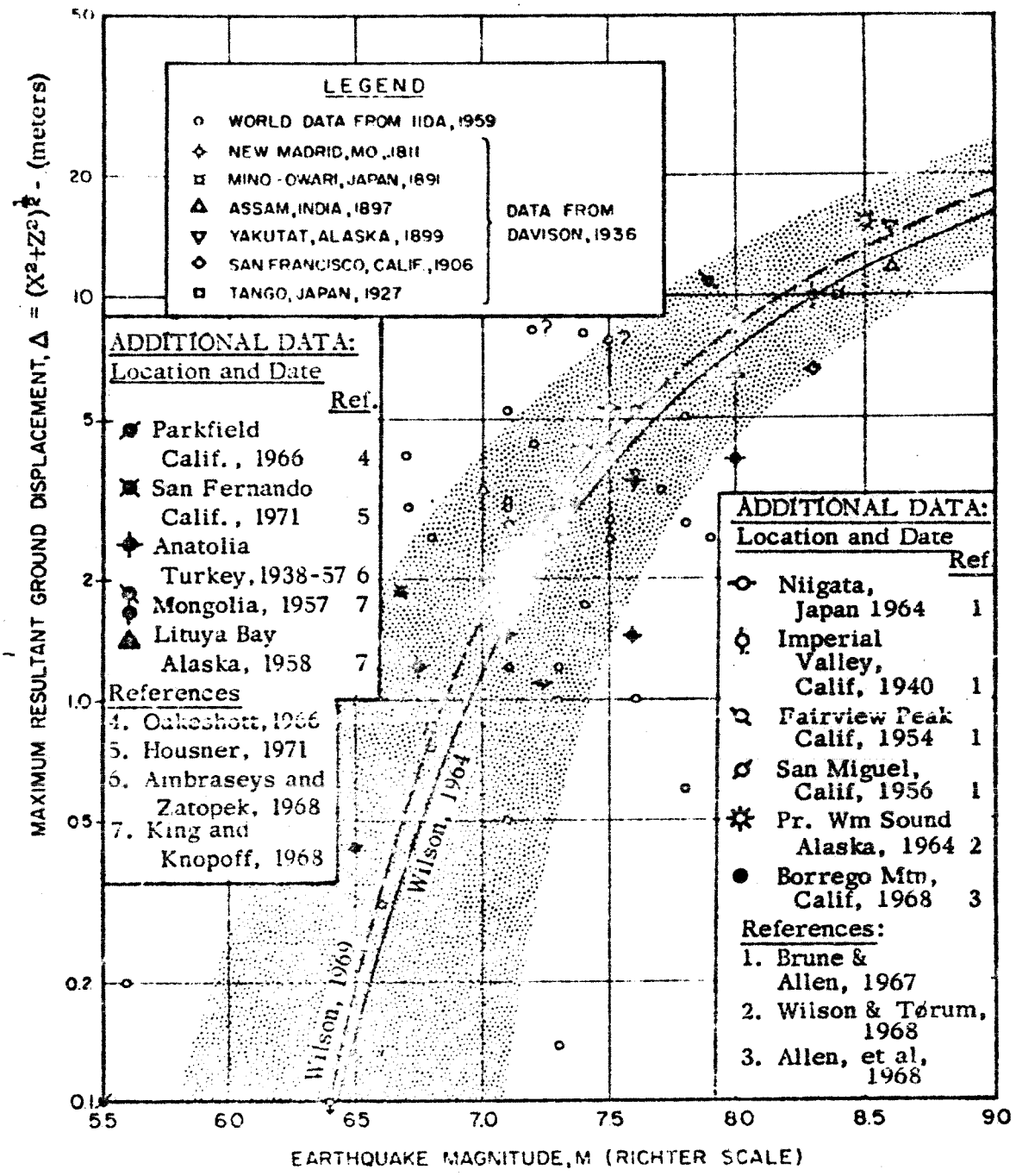


FIG. 3 - APPARENT TRENDS OF DEPENDENCE OF MAXIMUM RESULTANT GROUND DISPLACEMENT ON EARTHQUAKE MAGNITUDE (adapted from Wilson, 1964, 1969)

On this basis we feel encouraged to use the curves to adopt a mean working value of Δ,

$$\Delta \approx 4 \text{ m} \tag{4}$$

and a nominal maximum displacement (upper limit of shaded zone, Fig. 3)

$$\Delta \approx 7.5 \text{ m} \tag{4a}$$

for the earthquake magnitude M = 7.5. The Eq. (4) value corresponds with the Tango (Japan) earthquake data point which is exactly in-between the full and dash-line curves for M = 7.5.

For the stipulated strike-slip : dip-slip ratios of 10 : 1, 10 : 2 and 10 : 3, we have, then, by use of Eqs (3) and (4), values of maximum strike-slip, X, and dip-slip, Z, in accord with Table I. Corresponding values from Eqs (3) and (4a) are given in Table IA.

Of greatest consequence to the present study are the values of Z which vary from about 1.3 to 3.8 ft for the median value of Δ = 4 m (Table I) and from about 2.5 to 7.1 ft for the more extreme value of Δ = 7.5 m (Table IA).

We shall make the assumption that these maximum displacements will prevail along at least part of the fault; in particular, that they will be approximately constant in the region between Dana Point and Oceanside (Fig. 1).

The elastic rebound concept of Reid (1910) in explanation of earthquake dislocations along faults would require an exponential type decay of basement rock displacement with distance normal to the fault. This concept is now widely accepted by seismologists (cf. Benioff, 1964) and has, in fact, been verified by measurements in the field, particularly in areas where fault breaks have penetrated to the surface of the overlying alluvium.

TABLE I - MOST PROBABLE MAXIMUM EARTHQUAKE SURFACE DISPLACEMENTS (M = 7.5)

Ratio of Strike-Slip : Dip-Slip	Probable Maximum Surface Displacement					
	Strike-Slip X		Dip-Slip Z		Resultant Δ	
	(m)	(ft)	(m)	(ft)	(m)	(ft)
10 : 1	3.98	13.06	0.40	1.31	4.00	13.12
10 : 2	3.92	12.87	0.79	2.58	4.00	13.12
10 : 3	3.83	12.57	1.15	3.77	4.00	13.12

TABLE IA - POSSIBLE EXTREME MAXIMUM EARTHQUAKE SURFACE DISPLACEMENTS (M = 7.5)

Ratio of Strike-Slip : Dip-Slip	Extreme Maximum Surface Displacement					
	Strike-Slip X		Dip-Slip Z		Resultant Δ	
	(m)	(ft)	(m)	(ft)	(m)	(ft)
10 : 1	7.46	24.48	0.75	2.45	7.5	24.60
10 : 2	7.35	24.12	1.47	4.82	7.5	24.60
10 : 3	7.18	23.56	2.15	7.07	7.5	24.60

The Tango earthquake (M=7.5) of 1927 in Japan throws some light on earth movements of this kind involving both horizontal and vertical displacements. Fig. 4 which is adapted from Davison (1936), portrays the horizontal shear which took place along the Gomura fault, which has a dip of about 70° to the southwest. Actual magnitudes of horizontal movements at various distances from the Gomura fault along a line normal to the fault at Shimooka, are shown in Fig. 5. Evidently the displacement decayed exponentially with distance from the singularity at the fault. This decline of permanent set with distance from the fault was a noticeable feature also of the San Francisco earthquake of 1906 in which the movements were very largely horizontal (Lawson, 1908; Davison, 1936).

The vertical displacements across the Gomura fault, although generally much less than the horizontal, showed the same trend of decay with distance horizontally, as well as reversed vertical directions at the fault.

The El Centro earthquake (M=7.1) of 1940 in California is another example in which surface displacements have conformed with this pattern. Thus, according to Berg and Housner (1961), maximum relative displacement on the fault was approximately 12 ft. At a seismograph measuring site about 10 miles from the fault the displacement to NNW calculated from the component horizontal motions (see Fig. 6) was 1 ft, which is consistent with the same kind of displacement as that of the Tango earthquake on the Gomura fault, (for which the strike offset was also about 11 or 12 ft).

The curves of Fig. 5 can be approximated by a normalized empirical equation for strike-slip, $\xi(y)$, and dip-slip, $\zeta(y)$ in terms of the corresponding maxima, X and Z, at the fault

$$(2\,\xi/X) = (2\,\zeta/Z) = e^{-\beta y} \qquad (5)$$

where y is horizontal distance at right angles to the fault at which the values ξ and ζ apply, and β has the dimensions of $(\text{length})^{-1}$.

The value of β which approximates the full-line curves of Fig. 5 is

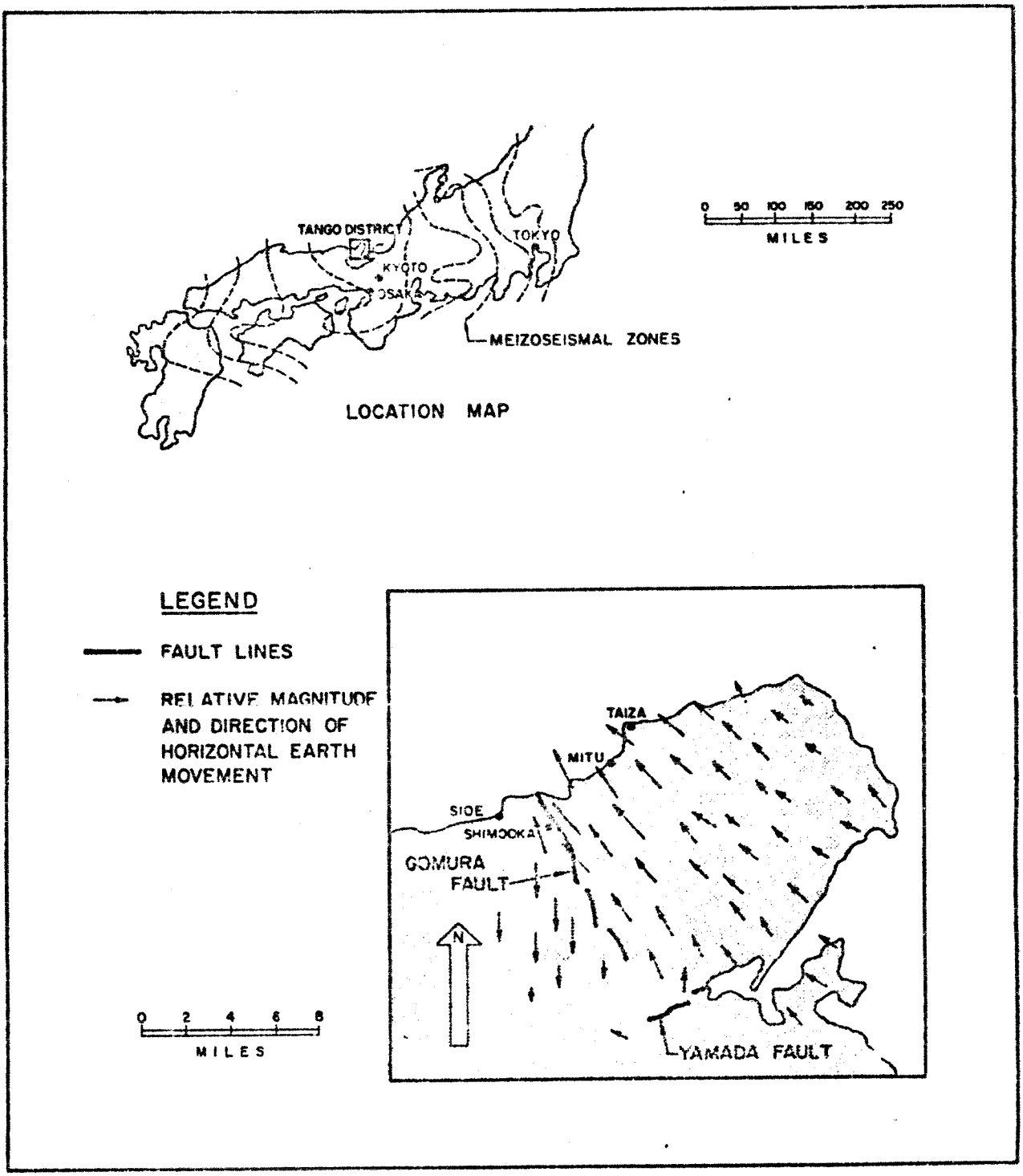


FIG. 4 - HORIZONTAL EARTH MOVEMENTS IN THE TANGO EARTHQUAKE OF MARCH 7, 1927, ISLAND OF HONSHU, JAPAN (adapted from Davison, 1936).

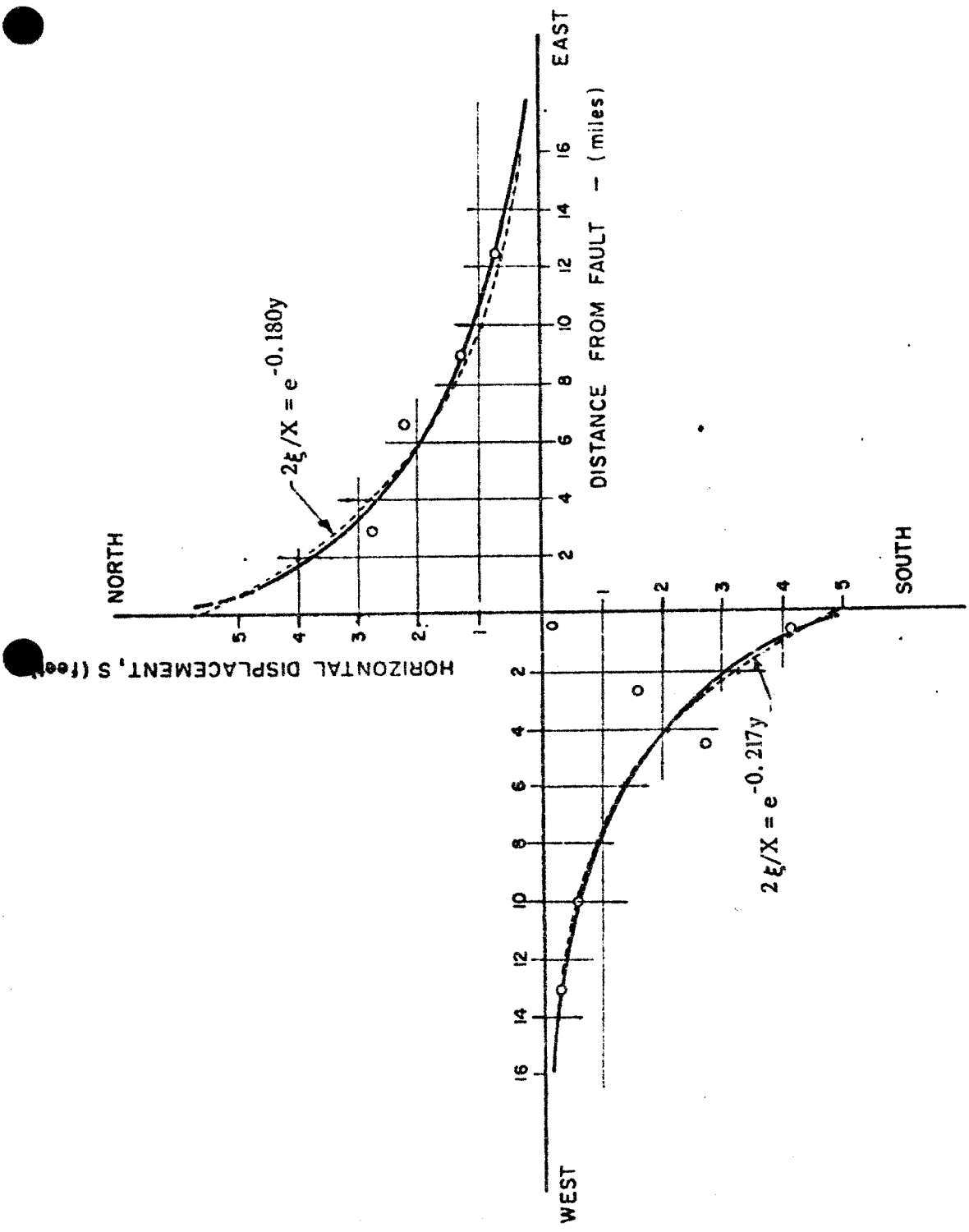


FIG. 5 - HORIZONTAL DISPLACEMENTS EAST AND WEST OF THE GOMURA FAULT NEAR SHIMOOKA, TANGO EARTHQUAKE OF MAR. 7, 1927, JAPAN.

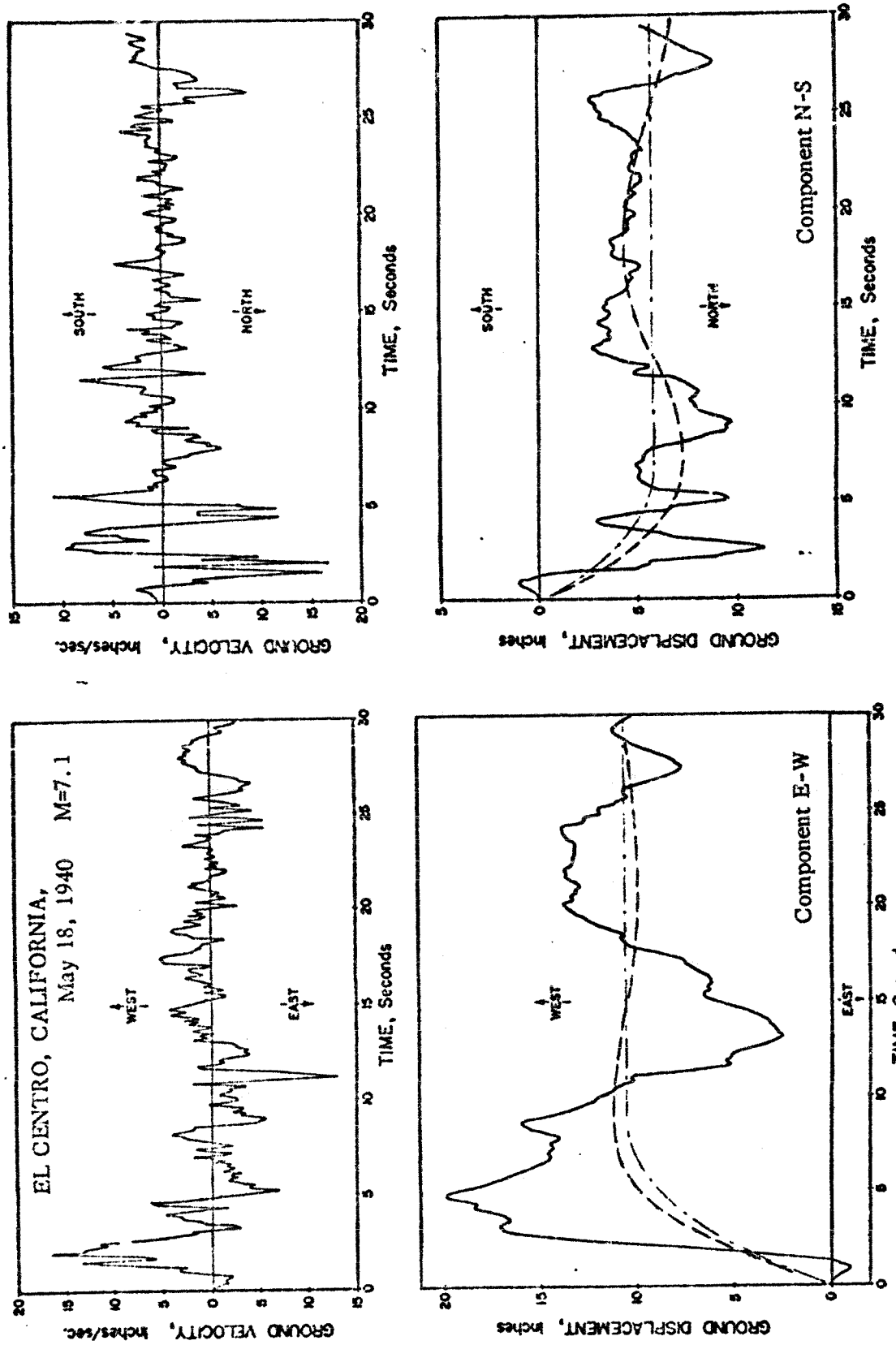


FIG. 6 - INTEGRATED HORIZONTAL COMPONENTS OF VELOCITY AND DISPLACEMENT OF GROUND MOTION (about 30 miles from epicenter) IN EL CENTRO, CALIFORNIA, EARTHQUAKE OF MAY 18, 1940 (adapted from Berg and Housner, 1961)

(i) $\beta = 0.1796 \text{ (miles)}^{-1}$ .....[for right hand curve of Fig. 5]

(ii) $\beta = 0.2170 \text{ (miles)}^{-1}$ .....[for left hand curve of Fig. 5]

Eq. (5) for each of these values of β is plotted as a dash-line curve in Fig. 5 as an indication of goodness of fit. Obviously the empirical equation is a good model of the measured dependence of horizontal displacement ξ on distance y. It seems reasonable to assume that Eq. (5), with the same value of β, will also satisfy the dependence of vertical displacement ζ on y.

For present purposes it seems valid then to adopt a mean value for β of

$$\beta = 0.200 \text{ (miles)}^{-1} \quad (6)$$

4. Duration Time of Earthquake Dislocation

We have already shown that the assumed fault length, L, of 65 miles would accord with a relationship which would be median between Eqs (1) and (2). Such an averaging would yield:

$$\text{Log}_{10} L = 1.07M - 6.0 \quad (7)$$

for L in kms. If the duration time t_d of severe shaking in an earthquake represented only the time for rupture to travel along the fault at the velocity of shear (S) waves in basement rock ($\approx$ 3.25 kms/sec), so that

$$t_d \approx L/3.25 \text{ secs} \quad (8)$$

for L in kms, then Eqs (7) and (8), combined to eliminate L and express t_d in terms of earthquake magnitude M, would indicate:

$$\text{Log}_{10} t_d = 1.07M - 6.51 \quad (9)$$

for t_d in secs. A plot of this relationship is shown in Fig. 7 along with readily available data on the duration time of severe earth shaking observed in a variety of earthquakes and drawn from sources such as Davison (1936), St. Amand (1961), Housner (1965) and Wilson and Tørum (1968). It seems evident from this that actual duration times of strong shaking tend to exceed the travel time of rupture along the fault more especially for lesser magnitude earthquakes.

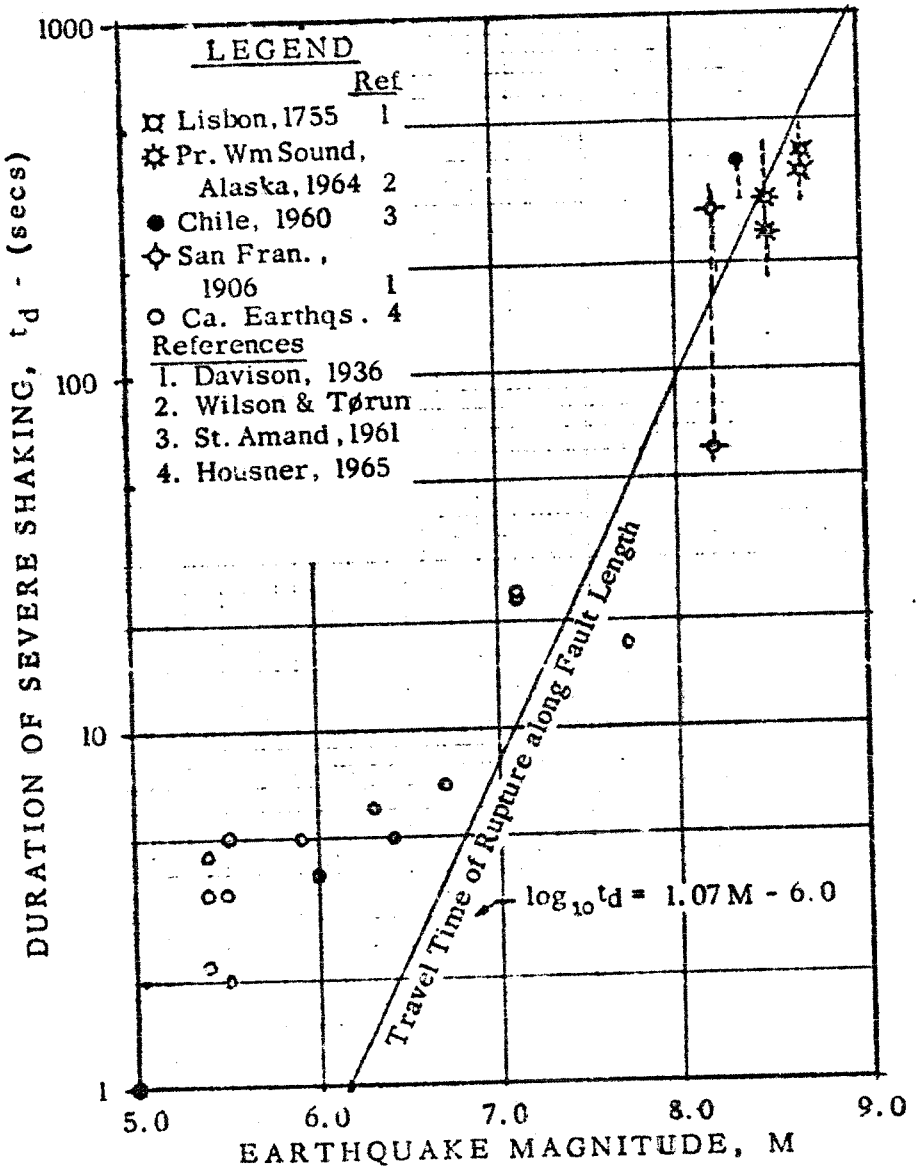


FIG. 7 - RELATIONSHIP BETWEEN DURATION OF STRONG SHAKING AND EARTHQUAKE MAGNITUDE

Examination of two specific earthquakes of magnitude M = 7.1 for which strong shaking was given as 23 and 24 secs, namely, the El Centro earthquake of 1940 in California and the Olympia earthquake of 1949 in Washington. (Berg and Housner, 1961), suggests that these duration times, in each case, incorporate one or two long Rayleigh waves of elastic ground shaking. This can be seen in Figs 6, 8 and 9 (adapted from Berg and Housner, 1961) from the integrated displacement curves in three component directions, obtained from acceleration records at distances of 10 miles (El Centro) and 45 miles (Olympia) from the earthquake epicenters. The displacements for the two earthquakes are quite remarkably similar in character and reveal that, besides the transient elastic vibration of the ground, a permanent set displacement was established within a time interval of about 8 secs from commencement of each earthquake.

Housner (1965) has drawn some interesting inferences from Fig. 6 in regard to the probable velocity of shaking of the basement rock in the El Centro earthquake of 1940. He assumes that the 20 ins transient E-W displacement in relation to the 10 ins E-W permanent displacement represents a factor of 2 amplification of motion in the alluvium, and that maximum velocity in the underlying rock was thus about $\frac{1}{2}$ of the registered maximum value of 1.8 ft/sec, or 0.9 ft/sec. From this he calculates that the time of slippage during which differential displacement of about 7.5 ft was occurring on each side of the fault was approximately 8 secs. Fig. 6 confirms that the E-W permanent set was reached in about this interval of time.

It is of interest also that the writer, in Wilson and Tørum, (1972), has inferred from indirect (hydrodynamic) arguments that the large earth movements of the Prince William Sound earthquake of March, 1964, may have been completed within about 8 secs.

On the basis of the median (dash-dot) curves of Figs 8 to 10, we may attempt to define a reasonable value for α (units of frequency) in an empirical simulation of time dependency, $\tanh(\alpha t)$ as part of an expression for permanent ground

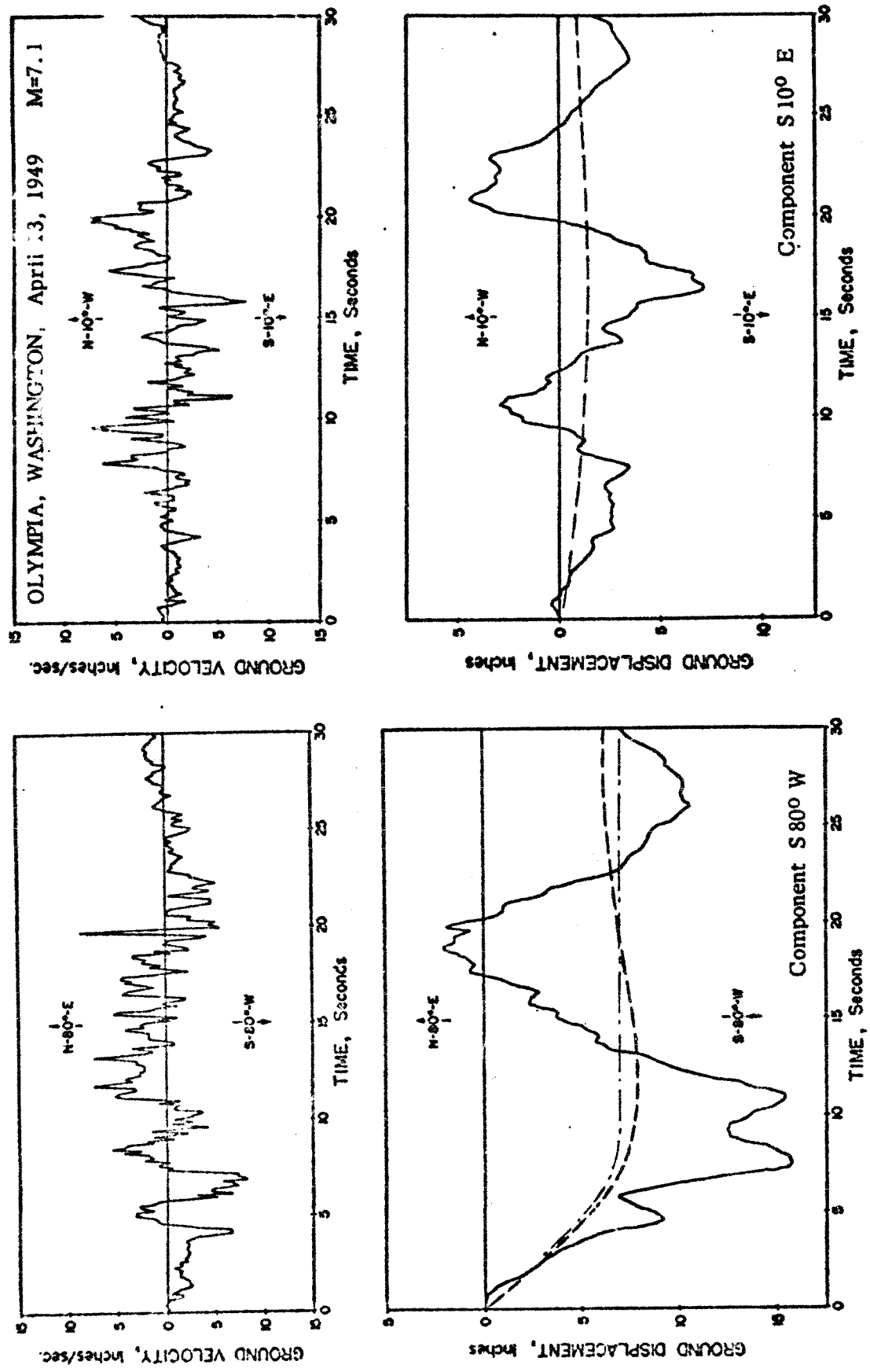


FIG. 8 - INTEGRATED HORIZONTAL COMPONENTS OF VELOCITY AND DISPLACEMENT OF GROUND MOTION (about 45 miles from epicenter) IN OLYMPIA, WASHINGTON, EARTHQUAKE OF APRIL 13, 1949 (from Berg and Housner, 1961).

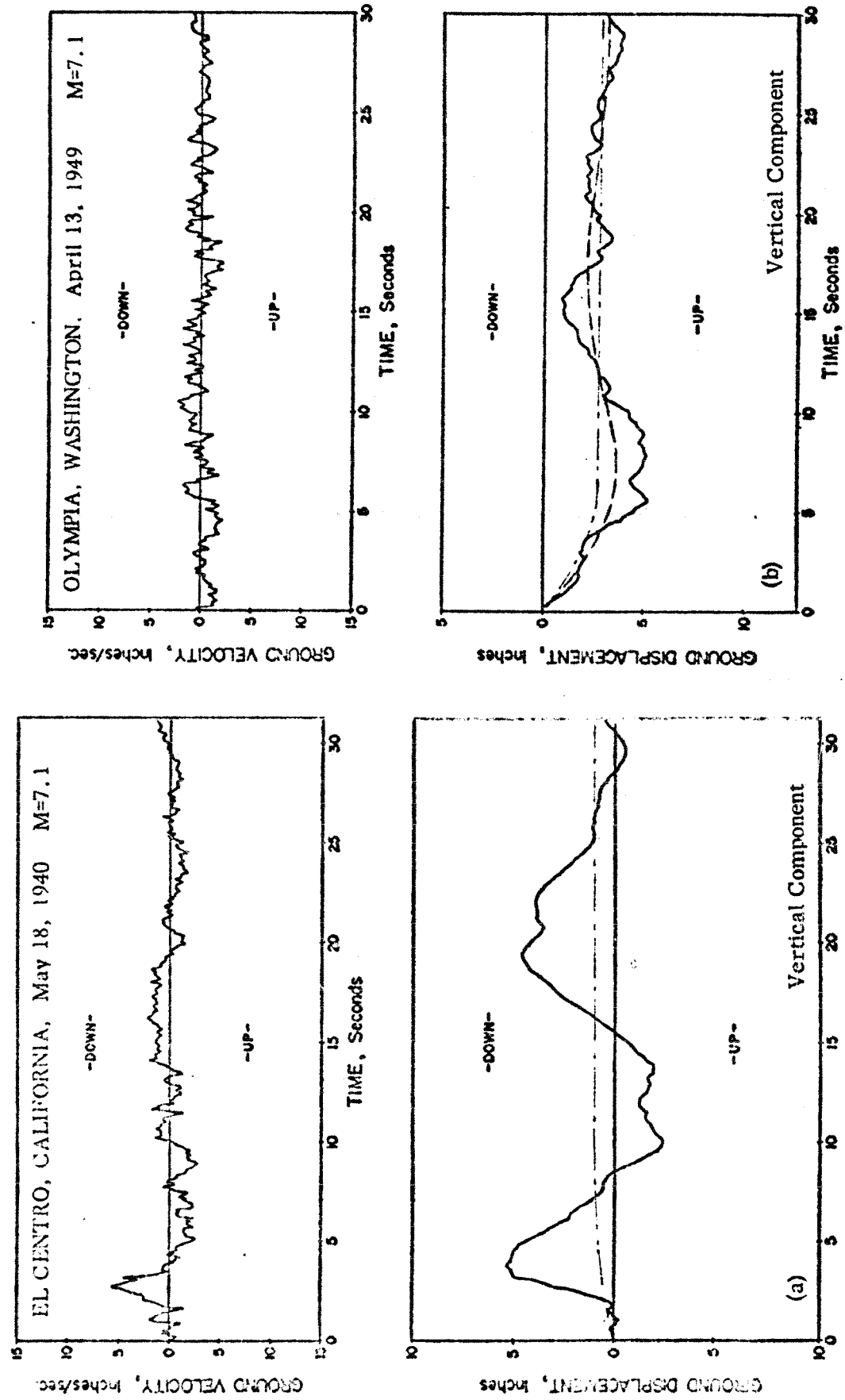


FIG. 9 - INTEGRATED VERTICAL COMPONENTS OF EARTHQUAKE GROUND VELOCITY AND DISPLACEMENT; (a) EL CENTRO, CALIFORNIA, EARTHQUAKE OF MAY 18, 1940; (b) OLYMPIA, WASHINGTON, EARTHQUAKE OF APRIL 13, 1949 (from Berg and Housner, 1961).

displacement of the form:

$$(2\xi/X) = (2\zeta/Z) = e^{-\beta y} \tanh(\alpha t) \quad (10)$$

Generalized, this expression is

$$(2\xi/X) = (2\zeta/Z) = f(y) \cdot f(t) \quad (11)$$

where f(y), a function of y only, has already been approximated through Eqs. (5) and (6), and f(t) is here taken of the form

$$f(t) \approx \tanh(\alpha t) \quad (12)$$

Table II gives values of f(t) as measured from the dash-dot curves of Figs 8 and 9 and corresponding values of $\tanh(\alpha t)$ for selected values of α, which show reasonable compliance with the identity expressed by Eq. (12).

TABLE II - TEST OF ADEQUACY OF $f(t) \approx \tanh(\alpha t)$

Time t (secs)	EL CENTRO, Ca., Earthquake, May 1940 (Ground Displacement Data from Fig. 8)				OLYMPIA, Wash., Earthq. April, 1949 (Data from Fig. 9)	
	E-W Component		N-S Component		S 80° W. Component	
	f(t)	$\tanh(\alpha t)$ (α=0.262)	f(t)	$\tanh(\alpha t)$ (α=0.314)	f(t)	$\tanh(\alpha t)$ (α=0.200)
0	0	0	0	0	0	0
1	0.236	0.256	0.310	0.304	0.154	0.197
2	0.425	0.481	0.543	0.557	0.309	0.380
3	0.590	0.656	0.724	0.736	0.471	0.537
4	0.736	0.781	0.845	0.850	0.625	0.664
5	0.835	0.864	0.931	0.917	0.765	0.761
6	0.915	0.917	0.983	0.955	0.860	0.834
7	0.962	0.950	0.991	0.976	0.941	0.885
8	0.991	1.000	1.000	0.987	0.985	0.922
9	1.000	1.000	1.000	0.993	0.997	0.947
10	1.000	1.000	1.000	0.996	1.000	0.964

In summary the values of α which satisfy Eq. (12) to good approximation are:

El Centro, California, Earthquake, May 1940

(i) E-W Component $\alpha = 0.262 \text{ (sec)}^{-1}$
(ii) N-S Component $\alpha = 0.314 \text{ (sec)}^{-1}$

(13)

Olympia, Washington, Earthquake, April 1949

S-80° W. Component $\alpha = 0.200 \text{ (sec)}^{-1}$

We shall adopt a mean value $\alpha = 0.29 \text{ (sec)}^{-1}$ as being appropriate to California.

It would appear then that basement rock ground displacement, at any point distant y from the line of strike-slip faulting near the epicenter of an earthquake, and at any time t from initiation of the earthquake, can be modelled reasonably well by a general empirical equation such as

$$(2\xi/X) = (2\zeta/Z) \approx e^{-0.20y} \tanh (0.29t) \qquad (14)$$

for y (>0) in miles and t (>0) in secs, and

$$\text{(i)} \quad (2\xi/X) \approx e^{0.20y} \tanh (0.29\,t)$$
$$\text{(ii)} \quad (2\zeta/Z) \approx e^{0.20y} \tanh (0.29\,t) \qquad \text{for } y<0;\, t>0 \qquad (15)$$

It should be noted that the function $(1 - e^{-\alpha t})$ which was initially proposed for use has been abandoned here in favor of $\tanh (\alpha t)$ because of the failure of the former to show reasonable agreement with f(t) as given in Table II.

5. Elastic Displacements

There remains to remark that actual surface ground movement will tend to include not only the permanent set of the basement rock but also the transient displacement from the elastic waves generated by the strain release. It would appear from Figs 6, 8 and 9 that the transient displacement, superimposed upon the permanent set displacement, can be a significant part of the strike slip or dip slip upheaval. It must also be supposed that the basement rock itself will vibrate similarly, though to a lesser extent than the over-riding sediments, and that its

extent of strike and dip motion there will tend to exceed the permanent set with a sort of whip-lash effect.

This question has been discussed extensively with Dr. Paul C. Jennings, a specialist in earthquake engineering, who cautions that while the writer's interpretation of Figs 6, 8 and 9 could be correct, it might also be inaccurate because of the uncertainty of accuracy in the digitization and double integration of low frequencies in the accelerograms which had been performed several years ago. He points out that the more recent trend in analysis of seismograms is to filter out both very low and very high frequencies. This, of course, makes it impossible to interpret any permanent type low frequency displacement in the calculated displacement, though it may indicate correctly the combined elastic displacement and initial (probably incomplete) permanent set at the first large wave of movement. Dr. Jennings conceded that the state of knowledge on earth movements was really insufficient to verify or disprove the writer's interpretations of permanent set and transient ground displacements, but that in the light of the associated deductions, the results seemed reasonable and could be a logical basis for proceeding.

Dr. Jennings indicated that fault displacement of the type hypothesized had been reported in the Gobi Altai earthquake of December, 1957, by Florensov and Solenko (1963). These authors state (p. 347):

> ".... the movements show that during the earthquake the active flanks of the faults were carried by the force of momentum up and beyond the new equilibrium point of the rock masses. At a later stage the masses moved back towards this point, but the movement was so vigorous that they again passed it now in the opposite direction. Subsequently they were again shifted eastward with a simultaneous vertical displacement and reached the equilibrium point."

Again (p. 348):

> "The dislocation of large masses (of sedimentary, metamorphic and igneous rocks) took place along complicated trajectories. In certain areas the amplitude of displacement was twice as large as that of irreversible

deformations. This indicates the important role played by elastic deformations."

The possibility of deformations occurring in a submarine earthquake in excess of the permanent displacements has not hitherto been considered in relation to the added momentum that the elastic deformations could impart to the water. The problem, however, seems to be of significant importance for tsunami generation.

Allowance for a whip-lash effect in the vertical motion (of dominant interest to us) would require modification of $(2\zeta/Z)$ in Eqs (14) and (15) to the form:

$$\begin{aligned} &\text{(i)} \quad (2\zeta/Z) = e^{-\beta y}\{\tanh \alpha t + \gamma e^{-\delta t} \cos (Ky) \sin (\omega t)\} \\ &\qquad\qquad \text{for } y>0;\ t>0 \\ &\text{(ii)} \quad (2\zeta/Z) = -e^{\beta y}\{\tanh \alpha t + \gamma e^{-\delta t} \cos (Ky) \sin (\omega t)\} \\ &\qquad\qquad \text{for } y<0;\ t>0 \end{aligned} \tag{16}$$

in which

$$\gamma = 2A/Z \tag{17}$$

expresses the ratio of the amplitude of the elastic wave displacement to that of the permanent offset Z at the fault, K is the surface wave number and ω the frequency of the standing wave oscillation, normal to the fault, whose decay with time is taken to be exponential at the logarithmic decrement $T\delta$, δ being the decay frequency and T the oscillation period. The assumption for this model of earth movement is that motions on opposite sides of the fault are equal and opposite and that the elastic standing wave is in the nature of a Rayleigh earthwave whose velocity C is of the order of 4.2 kms/hr. Thus

$$C = \omega/K \approx 4.2 \text{ km/hr.} \tag{18}$$

If the period T of the standing wave be taken as 15 secs, in conformity with Fig. 9, then plausible values of K and ω in Eq. (18) would be

$$\begin{aligned} &\text{(i)} \quad \omega = (2\pi/T) = 0.4189 \text{ (sec)}^{-1} \\ &\text{(ii)} \quad K = (\omega/C) = 0.0997 \text{ (kms)}^{-1} \end{aligned} \tag{19}$$

yielding a wavelength of the standing wave

$$L = (2\pi/K) \approx 63 \text{ kms} \tag{20}$$

This would mean that the distance from the fault to the first node would be approximately L/4 or 16 kms (10 miles) and that, accordingly, the 5-mile width of continental shelf from the fault to San Onofre would rise and fall almost in unison with a period of 15 secs.

For the exponential decay with time of the elastic deformation we adopt a value

$$\delta = 0.034\ (\text{sec})^{-1} \tag{21}$$

arrived at by adopting an amplitude ratio of decay of 0.6, suggested by Figs. 6, 8 and 9, yielding

$$e^{-\delta T} \approx 0.6$$

Finally, as a value for γ in Eq. (17), in the light of Fig. 9 and the comments of Florensov and Solenko (1963), we shall adopt

$$\gamma = 1, \tag{22}$$

which makes the amplitude of the elastic deformation A at the fault equal to the upward (downward) permanent set (Z/2) at the fault. This value is assumed applicable to basement rock because it is known that the continental shelf off Southern California contains no soft sedimentary cover, (Shepard, 1963).

6. Practical Evaluation of Vertical Earth Movement

Adopting the values of α, β, γ, δ, K and ω given in Sections 3-5, Eqs (16) become

$$\text{(i)} \quad (2\zeta/Z) = e^{-0.20y}\{\tanh(0.29t) + e^{-0.034t}\sin(0.42t)\cos(0.16y)\} \quad \text{for } y>0,\ t>0$$

$$\text{(ii)} \quad (2\zeta/Z) = -e^{0.20y}\{\tanh(0.29t) + e^{-0.034t}\sin(0.42t)\cos(0.16y)\} \quad \text{for } y<0,\ t>0 \tag{23}$$

for y in miles and t in secs.

Over the five miles of continental shelf from the fault to San Onofre, the value of cos(0.16y) varies from 1.0 at the fault to 0.70 at San Onofre. Eqs. (23) may therefore be shortened to:

$$\text{(i)} \quad (2\zeta/Z) \approx e^{-0.20y}\{\tanh(0.29t) + e^{-0.34t}\sin(0.42t)\} \quad \text{for } y>0,\ t>0$$

$$\text{(ii)} \quad (2\zeta/Z) \approx -e^{+0.20y}\{\tanh(0.29t) + e^{-0.034t}\sin(0.42t)\} \quad \text{for } y<0,\ t>0 \qquad (24)$$

Fig. 10 gives a plot of the function $(2\zeta/Z)$, at three distances between the fault and San Onofre site, as a function of time from the start of the design earthquake. The curves show the permanent deformation at each of the three locations and part of the first wave of the superimposed transient elastic deformation. Fig. 10 bears comparison with Fig. 9.

7. The Hydrodynamic Problem of Tsunami Wave Generation

In the first phase of an endeavor to determine the character of the sea disturbance arising over the strike-slip fault shown in Fig. 1, we shall neglect all effects of the horizontal strike-slip displacement and consider only the vertical dip-slip component, ζ, modeled by the empirical Eqs (24).

The problem is complicated by the fact that in the direction normal to the vertical fault, the sea-bed on the continental shelf slopes upward towards the coast on the east side and downward towards the continental shelf edge on the west side. The gradient of the shelf, however, is sufficiently slight (about 1%) to permit the approximation of a uniform depth condition, at least in the near field of the fault. The consequences of the shoaling depth can be dealt with later once the nature of the tsunami is established by the uniform depth approximation.

The problem will also be simplified by neglecting any variation of conditions in the x-direction along the fault, so that it becomes strictly one-dimensional in the vertical plane, normal to the fault.

Fig. 11 is a schematic representation of the earthquake fault as viewed from a direction parallel to the earthquake fault. The origin O of the reference plane ZOY is taken on the undisturbed sea-bed at the fault, with the axis of z vertical and positive upwards and the axis of y horizontal and positive in an easterly

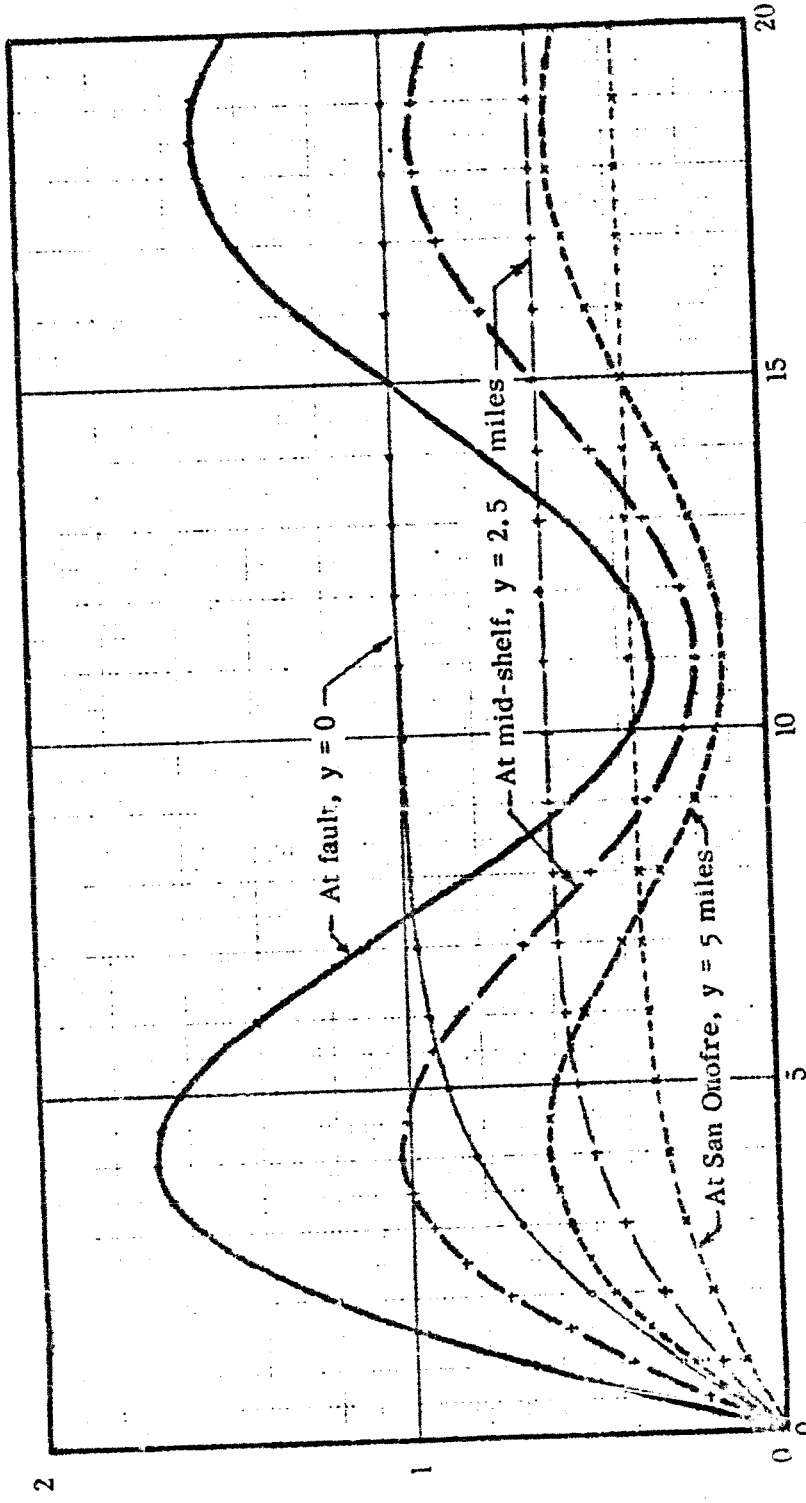


FIG. 10 - VERTICAL COMPONENT OF SEA-BED MOVEMENT (EMPIRICAL MODEL, EQ. 24 i) AT THREE LOCATIONS OFF SOUTHERN CALIFORNIA COAST

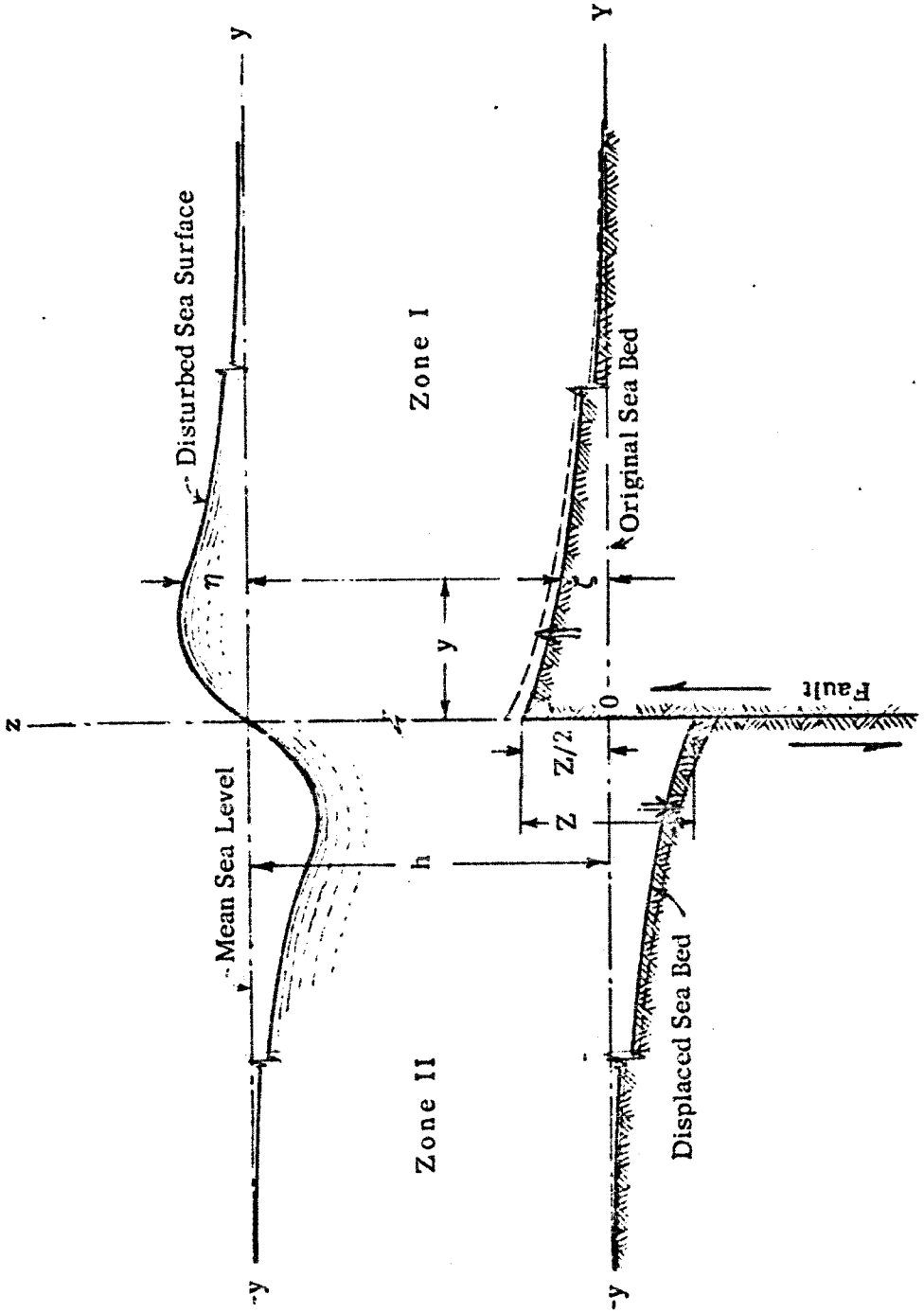


FIG. 11 - SCHEMATIC DIAGRAM OF VERTICAL (DIP-SLIP) MOVEMENT ON EARTHQUAKE FAULT AND ACCOMPANYING EFFECT ON SEA SURFACE.

direction towards San Onofre. The fluid regime is considered to be divided in two zones, I, east of the fault and II, west of the fault. Certain conditions govern the behavior of the water across the extension of the fault plane ZOY at all times:

(a) The water surface elevations η must match at all times; thus, if subscripts 1 and 2 identify the zones I and II respectively,

$$\eta_1 = \eta_2 \qquad \text{for } t \geq 0;\ \text{at } y = 0 \tag{25}$$

(b) The water surface gradient, $\frac{d\eta}{dy}$, must match at all times

$$\left(\frac{d\eta}{dy}\right)_1 = \left(\frac{d\eta}{dy}\right)_2 \qquad \text{for } t \geq 0;\ \text{at } y = 0 \tag{26}$$

(c) The horizontal velocity of water flow u across the depth, h, reduced by the uplift of the sea-bed ζ, must be common in value and direction

$$u_1 = u_2 \qquad \text{for } t \geq 0;\ y = 0 \tag{27}$$

It is apparent that over the small vertical distance $(\zeta_1 - \zeta_2)$, representing the offset of dip-slip, horizontal velocity would have to be zero against the scarp, but because $(\zeta_1 - \zeta_2)$ is, at maximum, very small compared with the water depth, h, its effect in blocking horizontal flow will be neglected.

We may proceed to examine the effects on the water of the earthquake disturbance in terms of a velocity potential ϕ and the governing Laplacian equation for potential flow, namely

$$\frac{\partial^2 \phi}{\partial y^2} + \frac{\partial^2 \phi}{\partial z^2} = 0 \qquad \left\{ \begin{array}{l} \text{for } t \geq 0 \\ -\infty < y < \infty \\ 0 < z < h \end{array} \right\} \tag{28}$$

At the free surface the generalized Bernoulli equation is

$$\frac{\partial^2 \phi}{\partial t^2} + g\frac{\partial \phi}{\partial z} = 0 \qquad \left\{ \begin{array}{l} \text{for } t \geq 0 \\ z = h \end{array} \right\} \tag{29}$$

where g is the acceleration due to gravity.

At the sea-bed the vertical velocity of the water must equal the vertical velocity of the earth in the two zones; thus

Zone I; [by use of Eq. (16 i), with cos (Ky) ≈ 1]

$$\frac{-\partial \emptyset}{\partial z} = \frac{\partial \zeta}{\partial t} = G_1(y).H(t) \qquad \left\{ \begin{array}{l} \text{for } t \geq 0 \\ z = 0 \\ y > 0 \end{array} \right\} \qquad (30)$$

Zone II; [by use of Eq. (16 ii), with cos (Ky) ≈ 1]

$$\frac{-\partial \emptyset}{\partial z} = \frac{\partial \zeta}{\partial t} = G_2(y).H(t) \qquad \left\{ \begin{array}{l} \text{for } t \geq 0 \\ z = 0 \\ y < 0 \end{array} \right\} \qquad (31)$$

in which

$$\text{(i)} \quad G_1(y) = (Z/2)e^{-\beta y}$$

$$\text{(ii)} \quad G_2(y) = -(Z/2)e^{\beta y} \qquad (32)$$

$$\text{(iii)} \quad H(t) = [\alpha \operatorname{sech}^2(\alpha t) + e^{-\delta t}(\omega \cos \omega t - \delta \sin \omega t)]$$

The further requirement of the problem is that there be no motion of the fluid at the instant t = 0, so that

$$\text{(i)} \quad \emptyset = 0$$

$$\text{(ii)} \quad \frac{\partial \emptyset}{\partial t} = 0 \qquad \left\{ \begin{array}{l} \text{at } t = 0 \\ -\infty < y < \infty \end{array} \right\} \qquad (33)$$

For a simple solution of Eq. (28), we shall seek a Fourier transform of $\emptyset(y, z, t,)$ in the form of $\varphi(k, z, \sigma)$, in which k and σ are in the nature of a wave number and frequency respectively. Such a transform, inserted in Eq. (28), yields

$$-k^2\varphi + \frac{\partial^2 \varphi}{\partial z^2} = 0 \qquad (34)$$

enabling Eq. (34) to be solved in the form:

$$\varphi(k, z, \sigma) = a(k, \sigma)e^{kz} + b(k, \sigma)e^{-kz} \qquad (35)$$

Here a and b are functions of k and σ and their values must be determined from other conditions.

Applying Eq. (35) to Eq. (29), we have

$$-\sigma^2\varphi + g\frac{\partial \varphi}{\partial z} = 0$$

which, for z = h, and by substitution from Eq. (35), yields

$$a(k,\sigma)\, e^{kh}(gk - \sigma^2) = b(k,\sigma)\, e^{-kh}(\sigma^2 + gk)$$

By making each side of this equation equal to

$$\{P(k,\sigma)/2\}[(gk)^2 - \sigma^4],$$

we can represent the unknowns a and b in terms of a single unknown P, thus reducing the solution for the Fourier transform to

$$\varphi(k,z,\sigma) = P(k,\sigma)\,[gk \cosh k(z-h) + \sigma^2 \sinh k(z-h)] \tag{36}$$

Application of the Fourier transform to Eqs (30) and (31) will result in

$$-\frac{\partial \varphi}{\partial z} = G(k).H(\sigma), \text{ for } z = 0 \tag{37}$$

provided G(k) is the transform of G(y), represented as an <u>odd function</u> for which

$$G_1(y) = -G_2(-y).$$

Then, use of Eq. (36) in (37) gives, for the condition z = 0,

$$P(k,\sigma) = H(\sigma)\{G(k)/k\}[gk \sinh kh - \sigma^2 \cosh kh]^{-1}$$

permitting elimination of $P(k,\sigma)$ in Eq. (36) and specification of the Fourier transform $\varphi(k,z,\sigma)$ as

$$\varphi(k,z,\sigma) = \frac{G(k)\,.\,H(\sigma)}{k} \cdot \frac{\{gk \cosh k(z-h) + \sigma^2 \sinh k(z-h)\}}{\{gk \sinh kh - \sigma^2 \cosh kh\}} \tag{38}$$

Finally the desired potential function $\Phi(x,z,t)$ is given in terms of its transform as

$$\Phi(y,z,t) = \frac{1}{\pi} \int_{-\infty}^{\infty} \int_{-\infty}^{\infty} \varphi(k,z,\sigma)\, e^{iky}\, e^{i\sigma t}\, dk\, d\sigma \tag{39}$$

and the transforms G(k) and H(σ) in terms of G(y) and H(t) as

$$G(k) = (2\pi)^{-\frac{1}{2}} \int_{-\infty}^{\infty} G(y)\, e^{-iky}\, dy \tag{40}$$

$$H(\sigma) = (2\pi)^{-\frac{1}{2}} \int_{-\infty}^{\infty} H(t)\, e^{-i\sigma t}\, dt \tag{41}$$

where $i = \sqrt{(-1)}$.

Because $\frac{\partial \eta}{\partial t} = \frac{-\partial \phi}{\partial z}$ for $z = h$, at the water surface, Eq. (29) can also be written as

$$\frac{\partial^2 \phi}{\partial t^2} - g\frac{\partial \eta}{\partial t} = 0 \qquad (42)$$

Upon integration with respect to t

$$\eta = (1/g)\left[\frac{\partial \phi}{\partial t}\right]_{z=h}^{t}_{0} \qquad (43)$$

If the value of $\varphi(k, z, \sigma)$ at z=h, given by Eq. (38), is substituted in Eq. (39) and the latter is differentiated with respect to time t between the limits t and 0, then Eq. (43) gives finally the elevation of the water surface resulting from the earthquake:

$$\eta = \frac{1}{2\pi}\int_{-\infty}^{\infty} G(k)\, e^{iky}\, dk \int_{-\infty}^{\infty} \frac{i\sigma H(\sigma)\,(e^{i\sigma t} - 1)\, d\sigma}{(gk \sinh kh - \sigma^2 \cosh kh)} \qquad (44)$$

Here it is understood that only the real part of Eq. (44) is to be retained in the final result.

To evaluate Eq. (44) we proceed first with development of Eqs (40) and (41). Substitution of Eqs. (32 i) and (32 ii) in Eq. (40) yields on integration,

$$G(k) = -Z(2\pi)^{-\frac{1}{2}}[ik/(\beta^2 + k^2)] \qquad (45)$$

Evaluation of the function $H(\sigma)$ by substitution of Eq. (32 iii) in Eq. (41) proves to be more difficult. The substitution, when H(t) is taken as an even function, yields

$$H(\sigma) = (2\pi)^{-\frac{1}{2}}\left[\int_0^{\infty} \alpha \operatorname{sech}^2(\alpha t).\, e^{-i\sigma t}\, dt + \int_0^{\infty} e^{-(\delta + i\sigma)t}(\omega \cos \omega t - \delta \sin \omega t)dt\right. \qquad (46)$$

where it is to be noted that the lower limit of integration has been taken as 0 because the function has to be non-existent for negative time ($t < 0$). Considering initially just the first of the two integrals in Eq. (46), this can be developed to the form:

$$\int_0^\infty = \left[e^{-i\sigma t}\tanh(\alpha t)\right]_0^\infty + i\sigma \int_0^\infty e^{-i\sigma t}\tanh \alpha t.\, dt.$$

$$= i\sigma \int_0^\infty e^{-i\sigma t}\tanh \alpha t\, dt.$$

The difficulty arises in determining this integral in closed form. It is evaded only by making an approximation. Thus, as has been shown in the early part of this work, tanh αt attains a value of ($\approx$ 1) in about 8 secs. It is to be expected on the other hand that σ is a relatively small quantity, so that in integration between limits $e^{i\sigma t}$ will be a relatively long period cyclic function. Consequently for purposes of approximating the integral in closed form we should not be too far wrong in writing it

$$\int_0^\infty \approx i\sigma \int_0^\infty e^{-i\sigma t}\, dt. \approx -e^{-i\sigma t}\Big|_0^\infty \approx -1 \qquad (47)$$

The second intergral of Eq. (46) presents no problem, so that Eq. (46) is then determined as

$$H(\sigma) \approx (2\pi)^{-\frac{1}{2}}\left[\frac{i\sigma\omega\cos\omega t - \{\omega^2 + \delta(\delta + i\sigma)\}\omega t}{\omega^2 + (\delta + i\sigma)^2} - 1\right] \qquad (48)$$

In the further development of Eq. (44) we may note two things. First is that we can replace σ^2 in the denominator of the second integral (enclosed) by the approximation

$$\sigma^2 \approx k^2 . gh \qquad (49)$$

on the basis that the evolving waves will be long waves in shallow water. Secondly, because the integrand is a statement related to frequency, it cannot exist in the negative domain, so that the function is zero between the integration limits $-\infty < \sigma < 0$. This enables Eq. (44) to be rewritten, on incorporating results from Eqs (45) and (48), as

$$\eta = \frac{Z}{g(2\pi)^2}\int_{-\infty}^{\infty}\frac{e^{iky}\, dk}{(\beta^2 + k^2)(\sinh kh - kh\cosh kh)}\int_0^\infty \sigma\,(e^{i\sigma t} - 1)\{f(\sigma) - 1\}d\sigma \qquad (50)$$

in which $f(\sigma)$ is

$$f(\sigma) = \frac{i\sigma\omega\cos\omega t - \{\omega^2 + \delta(\delta + i\sigma)\}\sin\omega t}{\omega^2 + (\delta + i\sigma)^2} \qquad (51)$$

[Because evaluation of this double integral will necessarily have to be performed (in part) by numerical integration and cannot be accomplished within available time, it becomes necessary to discontinue the hydrodynamic evaluation of the water surface elevation via Eq. (50) and proceed by assuming a wave form for η. This is done in the next section].

8. Assumed Initial Form of Water Surface Elevation

To simulate the effect of the generated wave we shall consider the Fourier series representation of a saw-tooth wave form of maximum height H, (Fig. 12), which is assumed to prevail from west to east over a continental shelf of uniform depth h and width $(L + \ell)$, of which L represents the distance from the fault to the coast at San Onofre and ℓ the distance of the fault from the nominal edge of the shelf. Fig. 12 may be recognized as a crude version of Fig. 11.

The fact that the wave form at the instant of maximum generation is taken angular is not a serious limitation because its representation as a Fourier series of sine and/or cosine terms will to a large extent eliminate the angularity by the mere fact of retaining only the first few terms of the series. The main object of this exercise is to identify the principal wave components that can be considered to be present and to be representative of the approximate shape of the sea disturbance set up by the earthquake.

If the maximum wave form is defined as $\eta(y)$, then its representation as a Fourier series of sine terms (for an odd function), in relation to an origin in the water surface in the plane of the fault, (cf. Eagle, 1925) is

$$\eta(y) = [H/\{(k\ell)^2(L/\ell - 1)\}] [\sin k\ell \sin ky + \tfrac{1}{9} \sin 2k\ell \sin 2ky + 1/9 \sin 3k\ell \sin 3ky + \ldots\ldots] \quad (52)$$

It is considered sufficient to retain just three terms of this series since it converges rapidly. The height of any n-th wave component may be generalized as

$$H_n = 2 [H/\{(nk\ell)^2(L/\ell - 1)\}] \sin nk\ell \quad (53)$$

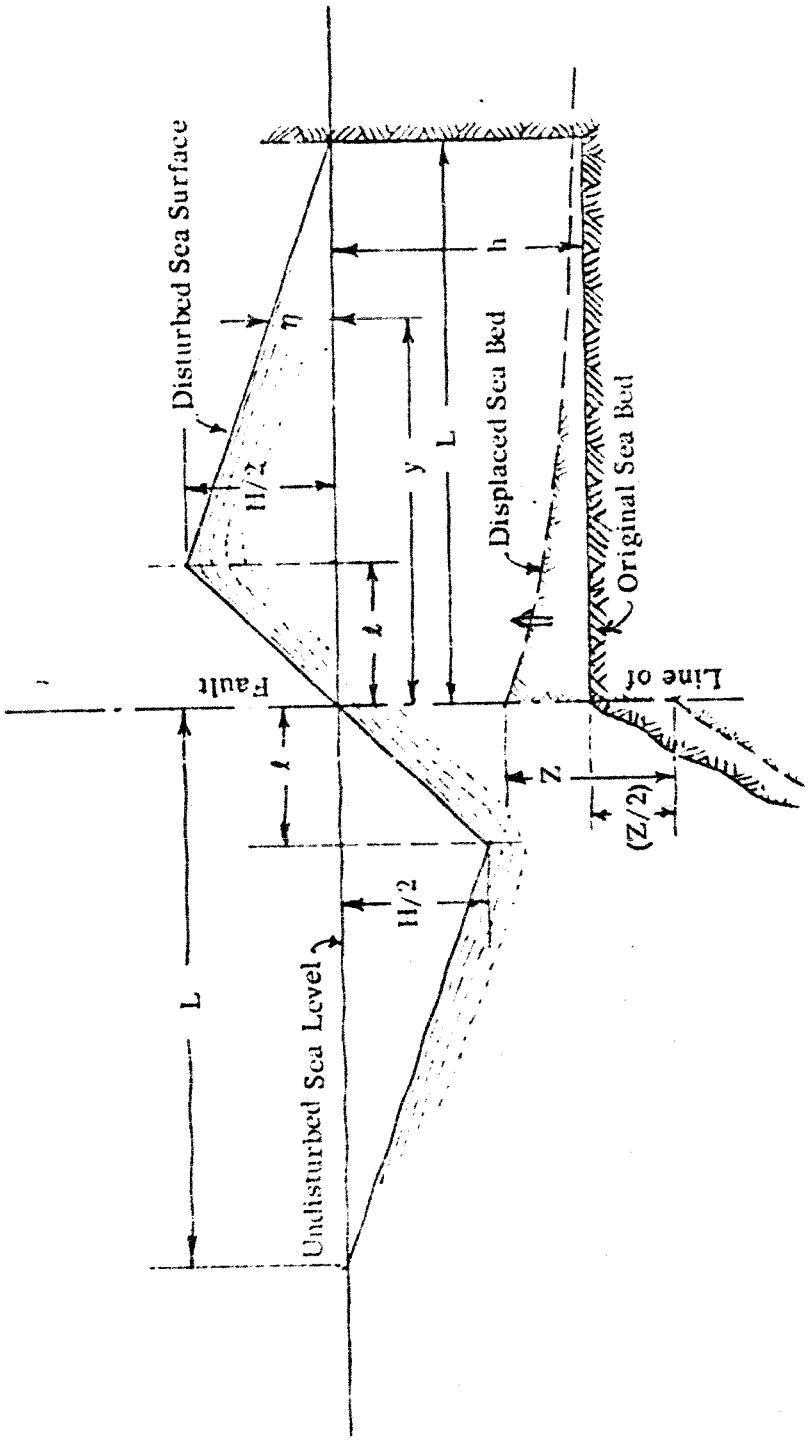


FIG. 12 - SCHEMATIC DIAGRAM OF SEA DISTURBANCE (EXAGGERATED SAW TOOTH MODEL) RESULTING FROM VERTICAL DIP-SLIP FAULTING OF SEA BED

in which n, an integer, has the values 1, 2, 3, ...

The fundamental wave of greatest height has a wave length λ (= $2\pi/k$) given by

$$\lambda = 2L \tag{54}$$

As a long wave in shallow water, its velocity c will be

$$c = (gh)^{\frac{1}{2}}$$

and its period T,

$$T = \lambda/c = 2L(gh)^{-\frac{1}{2}} \tag{55}$$

Generalizing, the period T_n of any n-th component in the wave system, (n = 1, 2, 3, ...) is

$$T_n = 2L/n(gh)^{\frac{1}{2}} \tag{56}$$

Now it is clear that the saw-tooth wave system comprising predominantly three systems of sinusoidal waves will collapse and propagate both shoreward and seaward. This means that the initial clapoti effect for each of the three wave systems will subside through the separation of each wave system into independent standing waves or, what is equivalent, into progressive waves passing through each other in opposite directions, both seaward and shoreward.

At this point it is desirable to evaluate the heights and periods of the three principal standing wave systems. These are tabulated in Table III for the following values of H, L, ℓ, and h and by use of Eqs (53) and (56)

(i) H = 1.2Z (assumed)

(ii) L = 5 miles ≈ 26,400 ft (distance fault to San Onofre)

(iii) ℓ = 1 mile ≈ 5,280 ft (assumed by judgement)

(iv) h = 40 m ≈ 150 ft (assumed average depth)

TABLE III - HEIGHTS AND PERIODS OF COMPONENT STANDING WAVES CAUSED BY THE HYPOTHETICAL EARTHQUAKE

Dip Slip Offset Z (see Tables I and IA)	Harmonic Sequence (n) of Standing Wave					
	1		2		3	
	Wave Period T_1 (mins)	Wave Height H_1 (ft)	Wave Period T_2 (mins)	Wave Height H_2 (ft)	Wave Period T_3 (mins)	Wave Height H_3 (ft)
1.31	12.7	1.17	6.3	0.47	4.2	0.21
2.58	12.7	2.30	6.3	0.93	4.2	0.41
3.77	12.7	3.36	6.3	1.36	4.2	0.60
2.45	12.7	2.19	6.3	0.88	4.2	0.39
4.82	12.7	4.30	6.3	1.74	4.2	0.77
7.07	12.7	6.32	6.3	2.56	4.2	1.14

As a check upon the results of Table III, we use the heights H_n to calculate the initial maximum water surface profile created by the assumed earthquake in accordance with Eq. (52) or what is equivalent:

$$\eta(y) = \sum_{1}^{n=3} (H_n/2) \sin nky \qquad (57)$$

Results are plotted in Fig. 13 for the first three cases of Table III. The initial uplift of water surface is greater than the assumed uplift of sea bed in each case because of the assumption made that H (in Eq. 52) is 1.2 Z. The factor 1.2 has been included to allow for the dynamic effect suggested by Fig. 10 and discussed in Sections 5 and 6.

It should be pointed out that Fig. 13 implies that the standing wave system represented by the uplift of the sea surface for any particular value of dip-slip Z,

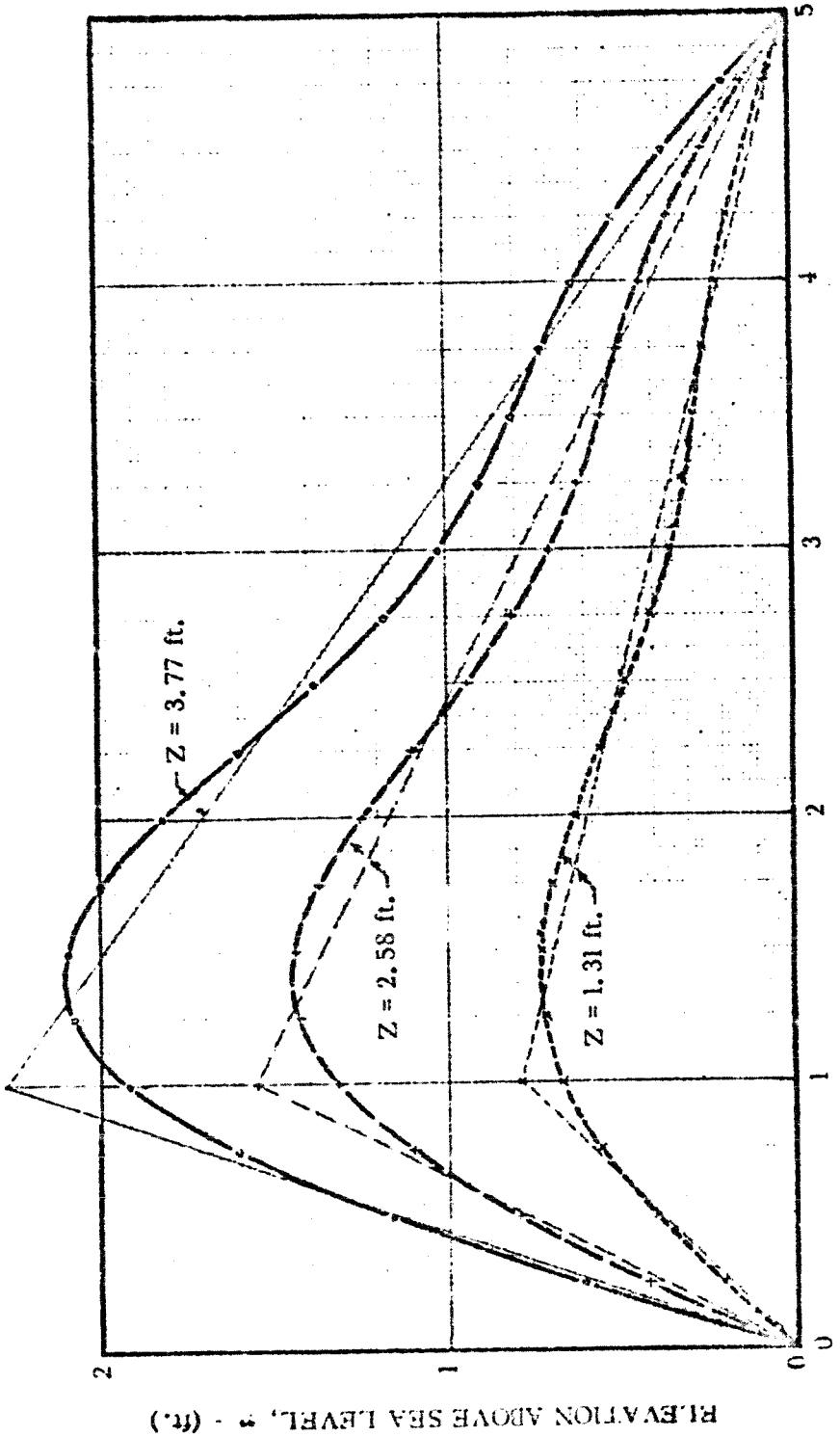


FIG. 13 - MAXIMUM PROFILE OF SEA SURFACE AT INSTANT OF TSUNAMI GENERATION FOR THREE ASSUMED DIP-SLIP DISPLACEMENTS OF THE SEA BED OF THE TYPE SHOWN IN FIG. 11

would have zero height at its eastern extremity (the coast), whereas Fig. 10 had indicated that at San Onofre the permanent uplift of the sea bed would be as much as $0.37(Z/2)$ and would thus momentarily give rise to a water surface elevation above mean sea level of a similar amount. Actually it would be less than $0.37(Z/2)$ because of the factor $\sin ky$, assumed as unity in Equation (24), but having an actual value at the coast of ≈ 0.7. This slight disparity does not over-rule the usefulness of the model of Fig. 12 in reaching for the essential make-up of the surface wave disturbance.

It is necessary also to emphasize that the model of Fig. 12 suggests a nodal condition for the standing wave at the coastal boundary (San Onofre), which is unrealistic. Standing waves are necessarily anti-nodal at a boundary. Again, this non-compliance with physical requirement need not invalidate the result that at the moment of generation of the sea disturbance, the system of waves formed was essentially composite of three harmonic components in accord with Table III. What becomes necessary now is to determine what three such oscillations, operating on the shelf edge, realistically could do to the water surface at the coast, allowing for the slope of the continental shelf.

9. Amplification of Wave Effects at the San Onofre Coastline

Each of the three harmonic components of the initial disturbance can be considered to be an oscillation on the edge of the shelf of the form, $\eta_i = A \cos \sigma t$, where A is the amplitude of the oscillation and σ its angular frequency. The problem now posed is that of determining the response at the coast, at the zero-depth boundary for a sloping sea bed of length L and irregular slope (h_c/L), to such a sinusoidal oscillation.

This problem has been treated by Lamb (1932, § 186) for the special case of a uniform slope, in the absence of friction. He shows that the water surface elevation $\eta(x)$ at any distance x from an origin in the water surface taken at the coast $[h(x) = 0]$, and normal to the coast, is

$$\eta(x) = A\left[J_0\left\{2(\tfrac{\sigma}{g}x)^{\frac{1}{2}}\right\}/J_0\left\{2(\tfrac{\sigma}{g}L)^{\frac{1}{2}}\right\}\right] \cos(\sigma t + \epsilon) \qquad (58)$$

where L is the length of the shelf slope, and ϵ a phase angle, k is a wave number defined by

$$k = \sigma^2 L/gh_0 , \tag{59}$$

h_0 is the water depth at the shelf edge (x = L), and J_0 is a Bessel function of zero order, of the first kind.

The free modes of oscillation of such a uniformly sloping shelf are given by the values of (kx) which yield

$$J_0\{2(kx)^{\frac{1}{2}}\} = 0 \tag{60}$$

that is, the zero-crossing values of $2(kx)^{\frac{1}{2}}$ which cause the Bessel function J_0 to be zero. From Eqs (59) and (60) it may be shown that the periods of free oscillation are (cf. Wilson, 1972):

$$\frac{T_m (gh_0)^{\frac{1}{2}}}{2L} = 2.618;\ 1.139;\ 0.728;\ 0.531;\ \ldots\ldots \tag{61}$$

where the subscript m refers to the mode number (m = 1, 2, 3, ...) corresponding to the numbers in sequence on the right hand side of Eq. (61).

So long as the forcing frequency σ is not too close in value to ω_m (= $2\pi/T_m$), a natural frequency of the shelf, the value of $\eta(x)$ at any point can be calculated from Eq. (58). However, when σ approaches ω_m in value the result from Eq. (58) becomes unreliable and is in fact indeterminate for $\sigma = \omega_m$.

Fig. 14 shows that the continental shelf off San Onofre cannot very satisfactorily be approximated by a single uniform slope so that the true values of the natural frequencies ω_m need to be computed by other means. We shall approach our problem therefore in a different way.

Considering any one of the three component waves given by Eq. (57), it is clear that for y = 0, at the shelf edge Eq. (57) yields $\eta(0) = 0$, and the seeming anomaly exists that no oscillation arises there. The water disturbance,

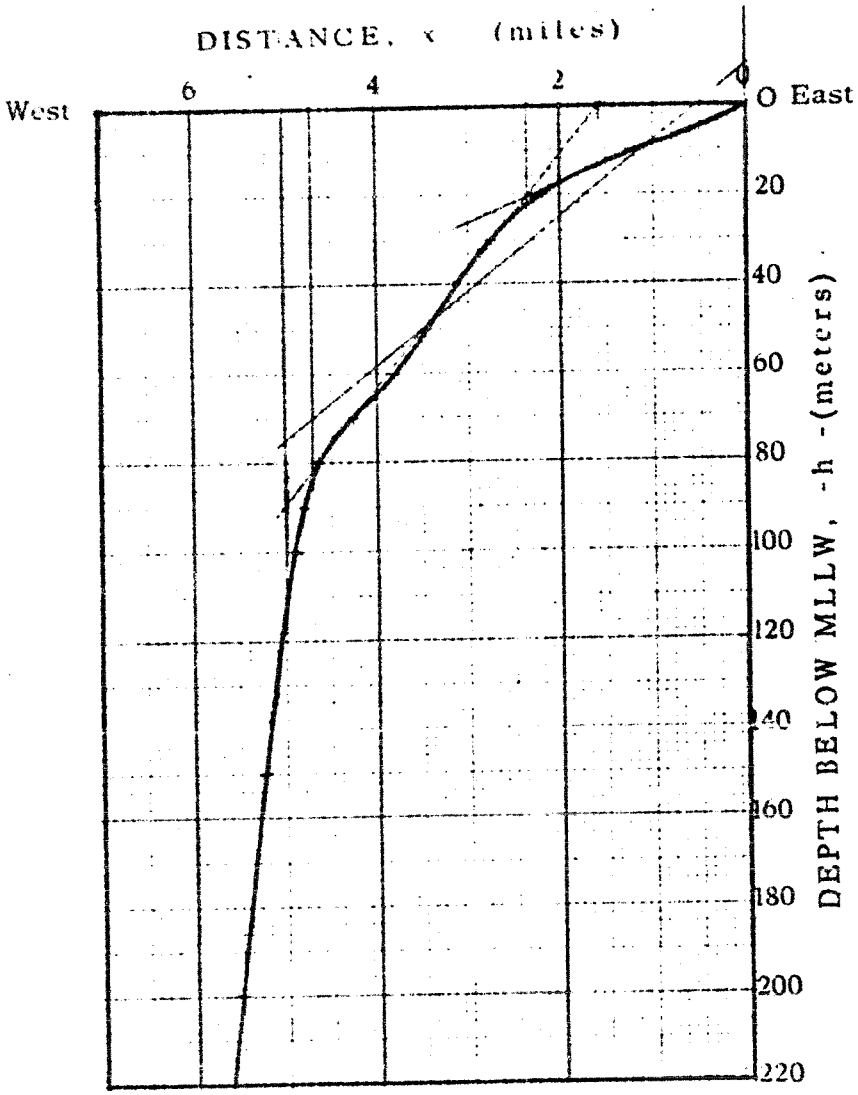


FIG. 14 - PROFILE OF CONTINENTAL SHELF OFF SAN ONOFRE, CALIFORNIA

initially, over the fault at the shelf edge, is nodal $[\eta(0) = 0]$ because of the assumed nature of the vertical displacements of the sea bed. In reality the sea condition at initiation of the tsunami can be considered to be the resultant of two *progressive* wave systems; one incident and one reflected, with initial elevations at the shelf edge of η_i and η_r respectively. These systems would be defined as

$$\text{(i)} \qquad \eta_i = (H/4) \sin (ky - \omega t) \tag{62}$$

$$\text{(ii)} \qquad \eta_r = (H/4) \sin (ky + \omega t)$$

where $\omega (= 2\pi/T)$ is the angular frequency of a component in the initial disturbance. It is readily shown that the superposition of these *progressive* incident and reflected wave systems gives

$$\eta = \eta_i + \eta_r = (H/2) \sin ky \cos \omega t \tag{63}$$

and if t is very small, as would be the case just after the earthquake, Eq. (63) would reduce to Eq. (57) for the sum of the three components.

We shall make use of Eq. (63) in due course as a means of providing the necessary boundary condition for solving the problem of the dynamic oscillation of the shelf waters.

In a general sort of way the problem is the parallel of a mechanical damped spring system as has been shown by Wilson (1972). The governing hydrodynamic equations can be written as

$$\text{(i)} \qquad \frac{\partial q}{\partial t} + Kq + gb(h + \eta) \frac{\partial \eta}{\partial y} = F(y,t) = -\left(\frac{h + \eta}{\rho}\right) \frac{\partial p_a}{\partial x} \tag{64}$$

$$\text{(ii)} \qquad \frac{\partial q}{\partial y} + b \frac{\partial \eta}{\partial t} = 0$$

where $\eta(y,t)$ and $q(y,t)$ are respectively the water surface elevation and horizontal volume flow over a variable width $b(y)$ (the volume being taken uniform with depth for long waves), $h(y)$ is variable water depth, K is a damping coefficient for linear damping and $F(y,t)$ a surface excitation, normally related to surface shear stress and pressure (cf. Wilson, 1972, p. 16) but here shown to comprise just a pressure term.

In Eq. (64 i), the disturbance F can be considered to be an atmospheric pressure variation equivalent to the sea bed disturbance given by Eqs (23) or (24). The main feature of the excitation, as discussed in Sections 5 and 6, is that it is of short period, about 15 secs (see Fig. 10). On the other hand, the expected period of free oscillation of the shelf waters is long (several minutes). Because of this the ratio of the forcing and natural frequencies, (σ/ω), is likely to be large and resonance will not be a problem. At the same time, the mechanical spring analogy tells us that the magnitude of the free oscillation will exceed the forced oscillation by the ratio (σ/ω). This fact enables us to discard consideration of the forced oscillation term, F, in Eq. (64 i) and solve Eqs (64) for the free oscillation, relying for the determination of magnitude upon the assumed initial (maximum) disturbance of the water surface [Eq. (52) and Fig. 13].

As the effect of damping, via the second term of Eq. (64 i), may also be expected to be quite small, we shall discard this also and consider the remaining terms of Eqs (64) in the following approximate forms:

$$\text{(i)} \qquad \frac{\partial^2 \xi}{\partial t^2} + g \frac{\partial \eta}{\partial y} = 0$$

$$\text{(ii)} \qquad \frac{1}{b} \frac{\partial}{\partial y} [bh\xi] + \eta = 0 \qquad (65)$$

Eqs (65) derive from (64) by writing $q = b(y)h(y) \frac{\partial \xi(y,t)}{\partial t}$ and by discarding η in comparison with h. The quantity $\xi(y,t)$ now represents the horizontal displacement of the water particles at any point y and time t in the free oscillation.

The solutions of Eqs (65) may be taken in the form:

$$\text{(i)} \qquad \eta = \zeta(y) \cos \omega t$$

$$\text{(ii)} \qquad \xi = \nu(y) \cos \omega t \qquad (66)$$

where ω is the angular frequency of the free oscillation and ζ and ν are amplitude functions (of y only) of the vertical and horizontal displacements η and ξ respectively. Inserting Eqs (66) into (65) and writing

$$S(y) = b(y)h(y) \tag{67}$$

where S(y) is the vertical cross-sectional area normal to the direction of oscillation, (that is, approximately parallel with the coast or the shelf-edge), Eqs (65) reduce to

$$\text{(i)} \quad \frac{\partial \zeta}{\partial y} = (\omega^2/g)\nu$$

$$\text{(ii)} \quad \zeta = -\frac{1}{b}\frac{\partial}{\partial y}(S\nu) \tag{68}$$

These equations are now written in finite difference form by adopting a suitably small increment of distance δ:

$$\text{(i)} \quad \zeta_{i+1} = \zeta_i + (\delta\omega^2/2g)(\nu_{i+1} + \nu_i)$$

$$\text{(ii)} \quad \zeta_{i+1} = -\zeta_i - \{4/(b_{i+1} + b_i)\delta\}(S_{i+1}\nu_{i+1} - S_i\nu_i) \tag{69}$$

Further by subtracting these equations and writing

$$\text{(i)} \quad B_i = 2/\delta(b_{i+1} + b_i)$$

$$\text{(ii)} \quad C = \delta\omega^2/4g \tag{70}$$

They are rendered as:

$$\text{(i)} \quad \nu_{i+1} = \{(B_iS_i - C)\nu_i - \zeta_i\}/(C + B_iS_{i+1})$$

$$\text{(ii)} \quad \zeta_{i+1} = \zeta_i + 2C(\nu_{i+1} + \nu_i) \tag{71}$$

From Eq. (71i) the value of ν_{i+1} can be calculated from values of ν_i and ζ_i for a preceding distance step. To pursue the numerical calculation it is necessary to have starting values of ν_i and ζ_i at an end boundary and to have values of C, B_i, S_i at increments of distance δ between the edge of the continental shelf and the coast. Once ν_{i+1} is known from Eq. (71i), ζ_{i+1} can be calculated from Eq. (71ii) and the iteration continued.

The recursive calculation can be started at the coast where the vertical amplitude ζ_o at i = 0 can be normalized to unit value. The horizontal amplitude there will be zero, $\nu_o = 0$ at i = 0, on the basis that the tsunami oscillation will flood against the vertical sea-wall. The value of ω in

Eq. (70 ii), of course, is unknown, but may be approximated by recourse to Eqs (61) and the adoption of a suitable value of h_o for a uniform shelf slope best approximating the irregular profile of the continental shelf off San Onofre. From Fig. 14, a value for h_o of 85 meters seems reasonable and approximate values of ω_m (m = 1, 2, 3, ..., the mode number) from Eqs (61) are, therefore:

$$\omega_m \approx 4.31;\ 9.91;\ 15.50;\ 21.23;\ \ldots (\times 10^{-3}) \text{ radians/sec.} \qquad (72)$$

The condition binding on successful solution of Eqs (71) is that ζ must be zero at the edge of the shelf (over the fault), that is

$$\zeta_{15} = 0 \quad (\text{at } i = 15 \text{ for } \delta = 1794 \text{ ft.}) \qquad (73)$$

If Eq. (73) is not satisfied by the adoption of any one of the values of ω_m in Eq. (72) then such value of ω_m must be altered incrementally up or down and the recursive process repeated until Eq. (73) shows that a solution has been reached.

10. Tsunami Wave Refraction over the Continental Shelf

To provide values of h_i, b_i and S_i for the numerical calculation in solution of the tsunami oscillation a wave refraction diagram has been developed for part of the shelf off San Onofre on the assumption that the oscillation will largely be dictated by the nature of wave transmission between the fault and the coastline. The refraction diagram has been calculated numerically and computer-plotted from a program adapted from one given by Orr and Herbich (1969).

Fig. 15 gives part of the grid pattern of depths h(x,y), in meters, used to define the topography of the area and Fig. 16 shows the wave fronts and rays as computer plotted from calculations which determine the refraction of the waves. The depth reticulation (Fig. 15) uses grid spacings of 1794 ft. which will be used also as the interval δ in the solution of Eqs (71).

The wave ray that bears directly on the site at San Onofre is shown in Figs 15 and 16 by a chain-line marked by station numbers 15 to 0 at intervals of δ = 1794 ft. The adjacent wave rays on either side of this chain-line are

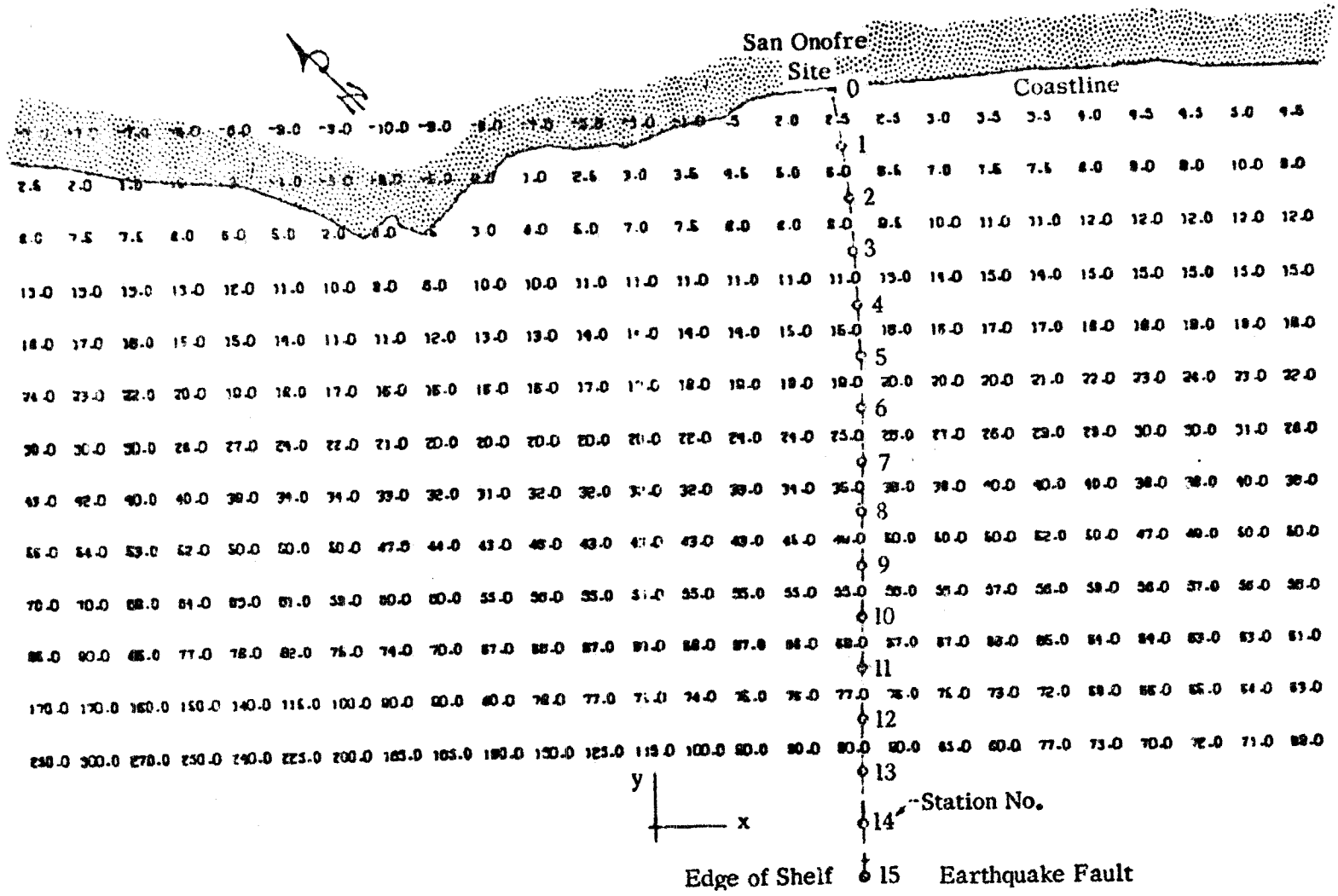


FIG. 15 - NETWORK USED FOR NUMERICAL COMPUTATION OF TSUNAMI WAVE REFRACTION OVER CONTINENTAL SHELF OFF SAN ONOFRE, CALIFORNIA. (Numbers indicate depths in meters at grid points; spacings of gridpoints are 1794 ft. in both x and y directions).

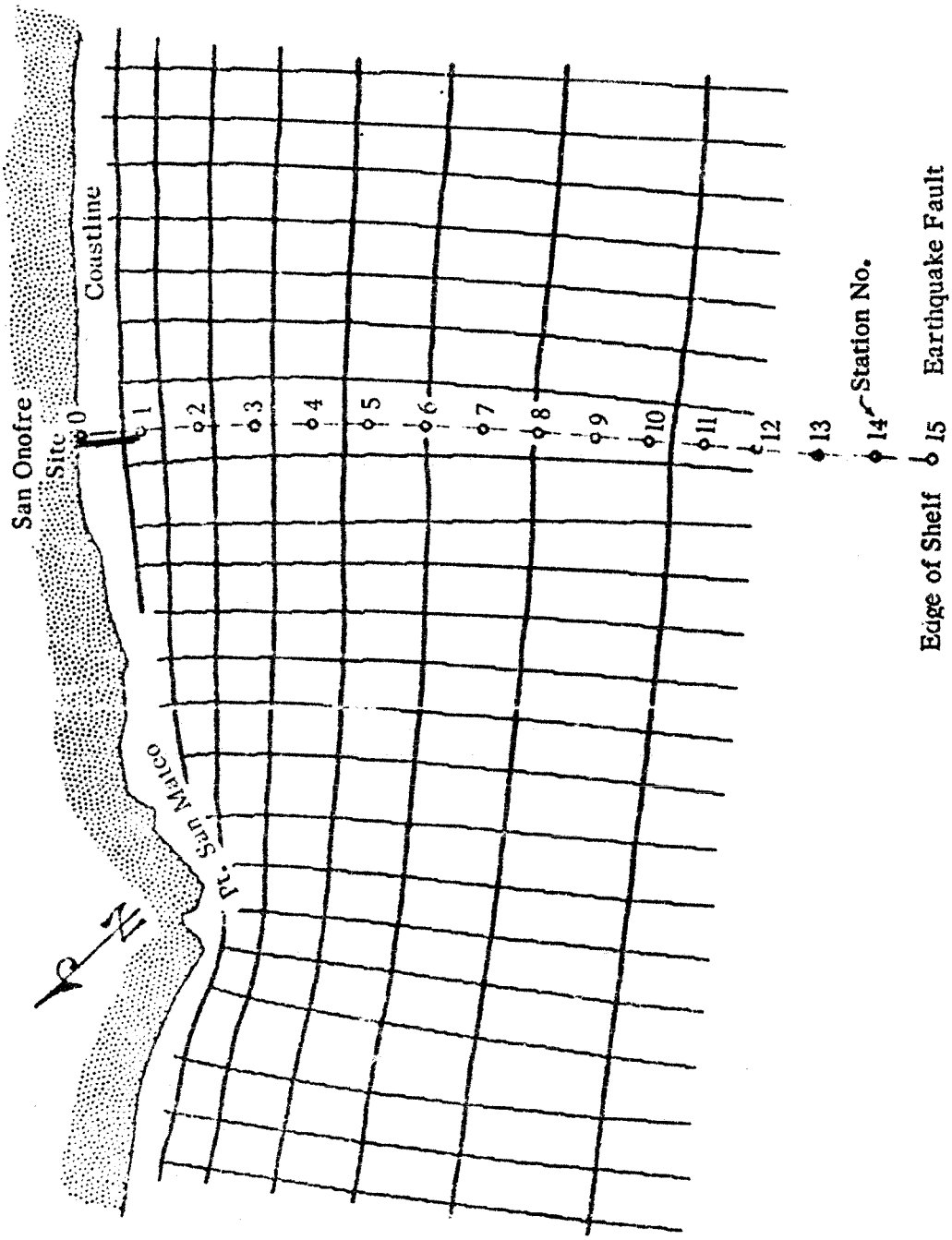


FIG. 16 - WAVE REFRACTION DIAGRAM SHOWING APPROACH OF TSUNAMI WAVES TO SAN ONOFRE, CALIFORNIA FROM ASSUMED EARTHQUAKE FAULT AT EDGE OF CONTINENTAL SHELF. [Wave fronts are given at time intervals of 1 min.; wave rays are spaced at 1 grid spacing (1794 ft.) at shelf edge.]

used for estimating the widths b_i in Eqs (70). The free oscillation of the shelf to be calculated is assumed to function (in effect) within this ray channel.

11. Modes of Free Oscillation of the Shelf off San Onofre

With everything now specified as required input to the numerical calculation using Eqs (71), the modes of free oscillation of the shelf are determined by the recursive process which homes in on the correct values of ω_n. Computations have been made for two water depths

(a) depth to MLLW

(b) depth to (MLLW + 8 ft.)

of which (b) represents a condition of extreme high tide (7 ft.) and allows for 1 ft. additional of storm tide elevation.

Results of these calculations are recorded in Tables IV and V in the form of values of ζ and ν, normalized to unit value of ζ at station 0, the coast. To obtain actual values, we refer back to Eqs (62) and (63) and the fact that at the shelf edge ($i = 15$, $y = 0$), the oscillation is nodal ($\eta = 0$) for the standing wave system expressed by Eq. (63). For such a system the horizontal particle displacement is given from linear long wave theory as:

$$\xi_n = -(H_n/2)(1/k_n h) \cos k_n y \cos \omega_n t \tag{74}$$

Consequently, the amplitude value of ξ_n is

$$\nu_n = -(H_n/2)(1/k_n h) \cos k_n y \tag{75}$$

Further, because by definition

$$\omega_n = k_n \sqrt{(gh)} \tag{76}$$

Eq. (75) becomes

$$\nu_n = -(H_n/2)\{(g/h)^{\frac{1}{2}}/\omega_n\} \cos k_n y \tag{77}$$

Accordingly, when $y = 0$ at the shelf edge (station 15), we obtain

$$\nu_n = -(H_n/2)\{(g/h)^{\frac{1}{2}}/\omega_n\} \tag{78}$$

TABLE IV: NORMALIZED PARAMETERS OF TSUNAMI OSCILLATION ON CONTINENTAL SHELF OFF SAN ONOFRE: WATER DEPTHS AT MEAN LOW LOW WATER (MLLW)

Station No. i	Water Depth h_i (m)	Width of Ray Channel l_i (ft)	Cross Sectnl Area S_i (sq. ft.)	Parameters of Tsunami Oscillation (normalized to unit value of ζ at i = 0 Computed Mode Frequencies and Periods: ω_n (rad./sec.); T_n (mins)							
				$\omega_1 = 3.7\times10^{-3}$	$T_1 = 28.28$	$\omega_2 = 8.71\times10^{-3}$	$T_2 = 12.02$	$\omega_3 = 1.43\times10^{-2}$	$T_3 = 7.32$	$\omega_4 = 2.10\times10^{-2}$	$T_4 = 4.99$
				$(\zeta_1)_i$ (ft)	$(\nu_1)_i$ (ft)	$(\zeta_2)_i$ (ft)	$(\nu_2)_i$ (ft)	$(\zeta_3)_i$ (ft)	$(\nu_3)_i$ (ft)	$(\zeta_4)_i$ (ft)	$(\nu_4)_i$ (ft)
			(x 10^6)								
0	0	---	0	1.000	0	1.000	0	1.000	0	1.000	0
1	4.3	2552	0.36	0.947	-135.9	0.743	-121.6	0.431	-99.9	0.077	-75.1
2	7.5	2683	0.66	0.842	-139.2	0.268	-103.1	-0.445	-54.0	-0.957	- 9.0
3	10.3	2575	0.87	0.732	-148.3	-0.123	- 82.1	-0.794	- 7.3	-0.624	36.1
4	13.0	2861	1.22	0.625	-132.0	-0.399	- 48.5	-0.701	23.7	0.229	33.4
5	17.1	2496	1.40	0.523	-133.8	-0.558	- 26.6	-0.350	37.8	0.792	12.4
6	22.0	2439	1.76	0.426	- 118.5	-0.627	- 6.0	0.057	33.8	0.814	-10.6
7	29.0	2355	2.24	0.342	-100.5	-0.624	7.2	0.378	22.4	0.434	-20.3
8	44.0	2231	3.22	0.275	- 73.8	-0.582	12.7	0.560	9.6	-0.021	-16.7
9	52.2	2161	3.70	0.221	- 66.9	-0.519	17.0	0.626	2.0	-0.379	-12.4
10	59.0	2144	4.15	0.172	- 61.5	-0.442	19.5	0.615	- 3.9	-0.612	- 6.5
11	65.0	2003	4.27	0.125	- 61.0	-0.354	22.3	0.544	- 8.7	-0.702	- 0.8
12	70.0	1912	4.39	0.079	- 60.1	-0.255	24.1	0.424	-12.2	-0.657	4.5
13	76.0	1858	4.63	0.034	- 57.4	-0.153	24.3	0.275	-14.1	-0.499	8.4
14	86.0	1858	5.24	0.002	- 50.8	-0.055	22.2	0.116	-13.7	-0.273	9.9
15	100.0	1857	6.09	0	- 43.6	0	19.1	0	-12.0	0	9.4

TABLE V: NORMALIZED PARAMETERS OF TSUNAMI OSCILLATION ON CONTINENTAL SHELF OFF SAN ONOFRE: WATER DEPTHS AT (MLLW + 8 FT.)

Station No i	Water Depth h_i (m)	Width of Bay Channel b_i (ft)	Cross Sectnl Area S_i (sq. ft) (x 10^7)	Parameters of Tsunami Oscillation (normalized to unit value of ζ at i = 0 Computed Mode Frequencies and Periods: ω_n (rad./sec.); T_n (mins)							
				ω_1= 3.80x10^{-3}	T_1= 27.56	ω_2= 9.50x10^{-3}	T_2= 11.02	ω_3= 1.5x10^{-2}	T_3= 6.67	ω_4= 2.30x10^{-2}	T_4= 4.55
				$(\zeta_1)_i$ ft	$(\nu_1)_i$ ft	$(\zeta_2)_i$ ft	$(\nu_2)_i$ ft	$(\zeta_3)_i$ ft	$(\nu_3)_i$ ft	$(\zeta_4)_i$ ft	$(\nu_4)_i$ ft
0	2.4	---	≈ 0	1.000	0	1.000	0	1.000	0	1.000	0
1	6.7	2552	0.58	0.966	- 81.4	0.805	- 77.5	0.544	- 66.3	0.228	- 52.6
2	9.9	2683	0.88	0.889	- 107.3	0.397	- 84.8	- 0.268	- 51.9	- 0.826	- 18.7
3	12.7	2575	1.09	0.796	- 122.6	- 0.008	- 76.5	- 0.758	- 19.5	- 0.803	20.3
4	15.4	2861	1.33	0.696	- 127.0	- 0.342	- 56.4	- 0.810	11.9	- 0.039	31.5
5	19.4	2496	1.60	0.595	- 124.0	- 0.570	- 33.9	- 0.530	29.0	0.678	17.1
6	24.4	2439	1.95	0.499	- 114.3	- 0.688	- 13.3	- 0.116	31.2	0.873	- 3.8
7	31.4	2355	2.40	0.412	- 101.1	- 0.717	1.8	0.263	24.1	0.579	- 16.1
8	46.4	2231	3.44	0.342	- 75.0	- 0.689	9.6	0.512	12.2	0.115	- 15.4
9	54.6	2161	3.88	0.283	- 69.7	- 0.627	15.2	0.630	4.9	- 0.298	- 12.7
10	61.4	2144	4.10	0.228	- 68.3	- 0.538	19.8	0.655	- 1.3	- 0.600	- 7.8
11	67.4	2003	4.30	0.174	- 66.8	- 0.431	22.9	0.601	- 6.5	- 0.743	- 1.9
12	72.4	1912	4.54	0.121	- 64.4	- 0.311	24.5	0.487	- 10.2	- 0.716	3.7
13	78.4	1858	4.78	0.070	- 61.8	- 0.187	25.0	0.330	- 12.6	- 0.544	7.9
14	88.4	1858	5.39	0.023	- 55.1	- 0.050	23.0	0.157	- 12.6	- 0.276	9.6
15	102.4	1857	6.24	0	- 47.6	0	19.9	0	- 11.3	0	9.1

It is now expedient to point out that in our estimate of initial water disturbance [Eq. (52) and Fig. 13] we neglected to include an allowance for the permanent uplift of the seabed. Had we done so, the effect on Fig. 13 would be roughly equivalent to tilting the curves upward at $y = 5$ miles about a hinge point at $y = 0$, the amount of tilt at $y = 5$ miles being of the order of the permanent set $2\zeta/Z$ at $t = 4$ secs given by Fig. 10, where ζ in this case refers to uplift of the seabed. Eq. (52) for the maximum initial disturbance would then have included a subharmonic term whose amplitude would be given by Eq. (24 i) for $y = 5$ mi, $t = 4$ secs. We need therefore to modify Eq. (57) to read

$$[\eta(y)]_{t=0} = (H_{\frac{1}{2}}/2) \sin (k/2)y + \sum_{1}^{n=3} (H_n/2) \sin nky \qquad (79)$$

with

$$H_{\frac{1}{2}} = 0.3Z \qquad (80)$$

The addition of the extra term in Eq. (79) will, of course, tend to enlarge the estimate of $[\eta(y)]_{t=0}$ at $y = 1.35$ mi. (Fig. 13) by the amount

$$0.15Z \sin (0.675k)$$

which, for $k = \pi/L$ and $L = 5$ mi, is:

$$0.0617Z$$

and would thus make the total estimate of the initial sea disturbance $H = 1.32Z$ instead of $1.2Z$ originally taken (p. 31).

It is of some considerable interest to note that our estimate of initial sea disturbance introduced harmonic components whose periods are quite remarkably close to the values found in Tables IV and V. The comparison is more easily made in Table VI. For greater accuracy therefore we may replace $\omega_{\frac{1}{2}}$ in Eq. (78) by ω_2 $(= 2\pi/T_2)$ given in Tables IV to VI.

If $(\nu_2)_{15}$ be the normalized value of the horizontal amplitude of displacement at station 15, as given in the last rows of Tables IV and V, and H_2 is the factor by which it must be multiplied to agree in value with Eq. (78) then

$$H_2 = -\{H_{\frac{1}{2}}/2(\nu_2)_{15}\}\{(g/h)^{\frac{1}{2}}/\omega_2\} \qquad (81)$$

TABLE VI: COMPARISON OF ESTIMATED AND TRUE MODAL PERIODS FOR TSUNAMI SHELF OSCILLATION

Estimated Periods Eqs (52) to (56)			Correct Periods (Hydrodynamic Solution; Eqs (64) to (71)		
Harmonic No. n	Period, T_n (mins)		Mode No. m	Period, T_m (mins)	
	Low Tide (MLLW)	High Tide (MLLW+8')		Low Tide (MLLW)	High Tide (MLLW+8')
∞	25.4	24.7	1	28.23	27.56
1	12.7	12.3	2	12.02	11.02
2	6.3	6.1	3	7.32	6.67
3	4.2	4.1	4	4.99	4.55

TABLE VII: COASTAL HEIGHTS AND PERIODS OF MODAL COMPONENTS OF TSUNAMI OSCILLATION CAUSED BY HYPOTHETICAL EARTHQUAKE (WATER DEPTHS TO MLLW)

Water Depth	Dip Slip Offset Z (see Tables I and IA	Modal Sequence of Hydrodynamic Solution (m)							
		1		2		3		4	
		Period T_1 (mins)	Height H_1 (ft)	Period T_2 (mins)	Height H_2 (ft)	Period T_3 (mins)	Height H_3 (ft)	Period T_4 (mins)	Height H_4 (ft)
MLLW	1.31	28.2	0.38	12.0	-1.10	7.3	0.43	5.0	-0.17
	2.58	28.2	0.75	12.0	-2.16	7.3	0.85	5.0	-0.33
	3.77	28.2	1.10	12.0	-3.16	7.3	1.24	5.0	-0.48
	2.45	28.2	0.71	12.0	-2.06	7.3	0.80	5.0	-0.31
	4.82	28.2	1.40	12.0	-4.05	7.3	1.59	5.0	-0.61
	7.07	28.2	2.05	12.0	-5.95	7.3	2.34	5.0	-0.90
(MLLW + 8')	1.31	27.5	0.33	11.0	-0.96	6.7	0.41	4.5	-0.16
	2.58	27.5	0.66	11.0	-1.88	6.7	0.81	4.5	-0.30
	3.77	27.5	0.97	11.0	-2.75	6.7	1.19	4.5	-0.44
	2.45	27.5	0.63	11.0	-1.79	6.7	0.77	4.5	-0.29
	4.82	27.5	1.24	11.0	-3.52	6.7	1.52	4.5	-0.57
	7.07	27.5	1.81	11.0	-5.17	6.7	2.23	4.5	-0.84

This quantity H_n in fact will be the true value of the modal component height of the tsunami at the coast, because $(\zeta_n)_0$ at i = 0 in Tables IV and V was normalized to the value 1.000. Values of H_n and corresponding periods T_n, calculated in this way are recorded in Table VII. Comparison of Tables III and VII shows that the original component heights and periods of the tsunami oscillation derived from the estimation of initial sea disturbance were good approximations to the nature of the oscillation which is hydrodynamically correct.

We may check the initial profile, $[\eta(y)]_{t=0}$ over the shelf width by calculating the sum of the products $[(\zeta_n)_i H_n]$

$$\eta_i = \sum_{1}^{n=4} [(\zeta_n)_i H_n] \tag{82}$$

over each station i (=0, 1, 2, ... 15), where $(\zeta_n)_i$ are the normalized values of ζ given in Tables IV and V and H_n are the corresponding factors from Table VII. Thus Fig. 17 gives the initial profile of the sea disturbance in conformity with the hydrodynamic properties of the continental shelf. Fig. 16 bears comparison with Fig. 13. The peak uplift of water level at stations 8 and 9 is now somewhat larger than the original estimates represented by Fig. 13. At the same time an initial drawdown on the coast is disclosed. At high tide (MLLW + 8 ft.) the peak uplift would be slightly larger and more seaward and the drawdown slightly less than at low tide relative to the prevailing sea level, as shown in Fig. 17.

12. Tsunami Runup and Drawdown at the Coast

The solutions to Eqs (71) given in Tables IV, V and VII provide the products $(H_n \zeta_n)$ and $(H_n \nu_n)$ whereby water particle movements, vertically on the surface, and horizontally in the body of shelf water, are defined completely at any station point i, as

$$\text{(i)} \quad [\eta(t)]_i = \sum_{1}^{n=4} H_n (\zeta_n)_i \cos \omega_n t$$

$$\text{(ii)} \quad [\xi(t)]_i = \sum_{1}^{n=4} H_n (\nu_n)_i \cos \omega_n t \tag{83}$$

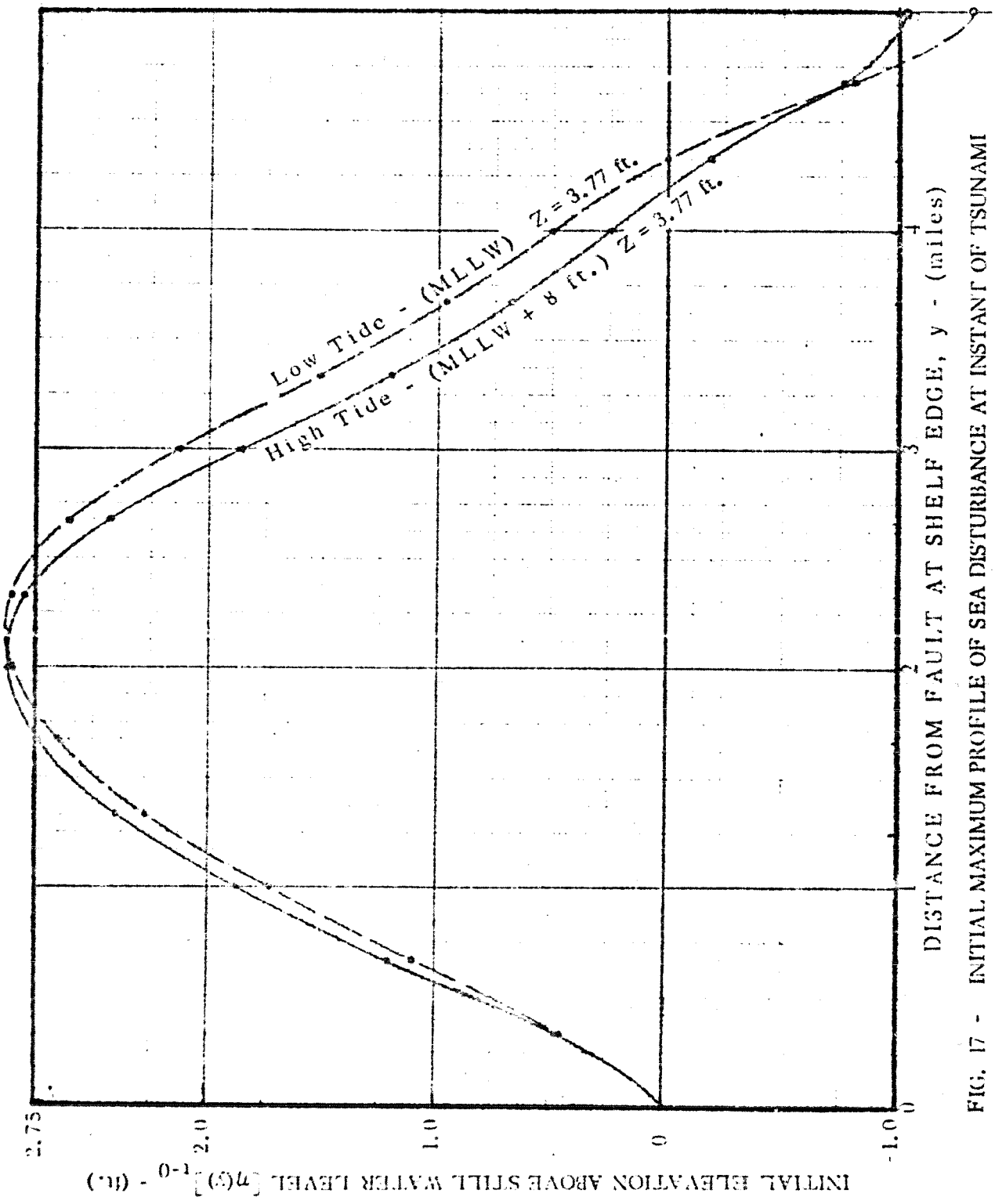


FIG. 17 - INITIAL MAXIMUM PROFILE OF SEA DISTURBANCE AT INSTANT OF TSUNAMI GENERATION, AS AT LOW TIDE AND HIGH TIDE, FOR DIP SLIP DISPLACEMENT ON THE FAULT Z=3.77 FT., CALCULATED IN ACCORDANCE WITH HYDRODYNAMIC PRINCIPLES

At the extreme coastal boundary (i = 0), Eq. (83 i) is readily calculated from the data of Tables IV, V and VII. Figs 18 and 19 give the time history of η at the coast for the different assumed values of the vertical dip-slip Z occurring on the fault in the hypothetical earthquake for the conditions of low tide (depths to MLLW) - Fig. 18 - and of high tide (depths to MLLW + 8 ft.) - Fig. 19.

In every case there occurs a nominally instantaneous drawdown of water as result of uplift of the land, but the amount is less than 2.5 ft. in the most extreme case (Z = 7.07 ft.). This is followed by the first big wave which would reach to 4.4 ft. above MLLW datum at low tide for Z = 3.77 ft. or to (4.0 + 8.0) = 12 ft. above MLLW at high tide for the same dip-slip. An unlikely extreme (Z = 7.07 ft.) would make this runup 8.2 ft. above MLLW at low tide and 15.6 ft. above MLLW datum at high tide. The first large wave would crest to about 6.5 mins after initiation of the sea disturbance and occurrence of the earthquake.

The large trough following the first crest would draw down sea level at the coast to 5.0 ft. below MLLW datum (Z = 3.77 ft.) and in the extreme to 9.4 ft. below MLLW (Z = 7.07 ft.) - Fig. 18. At the high tide - storm tide condition the drawdown would be to a level of 3.7 ft. above MLLW datum (Z = 3.77 ft.) and in the extreme to datum level (MLLW) itself (Z = 7.07 ft.).

Figs 18 and 19 show that after a minor intermediate wave, a crest larger than the first surges in at about 27 mins after the occurrence of the earthquake. That it is actually larger will depend on the effect of damping which has not been allowed for in arriving at the solutions of Eqs (83). The damping was briefly referred to in Eqs (64) by the factor K. Its effect is predictable through a time-dependent factor involving the exponential function

$$e^{-(K/2)t}$$

which gradually subdues the free oscillations of the shelf waters. This factor is often written in the alternative form:

$$e^{-\beta\omega t}$$

where β is a damping coefficient and ω the angular frequency of the oscillation ($\omega = 2\pi/T$; T = period of oscillation).

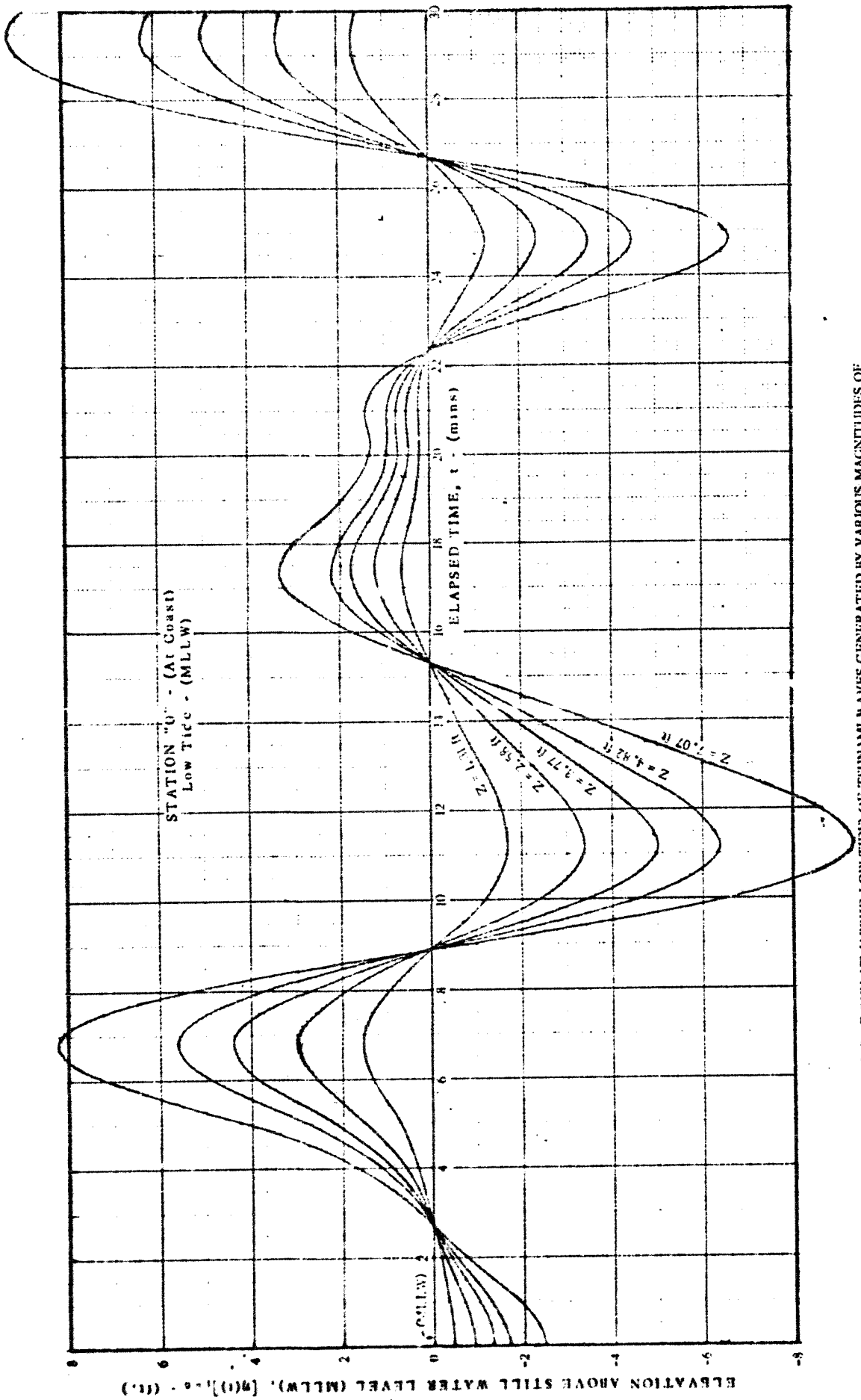


FIG. 14 - TIME HISTORIES OF RUN-UP (ABOVE LOW TIDE) OF TSUNAMI WAVES GENERATED BY VARIOUS MAGNITUDES OF VERTICAL DIP SLIP OFFSET, Z, FOR HYPOTHETICAL EARTHQUAKE ON SHELF-EDGE FAULT - (SAN ONOFRE)

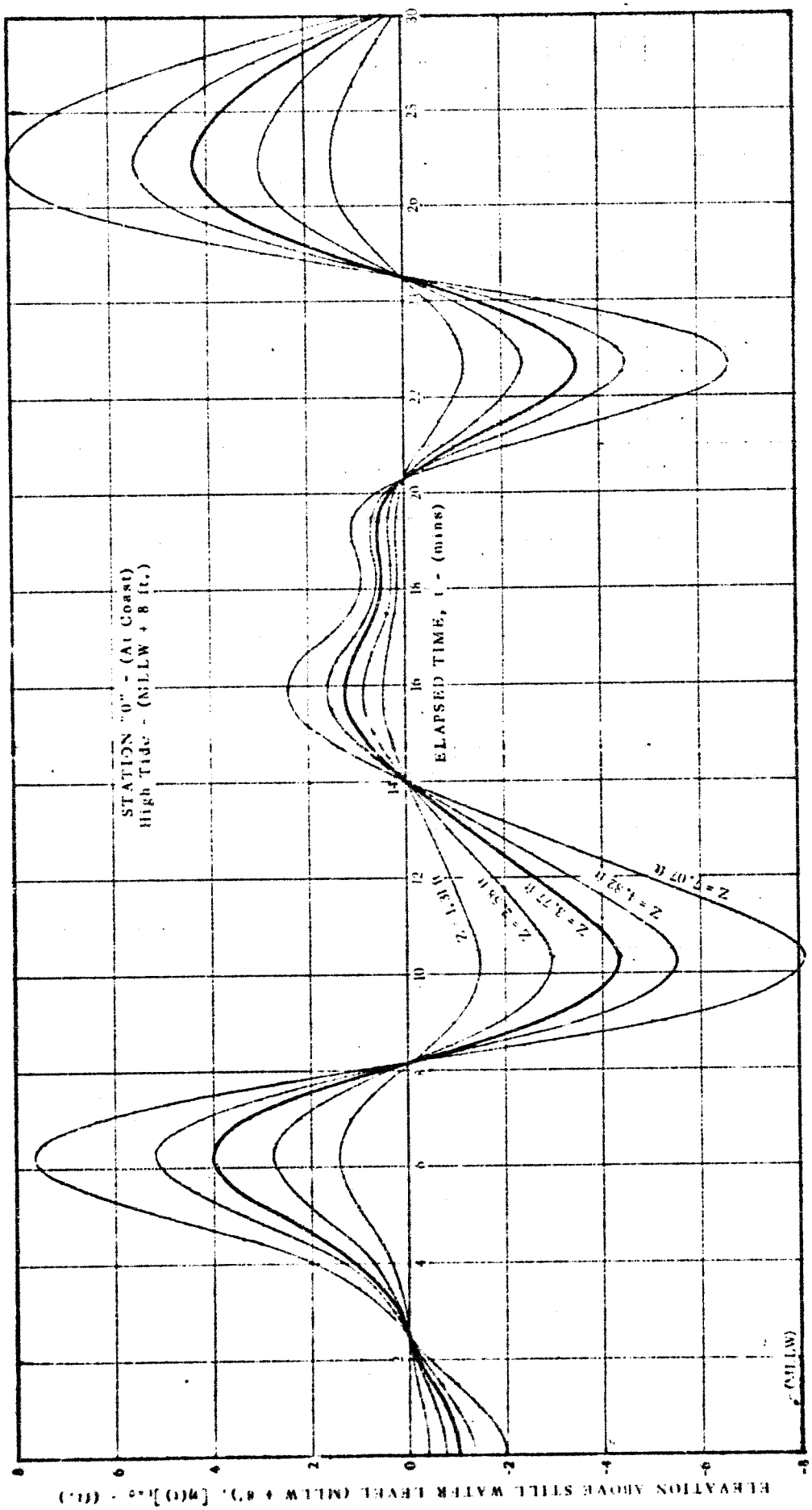


FIG. 19 TIME HISTORIES OF RUN-UP (ABOVE HIGH TIDE) OF TSUNAMI WAVES GENERATED BY VARIOUS MAGNITUDES OF VERTICAL DIP SLIP OFFSET, Z, FOR HYPOTHETICAL EARTHQUAKE ON SHELF-EDGE FAULT -- (SAN ONOFRE)

From measurements off tide records of the Alaskan tsunami at four west coast (California) stations, San Francisco, Rincon Island, Los Angeles and San Diego, the overall average height ratio of a tsunami wave to that of its predecessor is found to be 0.839 from which β is calculable from the equation

$$e^{-2\pi\beta} = 0.839 \tag{84}$$

yielding

$$\beta = 0.028 \tag{85}$$

This value is remarkably close to that of $\beta = 0.025$ found from a record of seiches occurring in San Francisco Bay (cf. Wilson, 1972, p. 32).

Adopting for the apparent wave period in Fig. 18 and 19 a value of T = 11 mins, the damping factor after t = 28 mins will be:

$$e^{-(2\pi\beta t/T)} = 0.639 \tag{86}$$

the value of which will make the crest height of the second large waves in Figs 18 and 19 appreciably less than the first waves. Attention may therefore be confined exclusively to the first high wave and trough.

Because the numerical calculation of $\eta(y,t)$ and $\xi(y,t)$ has been made for a somewhat course definition of sea bed topography via the distance increments δ = 1794 ft., there is some risk that the results obtained at the coastal boundary for $[\eta(t)]_{t=0}$ will insufficiently represent the true runup condition. Fig. 20 for instance, shows that in the neighborhood of the coast from A to E, the sea bed is quite irregular, whereas, within the range of distance of 6000 ft. included in the figure, it is defined by only four station points, 0 to 4, at the distance increments δ = 1794 ft.

To ensure that tsunami water levels at the coast, given by Figs 18 and 19 are not underestimates, we calculate the wave condition $\eta(t)$ as it might apply at station "$1\frac{1}{2}$", intermediate between stations 1 and 2, making use of the parameters given in Tables IV, V and VII. Figs 21 and 22, in this way, show the time histories of the tsunami waves as they might be recorded at station "$1\frac{1}{2}$" for the two cases of dip-slip at Z = 3.77 and Z = 7.07 ft. Considering just the

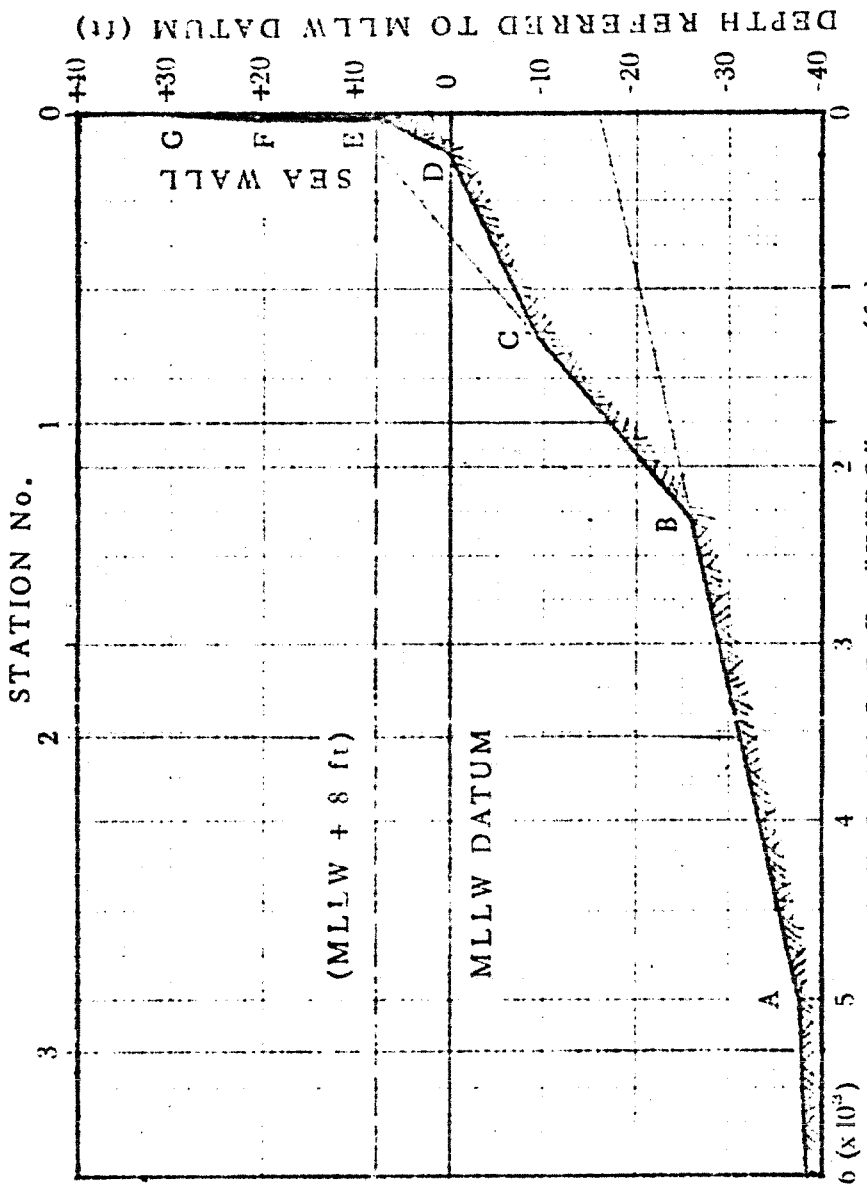


FIG. 20 - APPROXIMATE PROFILE OF SEA BED IN NEIGHBORHOOD OF SAN ONOFRE NUCLEAR POWER GENERATING PLANT

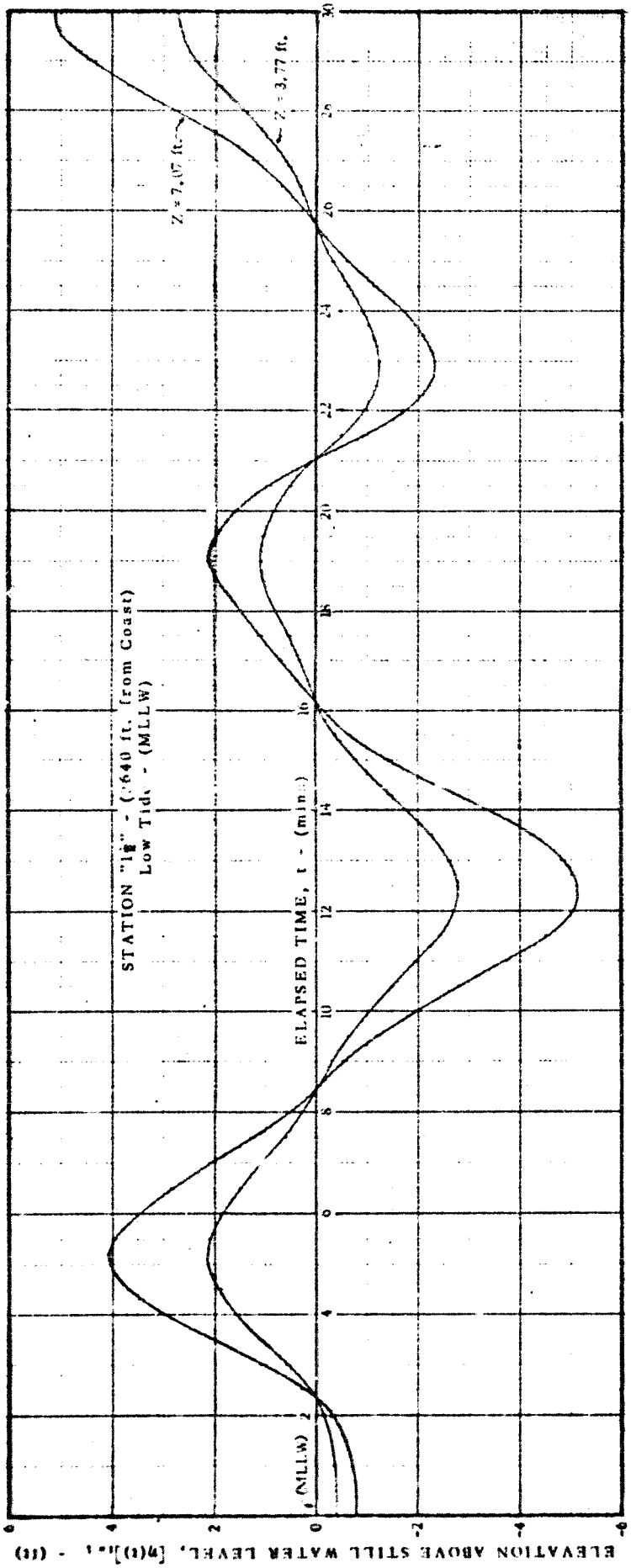


FIG. 21 - TIME HISTORIES OF TSUNAMI ELEVATION ABOVE LOW TIDE (MLLW) AT 2640 FT FROM COAST NEAR SAN ONOFRE FOR TWO MAGNITUDES OF DIP-SLIP OFFSET, Z, FOR HYPOTHETICAL EARTHQUAKE ON SHELF-EDGE FAULT

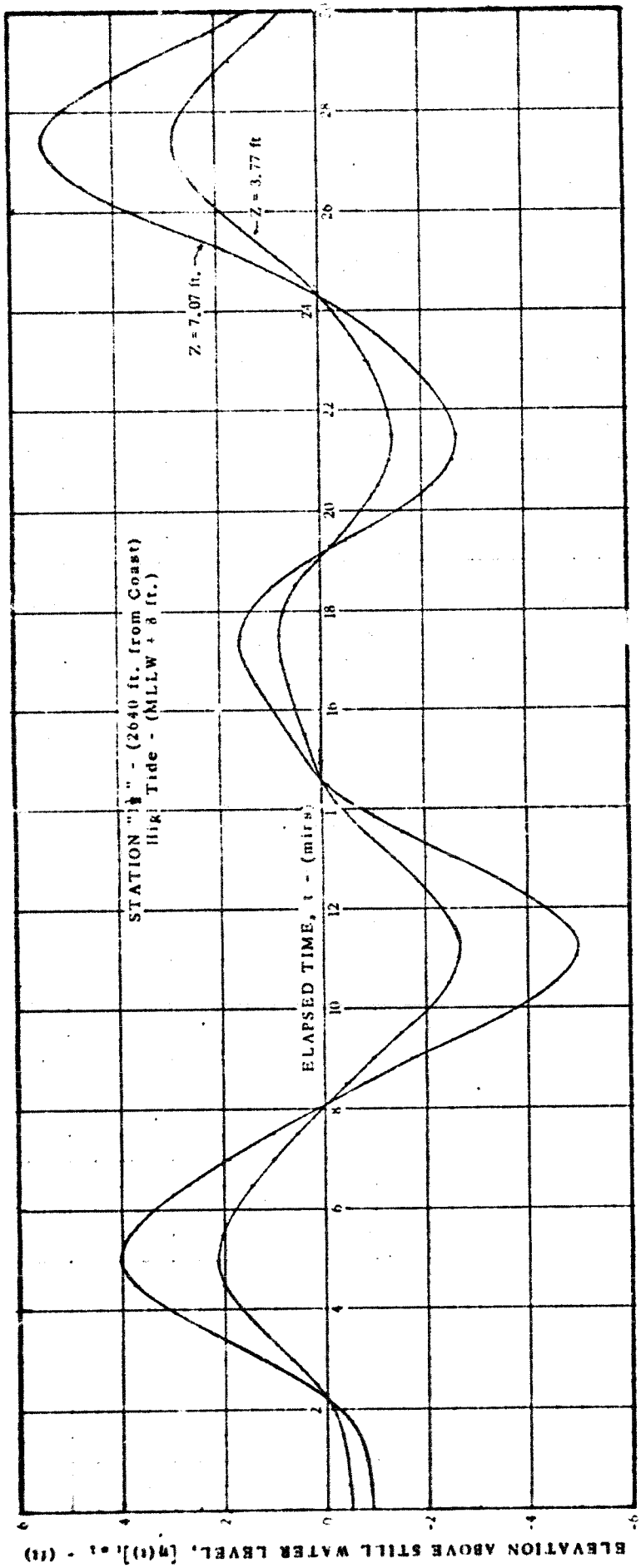


FIG. 22 - TIME HISTORIES OF TSUNAMI ELEVATION ABOVE HIGH TIDE (MLLW + 8 FT) AT 2640 FT FROM COAST NEAR SAN ONOFRE FOR TWO MAGNITUDES OF DIP-SLIP OFFSET, Z, FOR HYPOTHETICAL EARTHQUAKE ON SHELF-EDGE FAULT

first large crest and trough, the wave height (trough to crest) is about H = 5 ft. for Z = 3.77 and about H = 9 ft. for Z = 7.07 ft. at the toe of the slope BCDE in Fig. 19. The runup of the tsunami over the slope BCDE is then to be determined.

Although the tsunami oscillation has little real resemblance to a cnoidal or solitary wave type, we shall apply the known theoretical and experimental results for runup of solitary waves for estimation of the runup effect.

The most authoritative work known to the writer on the runup of solitary waves on slopes of various grades is that of Kishi and Saeki (1966), who have succeeded in unifying the theory and experiments of various authorities, besides themselves, who have worked in this field. These authors show that the runup experiments of Hall and Watts (1953) on steep slopes (> 1/10), of Kaplan (1955) on flat slopes (1/60) and of their own on intermediate slopes (1/30 to 1/10) can all be accommodated by the general empirical expression

$$R/h = a(H/h)^b \qquad (87)$$

where R is the runup measured above still water level, H the wave height at the toe of the slope, where the water depth is h, a a numerical constant and b a numerical exponent. Values of a and b are given in Fig. 23, which is reproduced from the paper of Kishi and Saeki (1966).

If from Fig. 20 we adopt an average slope from B to E of 34/2300 or 0.015 we find from Fig. 23

$$a = 0.33 \qquad b = 0.53$$

Accordingly, for the high tide-storm tide condition (MLLW + 8 ft.)

$$h = 34 \text{ ft.} \qquad H = 5 \text{ ft. (for } Z = 3.77 \text{ ft.)}$$

$$H = 9 \text{ ft. (for } Z = 7.07 \text{ ft.)}$$

and we obtain via Eq. (87):

$$R = 0.119\, h = 4.0 \text{ ft. (for } Z = 3.77 \text{ ft.)}$$

$$R = 0.163\, h = 5.5 \text{ ft. (for } Z = 7.07 \text{ ft.)}$$

above still water level, or

$$R = 12.0 \text{ ft. } (Z = 3.77 \text{ ft.})$$

$$R = 13.5 \text{ ft. } (Z = 7.07 \text{ ft.})$$

above MLLW datum.

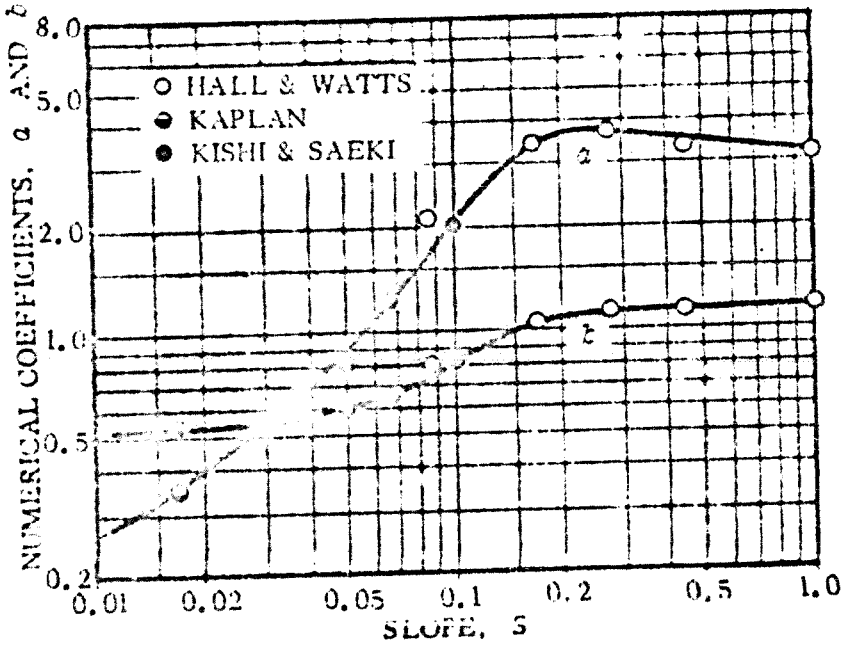


FIG. 23 - VALUES OF NUMERICAL COEFFICIENTS IN RELATIONSHIP FOR RUN-UP OF SOLITARY WAVES ON SLOPES OF VARIOUS GRADES (from Kishi and Seiki, 1966)

It is convenient now to summarize runup results in Table VIII.

TABLE VIII: ESTIMATED MAXIMUM RUNUP, R, AND DRAW-DOWN, D, OF TSUNAMI AT THE SAN ONOFRE SITE

Dip Slip Offset Z (see Tables I and IA) (ft)	Maximum Runup, R (ft) above MLLW Datum (at High Tide + Storm Tide) (Note: $_t$ = station no., Fig. 16)				Maximum Draw-down, D, (ft), below MLLW Datum (at Low Tide)	
	This Study from $[\eta(t)]_{t=0}$ (MLLW + 8' condition)		This Study from $[\eta(t)]_{t=1\frac{1}{2}}$ and Kishi-Saeki Formula (MLLW + 8' condition)		This Study from $[\eta(t)]_{t=0}$ (MLLW condition)	
	Max. Crest Amplitude ($_{t=0}$)	Max Crest Elevation	Max. Wave Height ($_{t=1\frac{1}{2}}$)	Max Crest Elevation	Max. Trough Amplitude ($_{t=0}$)	Max Trough Elevation
1.31	1.4	9.4	---	---	-1.7	-1.7
2.58	2.8	10.8	---	---	-3.4	-3.4
3.77	4.0	12.0	5.0	12.0	-5.0	-5.0
2.45	2.8	10.8	---	---	-2.8	-2.8
4.82	5.2	13.2	---	---	-6.4	-6.4
7.07	7.6	15.6	9.0	13.5	-9.3	-9.3

It is clear from Table VIII that the results of this study are consistent with results that are obtainable from use of the Kishi-Saeki empirical formula (Eq. 87). However, the value of runup height for Z = 7.07 given by this study is higher than that found by the formula and is considered more reliable as well as conservative.

We are in a position now to comply with the requirement of Question (l) in Appendix A and item (j) of Appendix B. Results of Table VIII are plotted in Fig. 24, from which extrapolation is possible, to infer (approximately no doubt), what unusual conditions would cause a local tsunami, generated at high tide in the presence of storm tide, to reach the height of 23 ft. above MLLW.

The runup, R, is found to be a linear function of Z, the vertical dip-slip at the fault, and can be fitted by an empirical equation:

$$R = 8.0 + 1.1Z \qquad (88)$$

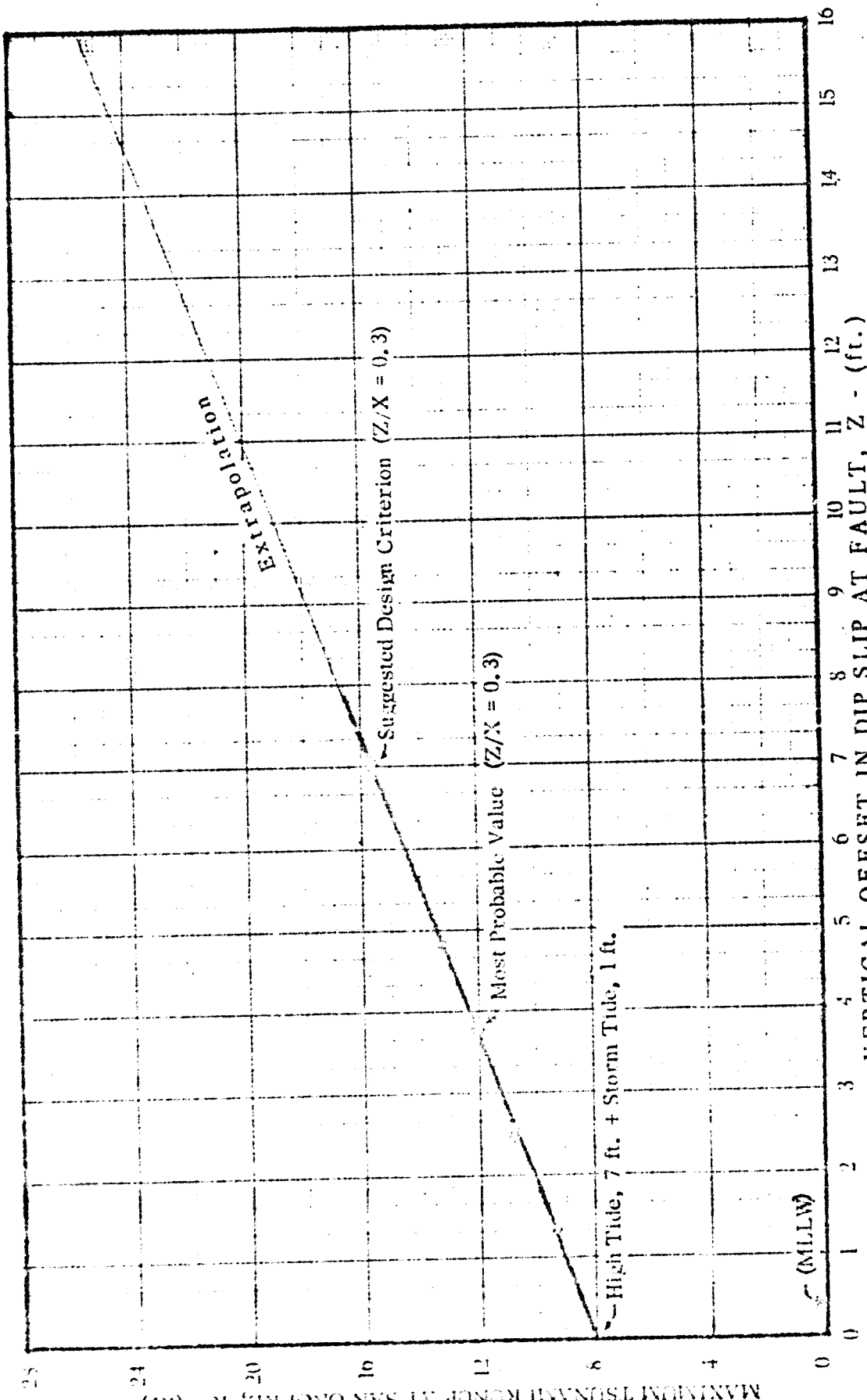


FIG. 24 - RELATIONSHIP BETWEEN MAXIMUM TSUNAMI RUNUP AT SAN ONOFRE AND VERTICAL DIP SLIP OFFSET ON THE SHELF-EDGE FAULT. (Runup referred to MLLW Datum)

for R and Z in feet. Hence for R = 28 ft., the vertical dip-slip displacement would have to be

$$Z = 18.2 \text{ ft. or } 5.5 \text{ m.}$$

At the ratio 10 : 3, strike slip to dip slip, the strike displacement of such an earthquake would be

$$X = 18.5 \text{ m}$$

and the resultant displacement

$$\Delta = 19.3 \text{ m}$$

According to Fig. 3 such an earth movement has no precedent even with the largest known earthquakes and may be considered outside the realm of possibility on a minor fault. The conclusion, therefore, is that the 28 ft. protective wall at San Onofre will never be overtopped by any tsunami that is likely to be generated locally.

Before leaving this section there remains one aspect for consideration concerning the continuity of operation of the cooling water intake. Drawing No. 5104344-1 of 1972, supplied to the writer, shows intake head level for Nuclear Generating Unit 3 at 15.0 ft below MLLW. We desire to know what value of dip-slip offset, Z, could cause a tsunami great enough to expose the intake head and interrupt the inflow of cooling water.

In answering this, we note first from Figs 18 and 21 for stations "0" and "1½" respectively, that the maximum trough amplitude following the first crest is greater than the crest amplitude in the ratio of about 1.2. With insufficient time on this project remaining to calculate $[\eta(t)]_z$ at the intake position directly, we must guess that for Z = 7.07 the maximum trough level of the tsunami at low tide would be about 4 ft below MLLW. For a tsunami with a trough of $|\eta_t|$ ft below MLLW at that point, we might then expect the value of Z necessary to produce it, would be

$$Z = (|\eta_t|/4)\, 7.07 \simeq 1.77\,|\eta_t| \qquad (89)$$

For the position of the intake at 3400 ft from shore, Eq. (10) indicates that sea bed uplift there (for y = 4.36 mi, t > 10 mins) will be $\zeta_s = 0.42Z$, where the subscript refers to the sea bed. Accordingly from Eq. (89), ζ_s, in terms of $|\eta_t|$

becomes

$$\zeta_b = 0.74\,|\eta_t| \tag{90}$$

For safety against exposure of the intake head, we must then have

$$\{15.0 - 0.74\,|\eta_t|\} > |\eta_t|$$

or

$$|\eta_t| < 8.6 \text{ ft.} \tag{91}$$

By Eq. (89), this means that the value of Z must be conditioned by

$$Z < 15.3 \text{ ft.} \tag{92}$$

13. Maximum Velocities of Uprush and Draw-down near San Onofre

We return to Eq. (83 ii) and differentiate this partially with respect to t, obtaining an expression for the velocity u(t) of the water particles at any station i, namely:

$$[u(t)]_i = \frac{\partial \xi}{\partial t} = \sum_{1}^{n=4} - H_n (\nu_n)_i\, \omega_n \sin \omega_n t \tag{93}$$

It should be noted that it is implicit in the long wave theory used in obtaining Eqs (64) - (see Wilson, 1972) - that the velocity distribution with depth is uniform. Hence the value given by Eq. (93) may be considered to apply at any depth at a specific station i.

Because the numerical integration procedure used in solution of ζ and ξ [Eqs (71)] proceeded from the coast seawards, whereas we desire to conform to the original sense of direction, positive towards the coast from an origin of abscissae, y, taken at the fault on the edge of the shelf, we change the sign of Eq. (93) and write it:

$$[u(t)]_i = \sum_{1}^{n=4} H_n (\nu_n)_i\, \omega_n \sin \omega_n t \tag{94}$$

A positive velocity, u, will then correspond to an inflow towards the coast and a negative velocity, vice versa.

Values of $[u(t)]_i$ are readily calculated for any particular station point i (i = 0, 1, 2,....15; see Fig. 16). Examples of these calculations are presented in Fig. 25 for Station 1, (i = 1), and for the cases of Z = 3.77 and 7.07 ft. at the low tide condition. Fig. 25 may be compared with the corresponding traces of $[\eta(t)]_{i=1\frac{1}{2}}$ in Fig. 21. Although the station points are different for these two figures, they are sufficiently close together to show that zero velocities correspond to maxima and minima of $\eta(t)$ values, a feature similar to slack waters at high and low astronomical tides.

Our primary interest, however, is in the maxima of the current velocities in up-rush and draw-down. These maximum values of u(t) are obtainable from data similar to those plotted in Fig. 25, calculated for stations i = 1, 2, ...6, close to the coast. The information is conveniently summarized in Table IX, which specifies both the maximum values of $[u(t)]_i$ and the times (in mins) at which they occur, referred to time "zero", [a few seconds (circa 5-8) after occurrence of the earthquake].

It will be noticed immediately from Table IX that draw-down velocities greatly exceed the up-rush maxima, and that the low tide conditions (MLLW) produce severer scour velocities than would tend to occur if the tsunami happened at high tide (MLLW + 8'). Consequently from a design point of view, considerations in respect of scour and possible bed movement must be related to the low tide condition.

Horizontal velocities, u(t), at the San Onofre seawall are necessarily zero because of this boundary restricting any horizontal flow. Seaward of this boundary the draw-down velocities peak at a short distance from the coast (about 1600 to 2000 ft.) and then decline at greater distances from San Onofre. This is shown in Fig. 26 where maximum draw-down velocities at low tide (MLLW) for different values of dip-slip offset, Z, are plotted against distance out to 2 miles. Depending upon which value of Z is adopted for final design, the maximum velocity of scour current can be obtained from Fig. 26 for any particular distance from the coast.

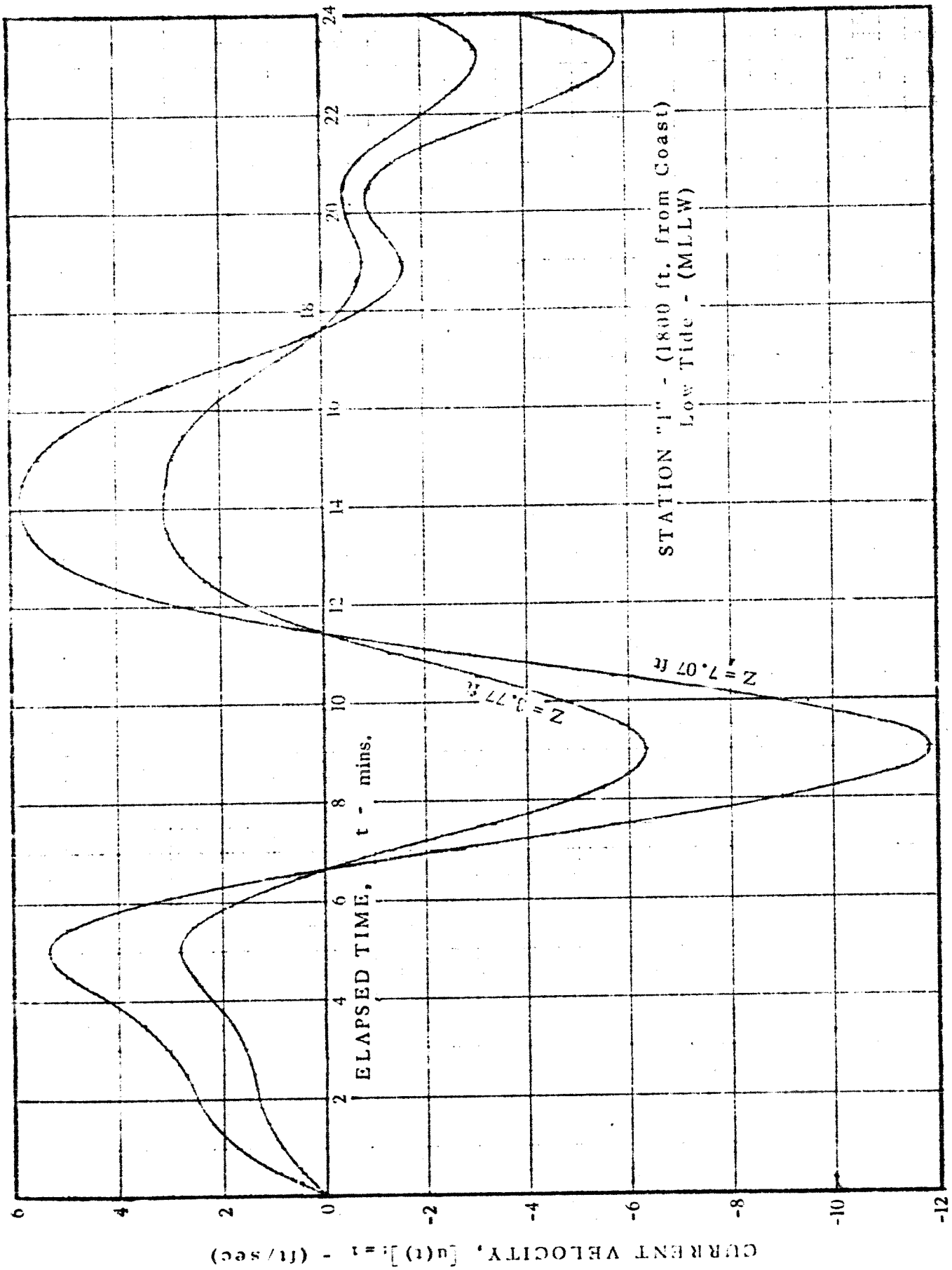


FIG. 25 - TIME HISTORY OF TSUNAMI CURRENT VELOCITY AT LOW TIDE (MLLW) AT 1800 FT.

TABLE IX: MAXIMUM VELOCITY VALUES AND TIMES OF OCCURRENCE OF UPRUSH AND DRAWDOWN CURRENTS FROM TSUNAMI AT DIFFERENT STATIONS OFFSHORE

Vertical Dip-Slip Offset (see Tables I and IA) Z (ft)	Station No. i	LOW TIDE (MLLW) Max Current Velocity, u; occurrence Time, t, and Direction +				HIGH TIDE (MLLW + 8') Max Current Velocity, u; Occurrence Time, t, and Direction +			
		Uprush (+)		Drawdown (-)		Uprush (+)		Drawdown (-)	
		u (ft/sec)	t (mins)	u (ft/sec)	t (mins)	u (ft/sec)	t (mins)	u (ft/sec)	t (mins)
1.31	0	0		0		0		0	
	1	+0.98	5.0	-2.20	9.0				
	2	+0.77	4.0	-1.53	9.0				
	3	+0.73	3.5	-0.91	9.5				
	4	+0.50	3.0	-0.52 -0.48	7.0 10.5				
	5	+0.34	2.0	-0.44 -0.31	6.5 11.5				
	6	+0.22	1.5	-0.33	5.5				
	15	+0.09	8.5	-0.27	2.5				
2.58	0	0		0		0		0	
	1	+1.93	5.0	-4.32	9.0				
	2	+1.51	4.0	-3.00	9.0				
	3	+1.43	3.5	-1.79	9.5				
	4	+0.98	3.0	-1.03 -0.94	7.0 10.5				
	5	+0.68	2.0	-0.88 -0.62	6.5 11.5				
	6	+0.44	1.5	-0.65	5.5				
	15	+0.17	8.5	-0.55	2.0				

TABLE IX (Continued)

Vertical Dip-Slip Offset (see Tables I and IA) Z (ft)	Station No. i	LOW TIDE (MLLW) Max Current Velocity, u; Occurrence Time, t, and Direction ±				HIGH TIDE (MLLW + 8') Max Current Velocity, u; Occurrence Time, t, and Direction ±			
		Uprush (+)		Drawdown (-)		Uprush (+)		Drawdown (-)	
		u (ft/sec)	t (mins)	u (ft/sec)	t (mins)	u (ft/sec)	t (mins)	u (ft/sec)	t (mins)
3.77	0	0		0		0		0	
	1	+2.82	5.0	-6.32	9.0	+1.90	4.5	-4.01	8.0
	2	+2.21	4.0	-4.39	9.0	+1.81	4.0	-3.68	8.0
	3	+2.09	3.5	-2.62	9.5	+1.76	3.5	-2.61	8.5
	4	+1.43	3.0	-1.50 -1.37	7.0 10.5	+1.50	3.0	-1.58	9.5
	5	+0.99	2.0	-1.28 -0.90	6.5 11.5	+1.07	2.5	-1.17 -1.00	6.0 10.0
	6	+0.63	1.5	-0.95	5.5	+0.73	1.5	-0.88 -0.70	5.5 11.0
	15	+0.25	8.5	-0.80	2.0				
2.45	0	0		0		0		0	
	1	+1.83	5.0	-4.10	9.0				
	2	+1.44	4.0	-2.85	9.0				
	3	+1.36	3.5	-1.71	9.5				
	4	+0.93	3.0	-0.98 -0.90	7.0 10.5				
	5	+0.64	2.0	-0.83 -0.58	6.5 11.5				
	6	+0.41	1.5	-0.61	5.5				
	15	+0.16	8.5	-0.52	2.0				

TABLE IX (Continued)

Vertical Dip-Slip Offset (see Tables I and IA) Z (ft)	Station No. i	LOW TIDE (MLLW) Max Current Velocity, u; Occurrence Time, t, and Direction ±				HIGH TIDE (MLLW + 8') Max Current Velocity, u; Occurrence Time, t, and Direction ±			
		Uprush (+)		Drawdown (-)		Uprush (+)		Drawdown (-)	
		u (ft/sec)	t (mins)	u (ft/sec)	t (mins)	u (ft/sec)	t (mins)	u (ft/sec)	t (mins)
4.82	0	0		0		0		0	
	1	+3.62	5.0	-8.09	9.0				
	2	+2.84	4.0	-5.62	9.0				
	3	+2.68	3.5	-3.36	9.5				
	4	+1.83	3.0	-1.92 -1.76	7.0 10.5				
	5	+1.27	2.0	-1.03 -1.15	6.5 11.5				
	6	+0.81	1.5	-1.21	5.5				
	15	+0.32	8.5	-1.02	2.0				
7.07	0	0		0		0		0	
	1	+5.32	5.0	-11.89	9.0	+3.57	4.5	-7.54	8.0
	2	+4.17	4.0	-8.26	9.0	+3.39	4.0	-6.92	8.0
	3	+3.94	3.5	-4.93	9.5	+3.31	3.5	-4.89	8.5
	4	+2.69	3.0	-2.82 -2.58	7.0 10.5	+2.83	3.0	-2.96	9.5
	5	+1.87	2.0	-2.40 -1.69	6.5 11.5	+2.01	2.5	-2.19 -1.87	6.0 10.0
	6	+1.20	1.5	-1.78	5.5	+1.37	1.5	-1.65 -1.32	5.5 11.0
	15	+0.47	8.5	-1.50	2.0				

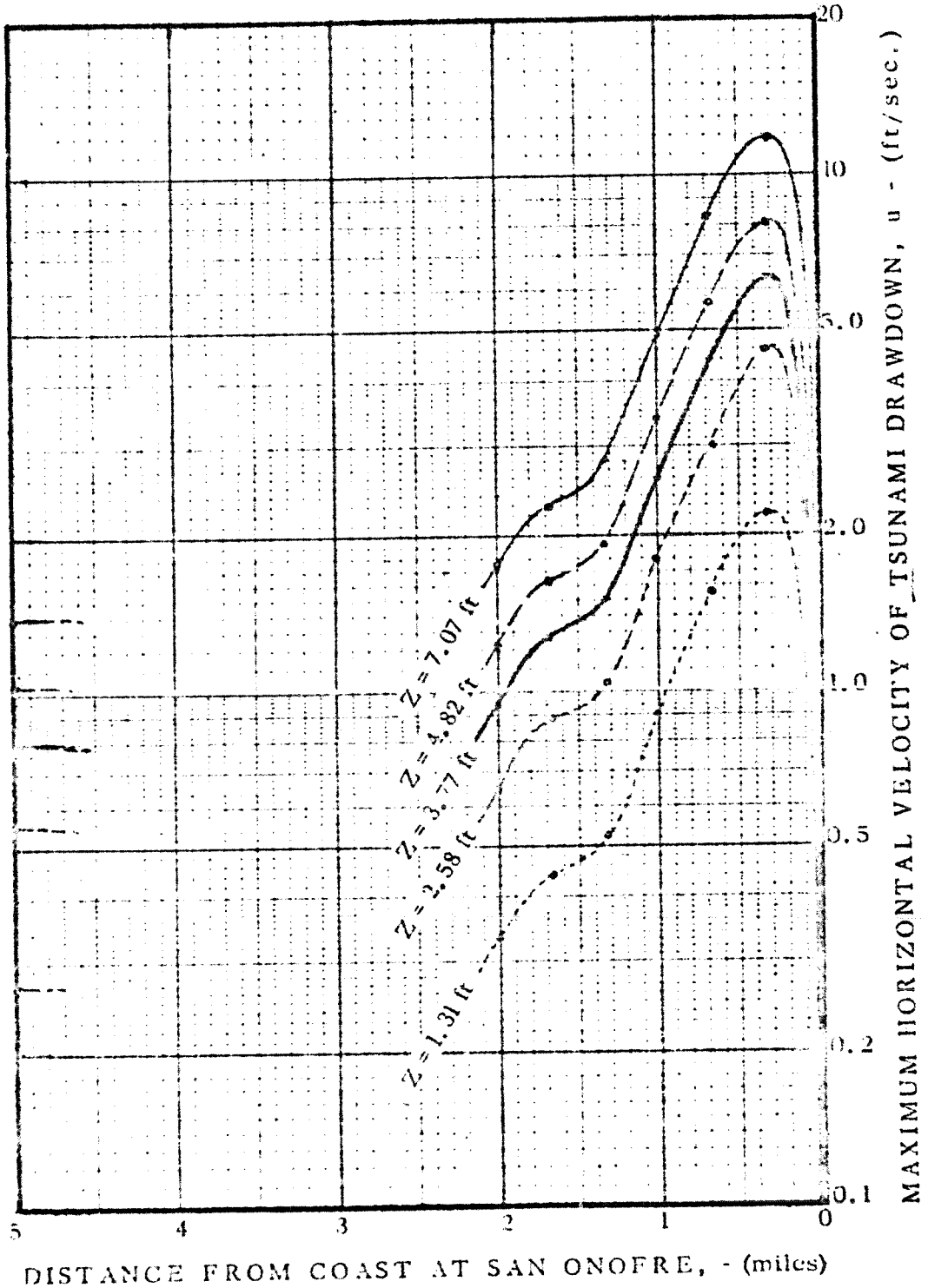


FIG. 26 - MAXIMUM VELOCITIES OF DRAW-DOWN CURRENTS IN THE TSUNAMI NEAR SAN ONOFRE FOR VARIOUS MAGNITUDES OF VERTICAL DIP-SLIP OFFSET, Z, ON THE SHELF-EDGE FAULT

It will not be possible within the time available for this study to comment adequately upon the effect of the draw-down velocites on the bed materials, this being a complicated subject in itself beyond the scope of this investigation.

It must be pointed out that all vertical structures such as diffuser ports and cooling water intake structures will need to be carefully designed to resist the hydrodynamic forces of the tsunami current plus additional accelerative currents such as those from astronomical tide, storm tide and regular wind waves and swells. The design magnitudes of the possible combinations of velocities and accelerations will depend upon the position of the structure and the selection of a design value of Z, but Fig. 26 should be helpful in arriving at suitable values of tsunami velocities and corresponding accelerations could be readily calculated, but are not given in this report.

14. Oscillating Properties of the Oceanic Basins

Question 3 of Appendix A and items (h) and (i) in answer thereof remain to be considered.

Figs 1 and 2 show the topography of the oceanic basins. In dealing hydrodynamically with the oscillating properties of these three-dimensional basins in an approximate manner we shall attempt to describe their topography through some simple geometrical shapes that represent them reasonably as to boundary shapes and depths. We shall deal with the shelf and oceanic basins in four separate ways:

(a) Shelf between Dana Point and Rose Canyon

(b) Ocean basin of the Gulf of Santa Catalina from Newport Beach to La Jolla

(c) Ocean basin between San Clemente Island and the San Onofre coastline

(d) Ocean basin between Santa Barbara channel islands, San Nicolas and San Clemente Islands and the southern California coastline

The first of these will treat only the shelf waters. The remaining three will consider oscillations in the oceanic basins.

(a) Dana Point - Rose Canyon Shelf

In the first instance we simulate the shelf in this area (see Fig. 1) as a semi-elliptic bowl of very large major/minor axis ratio. The length L, of this "basin" is about 32 naut. mi. and its semi-minor axis width (B/2), about 4.7 naut. mi. For an elliptical basin as elongated as this, its major responses are dictated almost entirely by the transverse modes of oscillation, which approximate closely the modes of free oscillation for an infinitely long straight shelf of semi-parabolic depth profile.

The concave semi-parabolic depth profile, however, is not a very good approximation to the true shape of the shelf between Dana Point and Rose Canyon, which is convex rather than concave in profile, as shown in Fig. 20. Since the three dimensionality of the problem largely falls away, we may substitute a more satisfactory geometric approximation to the true shape of the shelf bed by considering it to be one-half of a quartic curve with depth defined as

$$h(y) = h_0(1 - 4y^2/L^2)^2 \qquad (95)$$

in which h_0 is the depth at the edge of the shelf and y the distance measured normally from the shelf edge and taken positive towards the coast. The modes of free oscillation of such a shelf will be the same as the odd modes of oscillation of the full quartic basin formed by the shelf and its mirror image, for which the solution is known (cf. Wilson, 1972, p. 39). Periods T_n of these odd modes are given by

$$T_n (gh_0)^{\frac{1}{2}} / B = 4.965;\ 2.482;\ \ldots\ldots\ \ldots\ldots \qquad (96)$$

in which B is the width of the shelf and the numbers on the right hand side of Eq. (96) correspond to the shelf modes m = 1, 2, ... in sequence.

For B = 5 miles and h_0 = 100 m. = 328 ft., Eq. (96) gives

$$T_1 = 21.3 \text{ mins}$$
$$T_3 = 10.6 \text{ mins} \qquad (97)$$

These results are reasonably consistent with the more accurate numerical determinations of periods of shelf oscillation given in Table VI but provide a rough-and-ready check upon the latter.

(b) Gulf of Santa Catalina from Newport Beach to La Jolla

Fig. 27 shows another representation of the oceanic basins off the southern California coast with all areas of less than 600 ft depth shaded to emphasize virtual boundaries that exist for particular areas.

Considering just the ocean basin immediately flanking the coastal shelf edge from La Jolla to Newport Beach, it is evident from Fig. 27 that the area can be simulated quite effectively by a semi-elliptic basin of roughly paraboloidal bottom with its major axis in the deepest part of the Gulf in a NW-SE direction. Its major-axis dimension is $L \approx 66$ naut. mi. and its major/minor axis ratio $L/B \approx 3/2$.

The fundamental mode of transverse oscillation for this basin, having an antinode at the edge of the continental shelf and a node along its major axis has been shown (Wilson, 1971) to have a period

$$T_1 \approx 30.1 \text{ mins} \qquad (98)$$

A second mode in which the semi-elliptic basin could respond with a node along the major axis of the ellipse and a node along a concentric semi-ellipse, parallel to the boundary semi-ellipse, would have a period

$$T_2 \approx 24.5 \text{ mins} \qquad (99)$$

These natural periods are evidently not too greatly different from the natural periods of the shelf off San Onofre, as given in Table VI, so that the oceanic basin might be expected to show some response to the hypothetical earthquake. The important question lies in the magnitude of such response.

Without a very long and complicated analysis it is only possible to answer this now in very general terms. The essential difference between oscillation of the shelf waters and oscillation of the oceanic basin waters, as result of the initial sea disturbance visualized schematically in Fig. 12, is that while approximately equal potential energies are released in the two bodies of water, the volumes of water which must be moved by these releases are vastly different.

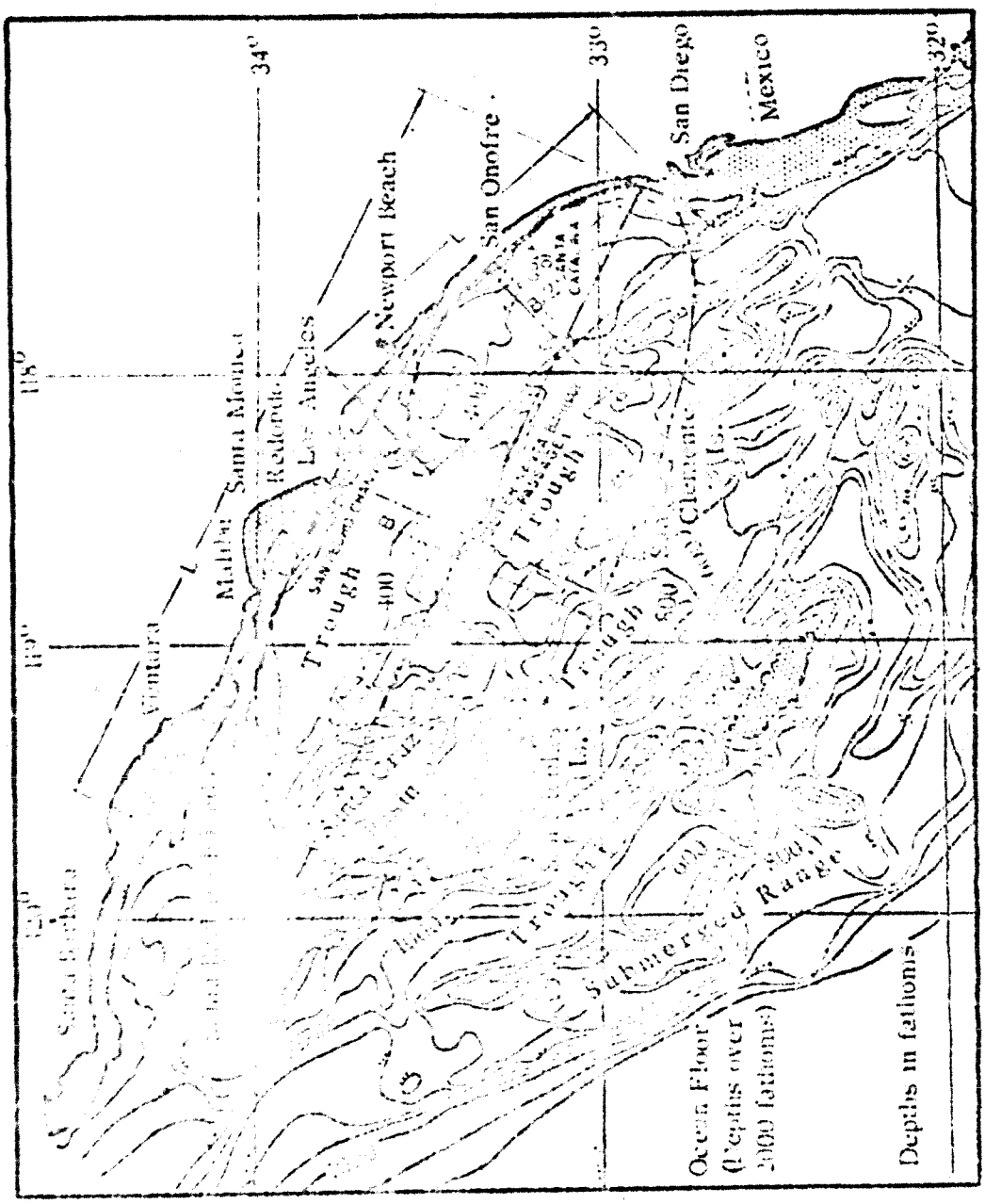


FIG. 27 - BATHYMETRY OF OCEANIC BASINS OFF SOUTHERN CALIFORNIA SHOWING GEOMETRIC ANALOGIES FOR BASINS ADJACENT TO SAN ONOFRE

The total energy per unit width in any induced seiche developing in an open-mouth basin, such as the shelf or oceanic quasi basin we are considering, can be approximated as

$$E \approx \tfrac{1}{4} \rho g \eta_b^2 L \tag{100}$$

in which η_b is the amplitude of the boundary elevation of the water and L is the length of the basin. If we use subscripts s and o to designate shelf and ocean respectively, and drop off the subscript b, then for equal energies E,

$$(\eta_o/\eta_s)^2 = L_s/L_o$$

or

$$(\eta_o/\eta_s) = (L_s/L_o)^{\frac{1}{2}} \tag{101}$$

Because $(L_s/L_o) \approx 0.21$, we could then expect

$$(\eta_o/\eta_s) \approx 0.46 \tag{102}$$

Eq. (102) implies that the oscillation in the oceanic basin would have less than half the height of that developing on the shelf.

It is not expected that this effect in the oceanic quasi-basin will greatly influence the results already calculated for the shelf. The shelf oscillation calculations have in effect already provided for the oceanic basin oscillation through the assumption of an *odd* function description of the initial sea disturbance. Thus Eq. (52) also describes the negative sea disturbance over the ocean for negative y ($y < 0$), and the determination of H_n via Eq. (81) is consistent with a flow at the edge of the shelf dictated by the interaction of the shelf and oceanic waters.

It has to be admitted that this kind of interaction at the shelf edge is approximate only. Strictly, for a more complete solution of the problem of the coupled basins we would need to have applied Eqs (71) to a chain of stations extending beyond No. 15 at the shelf edge, going into deep water as far as the major axis of the semi-elliptic basin. This however would open up the complexities of the three-dimensionality of the problem because the responses of the oceanic basin cannot properly be determined from the analysis of a narrow

filament of water in the manner done for the shelf oscillations.

It appears nevertheless that our results for the shelf oscillations should be conservative, because in terms of Eq. (102), flow velocities at the shelf edge should really be less than they were taken. There is, in any case, no question of resonance occurring because the forced oscillation is still only the earth movement with its rapid vibration at about 15 secs period (Eqs 24), and the behavior of the shelf and oceanic waters will merely constitute the free oscillation in the coupled system of basins arising from the initial disturbance.

(c) Oceanic Quasi-Basin between San Clemente Island and the Mainland

Much the same considerations as those discussed under (b), apply to the quasi-basin lying between San Clemente Island and the mainland (Fig. 27). Consideration of this quasi-basin on its own is just another rough-and-ready means of assessing the behavior of the oceanic waters off San Onofre. Actually the behavior of these waters will be a very complicated free oscillation influenced by the entire topography of the ocean bed and boundaries so that any treatments of the problem under these items (a) to (d) does not necessarily imply that each case gives an independent effect that can be superimposed on the others.

The profile of the ocean bed from San Clemente Island to the mainland is shown in Fig. 28. Figs 1, 27 and 28 show that San Clemente Island forms an almost vertical wall which would be capable of reflecting tsunami energy back towards the coast. The profile shape [taken approximately along the minor axis of the semi-ellipse considered previously (Fig. 27)] is so nearly rectangular that we may approximate the quasi-basin as one of rectangular plan shape, vertical ends and uniform depth. Approximate dimensions from Fig. 27 are $L \approx 43.8$ n.mi., $h \approx 480$ fathoms or 2880 ft.

Such a rectangular basin has natural modal periods, T_n given by

$$T_n = 2L/m(gh)^{\frac{1}{2}} \qquad (103)$$

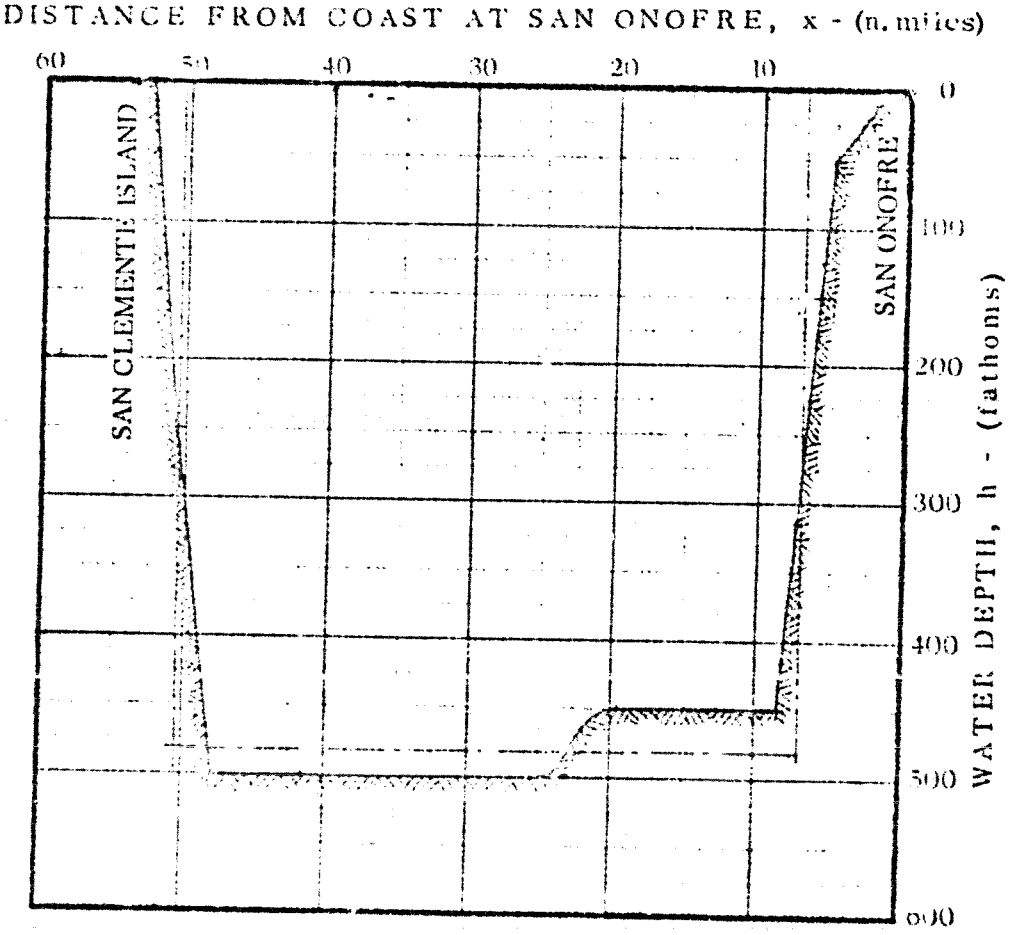


FIG. 28 - VERTICAL PROFILE OF OCEAN BED BETWEEN SAN ONOFRE AND SAN CLEMENTE ISLAND, CALIFORNIA

and for the dimensions given, their values, m = 1, 2, 3...., are

$$T_m = 29.1;\ 14.6;\ 9.7;\ 7.3;\ 5.8;\ 4.9;\ 4.1 \qquad (104)$$

The closeness in period values of the fundamental oscillations for this rectangular quasi-basin (29.1 mins) and the semi-elliptic basin of section (b) [30.1 mins, Eq. (94)] is evident, but expected. With the exception perhaps of T_2 (= 14.6 mins), the periods of Eq. (104)are quite close in value to the shelf modal periods. This will ensure some longevity for the shelf oscillations set up by the earthquake because of the tendency for some of the energy of the disturbance to become trapped in oscillations between San Clemente and the mainland coast.

The amount of energy per unit width so trapped would be given by Eq.(100) for L ≈ 43.8 n. miles. From Eq. (101), therefore, we could expect the ratio of amplitudes of boundary disturbance on the shelf (η_s) and in this ocean basin (η_o) to be

$$(\eta_s/\eta_o) \approx 0.31 \qquad (105)$$

which by the same argument discussed in section (b), would tend to make our calculations of the shelf oscillations still more conservative.

(d) Oceanic Quasi-Basin from the Santa Barbara Channel Islands to San Diego

The shaded boundary areas in Fig. 27 suggest that the entire southern California coastline from San Diego to the Santa Barbara Islands effectively forms a semi-ellipse and that San Nicolas and San Clemente Islands provide a large part of the mirror-image semi-ellipse, thus creating a pseudo-elliptical basin.

Although the depths of this quasi-basin are very irregular we shall apply the gross approximation that the sea bed is ellipsoidal and calculate the modes of oscillation of such a basin using the theory of Goldsbrough (1930). The major and minor axis lengths, L and B respectively, are

$$L \approx 143.3 \text{ n. mi.}$$

$$B \approx 52.0 \text{ n. mi.}$$

If we neglect the presence of Santa Catalina Island, near the center of the ellipse,

as an artifice to achieving useful results, we may assume maximum central depth h_o for the ellipsoidal bed as

$$h_o \approx 3600 \text{ ft.}$$

Some of the modal periods at which the waters of this elliptical basin could oscillate are obtainable directly from a summary of Goldbrough's results (Wilson, 1972). Thus in the longitudinal sense (with symmetry about the minor axis) the modal periods T_n ($n = 1, 2, 3, \ldots$) should approximate

$$T_n(gh_o)^{\frac{1}{2}}/L \approx 2.22;\ 1.02;\ 0.73;\ 0.40;\ \ldots. \tag{106}$$

In the transverse sense (with symmetry about the major axis) the modal periods should approximate

$$T_n(gh_o)^{\frac{1}{2}}/B \approx 2.22;\ 1.91;\ 1.51;\ 0.82;\ \ldots. \tag{107}$$

For the dimensions given, the modal periods from Eq. (107) are

$$T_n \approx 34.4;\ 29.6;\ 23.4;\ 12.7;\ \ldots\ldots \text{mins} \tag{108}$$

From Eq. (106) the modal periods would be

$$T_n \sim 94.7;\ 47.8;\ 31.1;\ 17.1;\ \ldots\ldots \text{mins} \tag{109}$$

Some few of these periods are in agreement with periods given in Table VI for the shelf oscillations, so that it would seem evident that we have a further-sustaining system for trapping wave energy in the region and preventing too rapid decay. Again, however, the argument [discussed in Section (b)] applies that this factor should not lead to amplification of effects on the shelf over those calculated in Sections 9 to 13 by virtue of the approach taken in those calculations.

15. Possible Tsunami Effects from the Strike-Slip Component of Earthquake Displacement on the Fault

In compliance with item 1 of Appendix B, we discuss here the possibility that the strike-slip movements X along the fault at the shelf edge (see Tables I and IA) could be instrumental in generating any tangible tsunami effects.

Fig. 27 shows that the shelf edge between Newport Beach and Rose Canyon is relatively straight. Horizontal slippage along the fault can affect the water

mass above it only through bottom stress or by the movement of a boundary that is steep and normal (or nearly so) to the direction of the fault. Bottom stress effect can be discounted at once as negligible. Normal boundary effect may also be considered negligible because within the 65 miles of postulated fault movement no boundaries with sufficient inclination to the fault direction are involved.

There is general support for this type of conclusion from the fact that the San Francisco earthquake of 1906 (magnitude M = 8.2), in which the San Andreas Fault movement was almost exclusively strike-slip, failed to generate any tsunami, notwithstanding that the epicenter was on the submarine extension of the fault, north of San Francisco.

Likewise the Tango earthquake of 1927 in Japan (Fig. 4) in which the earth movement was predominantly strike-slip along a fault running into the sea, with the epicenter in the Sea of Japan, also failed to generate any tsunami.

We conclude, therefore, that the strike-slip movement should not constitute any problem in generating sea disturbance off the coast at San Onofre.

REFERENCES

Allen, C.R., St. Amand, P., Richter, C.F. and Nordquist, J.M., (1965)
"Relationship between Seismicity and Geologic Structure in the Southern Calif. Region", Bul'n Seismolog. Soc. Am., v. 55(4), Aug. 1965, pp 753-797

Allen, C.R., Grantz, A., Brune, J.N., Clark, M.M., Sharp, R.V., Theordore, T.G., Wolfe, E.W., and Wyss, M. (1968)
"The Borrego Mountain, California, Earthquake of 9 April, 1968: A Preliminary Report", Bul'n Seismolog. Soc. Am., v. 58(3), June 1968, pp. 1183-1186

Ambraseys, N.N. and Zatopek, A. (1968)
"The Varto Ustrikran (Anatolia) Earthquake of 19 August 1966", Bul'n Seismolog. Soc. Am., v. 58(1), Feb. 1968, pp. 47-102

Benioff, H. (1964)
"Earthquake Source Mechanisms", Science, v. 143, Mar. 1964, pp. 1399-1406

Berg, V.B. and Housner, G.W. (1961)
"Integrated Velocity and Displacement of Strong Earthquake Ground Motion", Bul'n Seismolog. Soc. Am., v. 51(2), Apr. 1961, pp. 175-189

Brune, J.N. and Allen, C.R. (1967)
"A Low Stress-drop, Low-magnitude Earthquake with Surface Faulting: The Imperial Valley, California, Earthquake of March 4, 1966", Bul'n Seismolog. Soc. Am., v. 57(3), June 1967, pp. 501-514

Davison, C. (1936)
"Great Earthquakes", T. Hurby & Co., London, 1936

Eagle, A. (1925)
"A Practical Treatise on Fourier's Theorem and Harmonic Analysis", Longmans, Green & Co., London, 178 pp.

Florensov, N.A. and Solonenko, V.P. (1963)
"Gobi Altai Earthquake", Acad. of Science of the USSR Siberian Department, Eastern Siberian Geological Institute, Comm. for Sciences and Higher Education of the Mongolian Peoples Republic, Moscow 1963 (Israel Program for Scientific Translation, Jerusalem, 1965)

Goldsbrough, G.W. (1930)
"Tidal Oscillations in an Elliptic Basin of Variable Depth", Proc. Royal Soc., London, v. 130(A), 1930, pp. 157-167

Hall, J.V. and Watts, G.M. (1953)
"Laboratory Investigation of the Vertical Rise of Solitary Waves on Impermeable Slopes", Tech. Memo No. 33, Beach Erosion Board, U.S. Army corps of Engineers, Washington, D.C., March 1953, 14 pp.

References Continued

Housner, G.W. (1965)
"Intensity of Earthquake Ground Shaking near the Causative Fault", Proc. Third World Conf. Earthq. Eng., New Zealand, 1965

Housner, G.W. (1971)
General Features of the San Fernando Earthquake in "Engineering Features of the San Fernando Earthquake February 9, 1971", (P.C. Jennings, Editor), Earthquake Eng'g Research Lab., California Institute of Technology, June 1971

Iida, K. (1959)
"Earthquake Energy and Earthquake Fault", J. Earth Sci., Nagoya Univ., Japan, v. 13, 1965, pp. 115-132

Kaplan, K. (1955)
"Generalized Laboratory Study of Tsunami Run-up", Tech. Memo No. 60, Beach Erosion Board, U.S. Army Corps of Engineers, Washington, D.C., Jan. 1955, 30 pp.

King, C-Y and Knopoff, L. (1968)
"Stress Drop in Earthquakes", Bul'n Seismolog. Soc. Am., v. 58(1), Feb. 1968, pp. 249-257

Kishi, T. and Saeki, H. (1966)
"The Shoaling, Breaking and Runup of the Solitary Wave on Impermeable Rough Slopes", Proc. Tenth Conf. Coastal Eng'g, (Tokyo, Japan, Sept. 1966), ASCE, New York, N.Y., v. 1, Chap. 21, pp. 322-348

Lamb, H. (1932)
"Hydrodynamics", Cambridge Univ. Press, England, 6th Editn, (Dover Publications) New York, 1945, 738 pp.

Lawson, A.C. (1908)
"The California Earthquake of April 18, 1906", Report of the State Earthquake Investigation Commission, Carnegie Institution of Washington, Washington, D.C., v. I, 1908

Oakeshott, G.B. (1966)
"Parkfield Earthquakes of June 27-29, 1966, Monterey and San Luis Obispo Counties, California, Preliminary Report", Bul'n Seismolog. Soc. Am., v. 56(4), Aug. 1966, pp. 961-971

Orr, T.E. and Herbich, J.B. (1969)
"Numerical Calculation of Wave Refraction by Digital Computer", COE Report No. 114, Coastal and Ocean Eng. Div., Texas Eng. Experiment Station: Texas A & M Univ., Dec. 1969, 79 pp.

References Continued

Reid, H.F. (1910)
"The Mechanics of the Earthquake, The California Earthquake of April 18, 1906, Report of the State Investigation Commission", v. 2, Carnegie Inst. of Washington, Washington, D.C., 1910

Shepard, F.P. (1963)
"Submarine Geology", Harper and Row, New York, N.Y.

Wilson, B.W. (1964)
"Generation and Dispersion Characteristics of Tsunamis", Studies on Oceanography (Editor: K. Yoshida), Univ. of Tokyo Press, Japan, 1964; also Univ. Washington Press, Seattle, 1965, pp. 413-444

Wilson, B.W. (1969)
"Earthquake Occurrence and Effects in Ocean Areas", Tech. Report CR.69.027 (for U.S. Naval Civil Eng'g Lab., Port Hueneme, Ca.), Feb. 1969, 188 pp.

Wilson, B.W. (1972)
"Seiches", Advances in Hydroscience (Academic Press, New York), v. 8, pp. 1-94

Wilson, B.W., Webb, L. and Hendrickson, J.A. (1962)
"The Nature of Tsunamis: Their Generation and Dispersion in Water of Finite Depth", Tech. Report No. SN 57-2 (to U.S. Coast & Geodetic Survey), National Engineering Science Co., Pasadena, Ca., Aug. 1962

Wilson, B.W. and Tørum, A. (1968)
"The Alaskan Tsunami of March 1964: Engineering Evaluation", Tech. Memo. No. 25, Coastal Eng'g Research Center, U.S. Army Corps of Engineers, Washington, D.C., 1968, 401 pp. + Appendices

Wilson, B.W. and Tørum, A. (1972)
"Effects of the Tsunamis: An Engineering Study" in "The Great Alaska Earthquake of 1964: Oceanography and Coastal Engineering", National Academy of Sciences, National Research Council, Washington, D.C., 1972

APPENDIX A

SOUTHERN CALIFORNIA EDISON COMPANY ASSUMED PARAMETERS AND REQUIREMENTS OF INVESTIGATION

Parameters for investigation should be based on the following assumptions:

1. A postulated offshore fault extending between Newport and Rose Canyon could rupture along its entire postulated length of 65 miles.
2. The fault plane is vertical and trends subparallel to the coastline. Its position is five miles offshore of San Onofre and generally follows the edge of the continental shelf as shown on the attached drawing.
3. The sense of offset is predominantly strike slip (right lateral) with an associated small component of vertical dip-slip motion. Assume the east block will move up relative to the west block which moves down. There is no known reason to assume the development of either a graben or a horst.
4. Consider ratios of strike slip to dip-slip offset as being 10 : 1, 10 : 2, and 10 : 3.

Questions to be addressed in the investigation

1. What parameters of maximum fault offsets (horizontal and vertical) using the above assumptions would create a Tsunami run-up of 28 feet at the plant site? This would provide the most conservative mechanism of offset.
2. What would be the natural period of oscillation in the south coast offshore study area?
3. What effects on Tsunami run-up would be due to the presence of offshore islands and particularly San Clemente Island?
4. What would be the effects of draw-back on:
   a. Beach materials near the sea wall?
   b. Cooling water structures and continuity of operation?

APPENDIX B

PROPOSED APPROACH TO PROBLEM

(a) From the condition of a postulated rupture length of 65 miles along the offshore fault, establish a probable (design) earthquake magnitude from statistical data relating fault length with earthquake magnitude.

(b) For the earthquake magnitude found from (a), use statistical data relating maximum ground displacement to earthquake magnitude to determine a probable (design) value of maximum ground displacement (resultant of horizontal strike-slip and vertical dip-slip).

(c) Hence for the specified ratios of strike-slip : dip-slip of 10 : 1, 10 : 2, 10 : 3, establish values of strike-slip and of dip-slip likely to ensue under the postulated conditions. Assume that between Dana Point and Oceanside these ground displacements are reasonably constant.

(d) In the first consideration of tsunami generation, assume that the dip-slip vertical upthrust on the east side, and down throw on the west side, of the fault conform to an equation of the form

$$\zeta(y,t) = A(1 - e^{-\alpha t}) f(y) \qquad (1)$$

with

$$\text{(i)} \quad f(y) = e^{-\beta y} \quad (\text{for } y > 0)$$
$$\text{(ii)} \quad f(y) = -e^{+\beta y} \quad (\text{for } y < 0) \qquad (2)$$

where $\zeta(y,t)$ defines vertical ground displacement as a function of time t and horizontal distance y measured normally from the fault line and taken positive in an easterly direction. The quantity A is one-half the vertical displacement found from item (c). The parameter α (units of frequency) will be determined from statistical information relating the duration time of earthquake shaking with earthquake magnitude. The parameter β [units of $(\text{length})^{-1}$] will be determined from statistical information relating (horizontal) strike-slip displacement with distance from the fault and earthquake magnitude. Eqs (1) and (2), together, are

expected to model reasonably well the expected time-dependent vertical earth movement between Dana Point and Oceanside.

(e) Treating the continental shelf as uniformly sloping from zero depth at the coast to 100 m. at the shelf edge with the earthquake fault breaking surface at 100 m. depth, parallel to the coast and normal to the shelf slope, make a best effort attempt to solve the hydrodynamic equations for the model of ground displacement adopted under item (d) in order to establish the initial wave form of the tsunami. The hydrodynamic solution will be completed for just enough time to establish the nature of the waves advancing in the east and west directions from the fault. [If the hydrodynamic solution proves too time consuming, an assumption based on engineering judgement may have to be made in regard to the initial tsunami wave form.]Establish a period for the tsunami wave(s).

(f) Pursue the propagation of the tsunami wave from the fault to the coastline by the traditional methods of graphical refraction, allowing for shoaling, refraction, friction and reflection and taking into account changing wave form in accord with shallow water wave theories.

(g) Apply the most authoritative (theoretical and experimental) results for estimating the run-up of the tsunami wave at the San Onofre site from the height obtained under (f) near the coast (say in 10 m. water depth).

(h) Investigate the oscillating characteristics of the continental shelf between Dana Point and Oceanside by approximating the shelf as a semi-ellipsoidal bowl of large major/minor axis ratio. Estimate the possibilities and consequences of resonance between the exciting tsunami period and the free modes of oscillation of the shelf.

(i) Investigate the oscillating characteristics of the oceanic basin between San Clemente Island and the mainland coast and estimate the possibilities and consequences of resonance between the exciting tsunami period and the free modes of oscillation of the basin. Other forms of oceanic basins may be discussed and their possible effect commented upon.

(j) Plot final estimates of tsunami run-up at the San Onofre site so as to establish the parameters likely to yield a tsunami run-up of 28 ft. It is expected that sufficient results will be obtained to permit extrapolation, if needed.

(k) Examine, as possible, the effects of tsunami draw back and the flow velocities likely to occur near the

(i) sea wall

(ii) cooling water structures.

Draw conclusions regarding effects on bed materials and the continuity of operation of cooling water intake.

(l) Estimate the possible effects on the tsunami disturbance of the horizontal strike-slip component of earthquake displacement along the fault. These effects are expected to be small, but the influences of the north-south end boundaries to the Gulf of Santa Catalina oceanic basin (formed by the continental slopes to the San Pedro shelf and the San Diego shelf) will need to be investigated in association with the natural oscillating characteristics of this basin.

SONGS ISFSI Flooding Analysis
Follow-up material from 09-07-2023 technical discussion at SONGS
Prepared by Southern California Edison Company

1. SCE actions and deliverables

a. Whether each canister must be inspected before transportation to an offsite storage or disposal facility.
   i. As discussed during our meeting, as a practical matter, it is likely all SONGS canisters would be visually inspected prior to offsite transportation, regardless of transportation Certificate of Compliance (CoC) requirements. Such an inspection would provide additional assurance for the receiving facility.
   ii. There are three transportation CoCs associated with SONGS dry storage canisters. Whether a canister contains high burnup fuel (HBF) may influence whether a pre-shipment inspection is required. Storage of HBF within the 24PT1 canister is not authorized. Detail as follows:

Canister model (Stores)	Certificate of Compliance (CoC)	Canister inspection/integrity verification requirement for non-HBF?	Canister inspection/integrity verification requirement for HBF?
NUHOMS 24PT1 (Unit 1 Fuel)	71-9255	No	N/A
NUHOMS 24PT4 (Units 2/3 Fuel)	71-9302	Yes	Yes
Holtec MPC-37 (Units 2/3 Fuel)	71-9373	No	Yes

b. Provide hyperlinks to California Coastal Commission Staff Reports.
   2. The 2015 CCC Staff Report for construction of the Holtec UMAX ISFSI discusses findings from the Kuhn 2005 Paleoseismic Features Paper. Link as follows: https://documents.coastal.ca.gov/reports/2015/10/Tu14a-10-2015.pdf
   3. The 2022 CCC Staff Report for the permit extension of the NUHOMS ISFSI references the hazards reports prepared by Coastal Environments. Both of Coastal Environments' Geological Hazards and Tsunami Hazards reports are referenced in the CCC staff report and each use findings from the Kuhn 2005 Paleoseismic Features Paper (see Appendix A for Kuhn citation). Link as follows: https://documents.coastal.ca.gov/reports/2022/10/Th12a/Th12a-10-2022-report.pdf

a. Provide the foundation for 27-foot level as the design basis for SONGS including Dr. Basil W. Wilson's 1972 tsunami paper.
   i. FSAR Section 2.4, available on the NRC's online database, addresses how 27 feet was established as the SONGS design basis.

- Section 2.4.6.1 titled *Probable Maximum Tsunami* states *detailed specific analyses were completed by Dr. Basil W. Wilson.*
- The study concluded that the wave induced by 7-foot sea floor displacement and occurring during simultaneous high tide and storm surge would have a maximum runup to elevation +15.6 feet MLLW at the Unit 2 and 3 seawall.
- Section 2.4.5.3 describes wave action as producing *the lowest and highest instantaneous water elevations* while storm surge is described in section 2.4.5.2.3 and is the abnormal rise in seawater level during a storm, measured as the height of the water above the normal predicted astronomical tide.

ii. Section 2.4.6.6 titled *Effects on Safety-Related Facilities* states *When storm waves are superimposed, the predicted maximum runup is to elevation +27 MLLW, as discussed in paragraph 2.4.5.3*. Superimposing storm waves is conservative.

b. Provide a statement indicating that SCE cannot release Holtec's proprietary flood analysis in section 4.6.2.5 of its FSAR.
   i. *Flood* information in section 4.6.2.5 of the Final Safety Analysis Report for the HI-STORM UMAX Canister Storage System by Holtec International was withheld by Holtec in accordance with 10 CFR 2.390. SCE is not at liberty to disclose proprietary information belonging to another party.
   ii. Reference page 4.38 of the Holtec FSAR: https://adamswebsearch2.nrc.gov/webSearch2/main.jsp?AccessionNumber=ML12285A090

c. Retrievability.
   i. 10 CFR Part 72.122 (l) specifies the requirement for the retrieval of spent nuclear fuel as follows: *Retrievability. Storage systems must be designed to allow ready retrieval of spent fuel, high-level radioactive waste, and reactor-related GTCC waste for further processing or disposal.*
   ii. The retrievability requirement applies to all general license ISFSIs, such as for SONGS, and specific licensed ISFSIs. The NRC is responsible to verify by its review of license applications for ISFSIs and by pre-operational inspection of dry storage systems under a general license that the retrievability requirement of 10 CFR Part 72.122 (l) is met. The NRC carries out its reviews and inspections using NRC approved procedures and, where needed, NRC approved Interim Staff Guidance (ISG) documents, such as ISG No. 2, *Fuel Retrievability* (note that ISG No. 2 has been incorporated into NUREG-2215).
   iii. The SONGS dry storage systems have demonstrated their compliance with NRC regulations, including retrievability, by the NRC's extensive licensing reviews performed for both the UMAX and NUHOMS systems, which confirmed compliance with their respective Safety Analysis Report, Certificate of Compliance (CoC), and other applicable NRC regulations. During its licensing reviews the NRC determined, as documented in separate Safety Evaluation Reports (SERs), that both systems meet the requirements of 10 CFR Part 72, including retrievability.

iv. Prior to canisters containing spent fuel being loaded into the SONGS ISFSIs, the NRC also performed pre-operational inspections of each system in accordance with NRC Inspection Procedure 60854 (IP 60854). Among other objectives, IP 60854 requires verification of retrievability. As documented in the inspection reports, the demonstration tests required by each CoC and witnessed by the NRC in 2003 for the NUHOMS dry storage system and 2017 for the UMAX system confirmed compliance with all CoC requirements, including retrievability, and returning a canister to a pool to be opened, if required.

v. NUREG-2215, NRC's Standard Review Plan for Spent Fuel Dry Storage Systems and Facilities, section 16.4.5 defines ready retrieval as *the ability to safely remove the spent fuel from storage for further processing or disposal*. To demonstrate the ability for ready retrieval, a licensee should demonstrate it has the ability to perform any of the three options below. These options may be utilized individually or in any combination or sequence, as appropriate:

A. Remove individual or canned spent fuel assemblies from wet or dry storage.
B. Remove a canister loaded with spent fuel assemblies from a storage cask or overpack, as applicable.
C. Remove a cask or DSF storage container, as applicable, loaded with spent fuel assemblies from the storage location.

vi. The dry storage canisters stored within the SONGS ISFSIs are retrievable in accordance with option B above.

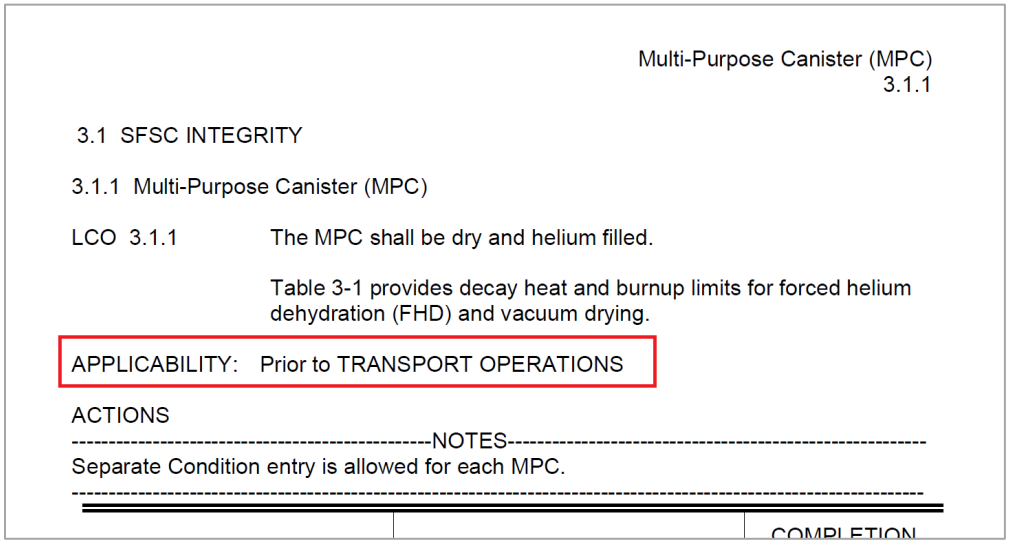
vii. Regular inspections of the SONGS ISFSIs continue to be performed by the NRC to assure compliance with applicable NRC regulations. These ongoing inspections will ensure retrievability is maintained over time.

viii. The NRC verified the NUHOMS canisters will remain retrievable during the period of extended operation (renewal). Reference the NRC's SER for renewed CoC 72-1029: https://www.nrc.gov/docs/ML2125/ML21258A020.pdf. For example:

- *The staff reviewed the applicant's supplemental evaluation to assess whether there was reasonable assurance that CISCC will not result in a loss of confinement or prevent retrieval of a CoC 1029 DSC during the period of extended operation, for a total of 60 years of storage. As noted in the CoC 1029 renewal application, the analysis was based on the CoC 1004 renewal application (ADAMS Accession No. ML16279A372), which the staff previously evaluated and documented in the CoC 1004 renewal application SER (ADAMS Accession No. ML17338A121). Specifically, Section 3.3.2 of the CoC 1004 renewal application SER addresses the staff's evaluation of the applicant's analysis of (1) DSC shell temperatures, (2) critical temperatures, relative humidity, and chloride concentration, (3) time for CISCC initiation, and (4) CISCC crack growth rate. Likewise, Section 3.4.13 of the CoC 1004 renewal application SER addresses the staff's evaluation of the applicant's analysis for DSC shell thickness to maintain the ASME Code limits during retrieval.*
- *The staff also reviewed the applicant's assessment that it relied on to support its conclusion that the evaluations conducted for the CoC 1004 renewal*

application are valid for the Standardized Advanced NUHOMS® System and sufficient for the CoC 1029 renewal application.

d. Applicability of LCO 3.1.1 *The MPC shall be dry and helium filled*.
   i. Reference: https://www.nrc.gov/docs/ML2034/ML20349A209.pdf
   ii. Required Action D. 1 states, with a completion time of 30 days: *Remove all fuel assemblies from the SFSC*.
   iii. The associated FSAR bases state:
      - D.1
      - If the MPC fuel cavity cannot be successfully returned to a safe, analyzed condition, the fuel must be placed in a safe condition in the spent fuel pool. The Completion Time is reasonable based on the time required to re-flood the MPC, cut the MPC lid welds, move the TRANSFER CASK into the spent fuel pool, remove the MPC [multipurpose canister] lid, and remove the spent fuel assemblies in an orderly manner and without challenging personnel.
   iv. As discussed during our meeting, Required Action D.1 is not applicable after the MPC has been dried, backfilled, and leak tested per Surveillance Requirements SR 3.1.1.1, 3.1.1.2, and 3.1.1.3. See below screen capture from the LCO:



Multi-Purpose Canister (MPC)
3.1.1

3.1 SFSC INTEGRITY

3.1.1 Multi-Purpose Canister (MPC)

LCO 3.1.1 The MPC shall be dry and helium filled.

Table 3-1 provides decay heat and burnup limits for forced helium dehydration (FHD) and vacuum drying.

APPLICABILITY: Prior to TRANSPORT OPERATIONS

ACTIONS

----------NOTES----------

Separate Condition entry is allowed for each MPC.

COMPLETION

e. Provide assessment of Kuhn study and context for understanding of carbon found at tsunami depositions within the last 20,000 years.
   i. In the 2005 Kuhn paper, Section 7 on Tsunamigenic Features discusses tsunami deposits and there is no mention of tsunami deposits coinciding with human activity at any of the elevations.
   ii. Confusingly, Figures 27, 28, and 29 related to liquefaction that describe human activity are located within Section 7 of the paper, and that section covers *Tsunamigenic features*. However, Figures 27, 28, and 29 are discussed in Section 6 (*Age of liquefaction features*). Liquefaction is a different mechanism than tsunami and can certainly occur up to elevation 100+ meters, even today.

iii. Reference: https://www.sciencedirect.com/science/article/abs/pii/S0013795205000785

iv. Moreover, SCE has engaged third-party experts to analyze the tsunami risk at San Onofre. The most recent research was conducted by Coastal Environments in connection with permitting processes required by the California Coastal Commission. That research found that the greatest risk of a significant tsunami at the site is from a far-field (versus a near-field) tsunami that originates from the eastern Aleutians. Findings are available in CCC Staff Reports, as follows:
   - 2015 Staff Report for construction of the UMAX ISFSI is available at https://documents.coastal.ca.gov/reports/2015/10/Tu14a-10-2015.pdf
   - 2022 Staff Report for extension of the NUHOMS ISFSI permit is available at https://documents.coastal.ca.gov/reports/2022/10/Th12a/Th12a-10-2022-report.pdf

f. Periodicity for radiation surveys of ISFSI storage system inlets and outlets.

i. SONGS technicians perform quarterly radiological surveys of both the UMAX and NUHOMS ISFSIs, which include obtaining radiation measurements for each storage module using sensitive handheld instruments and performing contamination surveys of the entire facility to identify the presence of loose surface contamination. UMAX surveys include the inlet and outlet vents. NUHOMS inspections cover the inlet vents. NUHOMS surveys do not include the storage module outlet vents, which are located approximately 20 feet above grade. Contamination surveys would determine whether any radioactive contamination had leaked from the canisters. Each quarterly radiological survey is formally documented and maintained as a plant record for regular inspection by the NRC.

ii. In addition to SCE's regular radiological monitoring, independent surveys of the SONGS ISFSIs were performed in 2018 and in 2020. The results of the independent surveys were consistent with SCE's radiation surveys.
   - On September 6, 2018, members of Residents Organized for a Safe Environment (ROSE) performed independent radiation monitoring of both SONGS ISFSIs using their own instrumentation. ROSE's survey results were consistent with SCE's radiation monitoring surveys. More on the survey by ROSE is available HERE.
   - On September 24, 2018, the County of San Diego Office of Emergency Services performed an independent radiation survey of both SONGS ISFSIs using its own handheld instruments. The survey results did not show evidence of risk to public health or the environment and confirmed radiation levels were well within NRC regulatory limits. Link: County SD Field Survey SONGS ISFSI.pdf (songscommunity.com)
   - On October 22, 2018, NRC inspectors performed independent measurements and verification of radiological conditions for both SONGS ISFSIs using their own handheld instruments. In its report the NRC concluded there were *no safety or regulatory concerns with loaded spent*

fuel canisters on the ISFSI pads at San Onofre. Link: https://www.nrc.gov/docs/ML1901/ML19011A457.pdf

- On October 19, 2020, an independent, third-party vendor surveyed the NUHOMS ISFSI. The survey was completed in response to comments from a member of the public during the August 2020 CEP meeting.
    - Link to video: https://www.songscommunity.com/news/releases/san-onofre-community-engagement-panel-meeting-to-include-updates-on-recent-radiation-survey-dismantlement-progress
    - Link to report: https://s3.amazonaws.com/cms.ipressroom.com/339/files/202010/Explanation+of+NUHOMS+Radiation+Survey+Results+FINAL.pdf

g. Send photographs taken during the tour that have been cleared by SCE Security to Blanch, Headrick, and Langley for their unrestricted use.

2. Paul Blanch actions

a. Request proprietary analysis from Holtec.